

**INVESTIGATIONS OF THE STRUCTURE AND DYNAMICS OF
NOVEL MUONIATED RADICALS**

by

Iain McKenzie

B.Sc., Simon Fraser University, 1999.

**THESIS SUBMITTED IN PARTIAL FULFILLMENT OF
THE REQUIREMENTS FOR THE DEGREE OF**

DOCTOR OF PHILOSOPHY

In the Department
of
Chemistry

© Iain McKenzie 2004

SIMON FRASER UNIVERSITY

March 2004

All rights reserved. This work may not be reproduced in whole or in part, by photocopy or other means, without permission of the author.

APPROVAL

Name: Iain McKenzie
Degree: Doctor of Philosophy
Title of Thesis: Investigations of the Structure and Dynamics of Novel Muoniated Radicals

Examining Committee:

Chair: Dr. Jason A. C. Clyburne
Assistant Professor

Dr. Paul W. Percival
Senior Supervisor
Professor

Dr. Ian D. Gay
Professor

Dr. Peter D. Wilson
Assistant Professor

Dr. Daniel B. Leznoff
Internal Examiner
Assistant Professor

Dr. Emil Roduner
External Examiner
Professor
Institut für Physikalische Chemie
Universität Stuttgart

Date Approved: March 25, 2004

SIMON FRASER UNIVERSITY



Partial Copyright Licence

The author, whose copyright is declared on the title page of this work, has granted to Simon Fraser University the right to lend this thesis, project or extended essay to users of the Simon Fraser University Library, and to make partial or single copies only for such users or in response to a request from the library of any other university, or other educational institution, on its own behalf or for one of its users.

The author has further agreed that permission for multiple copying of this work for scholarly purposes may be granted by either the author or the Dean of Graduate Studies.

It is understood that copying or publication of this work for financial gain shall not be allowed without the author's written permission.

The original Partial Copyright Licence attesting to these terms, and signed by this author, may be found in the original bound copy of this work, retained in the Simon Fraser University Archive.

Bennett Library
Simon Fraser University
Burnaby, BC, Canada

ABSTRACT

Muonium (Mu) can be considered as a light isotope of hydrogen in which the nucleus is a positive muon. Radicals labelled with Mu are used to probe the effect of isotopic substitution on the structure and dynamics of radicals. Novel muoniated radicals have been produced in which the muon is attached directly to the radical centre (α -muoniated radical) or the unpaired electron is in a σ orbital.

The CH_2Mu and CD_2Mu isotopomers of the methyl radical were produced by the reaction of Mu with ketene and deuterated ketene, respectively, and the hyperfine coupling constants (hfc) were measured between approximately 80 and 230 K. The temperature dependence of the hfc is due to interactions with the solvent which dominate because the large out-of-plane vibrational frequency, compared with CH_3 , results in negligible population of the excited vibrational level. Relaxation in the liquid phase is interpreted to be dominated by the spin-rotation mechanism. The reduced muon hfc (given by the muon hfc divided by the ratio of the muon and proton gyromagnetic ratios) is 3% larger than the proton hfc, consistent with the larger zero-point energy of the C-Mu bond compared with the C-H bond. An additional radical was observed just below the boiling point of ketene. Investigation revealed that this radical resulted from Mu addition to the ketene dimer, which forms at temperatures above 200 K.

Alpha-muoniated radicals were produced by the reaction of Mu with stable singlet carbenes. Four stable carbenes (1,3-bis(isopropyl)-4,5-dimethylimidazol-2-ylidene, 1,3-bis(2,4,6-trimethylphenyl)-imidazol-2-ylidene, 1,3,4-triphenyl-4,5-dihydro-1H-1,2,4-triazol-5-ylidene and 1,3-bis(2,4,6-trimethylphenyl)imidazolin-2-ylidene) were studied, and in every case Mu added exclusively to the carbeneic carbon. The radicals were identified by a comparison of the experimental hfc with values obtained from density functional theory calculations. The temperature dependence of the muon hfc cannot be accounted for by only considering vibrational motion at the radical centre.

The *N*-muono-*N*-*tert*-butylcarbonyl and *N*-muono-*N*-*tert*-butylthiocarbonyl radicals were generated by the reaction of Mu with *tert*-butylisocyanate and *tert*-

butylisothiocyanate. These radicals have the unpaired electron in a σ orbital and are the first acyl radicals to be observed directly by μ SR (muon spin rotation, resonance and relaxation spectroscopy).

DEDICATION

To my father.

ACKNOWLEDGEMENTS

I would like to express my gratitude to Professor Paul W. Percival, my senior supervisor, for his guidance and support. His leadership, knowledge and professionalism are admirable and I consider myself to be fortunate to have been his student.

Dr. Jean-Claude Brodovitch provided a great deal of technical assistance for the experiments described in this thesis. I am indebted to him for showing me how to pick weak μ LCR resonances out of background noise.

I would also like to thank the past and present graduate students and post-doctoral fellows of the SFU muonium chemistry group (Dr. Joachim Schüth, Dr. Brenda Addison-Jones, Dr. Khashayar Ghandi, Mrs. Sonja Kecman and Mr. Brett McCollum) for their assistance with experiments at TRIUMF and for their friendship.

Much of the work described in this thesis would not have been possible without the help of Dr. Jason A. C. Clyburne. His enthusiasm is infectious and the assistance that he provided was invaluable.

I must also thank my friends in the chemistry department of SFU, without whom this thesis would have been prepared much sooner. I am grateful to Mr. John Canal and Ms. Christine Wilcox for allowing me to use their glove-box.

I would like to thank my mother and father for their support. Although my father passed away before I began my Ph.D., he has greatly influenced my research.

Finally, I would like to thank my fiancé, Kathryn Benusic, for her love, support and putting up with the late nights and the interminable monologues about muoniated radicals.

TABLE OF CONTENTS

Approval.....	ii
Abstract.....	iii
Dedication.....	v
Acknowledgements.....	vi
Table of Contents.....	vii
List of Figures.....	xi
List of Tables.....	xiv
List of Abbreviations.....	xvi
CHAPTER 1. INTRODUCTION.....	1
1.1 The positive muon in chemistry.....	1
1.2 Production and decay of the positive muon.....	4
1.3 The transverse field muon spin rotation technique.....	6
1.4 Muonium.....	8
1.5 Muonium-substituted free radicals.....	11
1.6 Avoided muon level crossing resonance.....	13
1.7 Muoniated radicals.....	15
1.7.1 The muoniated trimethylsilylmethyl radical.....	16
1.7.2 <i>N</i> -muono-pyridinyl radical.....	16
1.7.3 Inorganic α -muoniated radicals.....	17
1.8 Routes to form α -muoniated radicals.....	18
1.8.1 Indirect formation.....	18
1.8.2 Direct formation.....	20
1.9 Collaborative versus individual work.....	21

CHAPTER 2. EXPERIMENTAL AND THEORETICAL METHODS.....	22
2.1 μ SR experiments	22
2.1.1 TRIUMF	22
2.1.2 Surface muons	23
2.1.3 Scintillator detectors	24
2.1.4 μ SR apparatus	24
2.1.5 Temperature control.....	24
2.1.6 TF- μ SR	25
2.1.7 μ LCR	27
2.1.8 Data analysis	29
2.2 Theoretical calculations	29
2.2.1 Introduction.....	29
2.2.2 Basis sets	31
2.2.3 Density functional theory.....	33
2.2.4 Software packages for electronic structure calculation.....	35
CHAPTER 3. THE MUONIATED METHYL RADICAL	36
3.1 Introduction.....	36
3.1.1 UV and IR spectroscopy of the methyl radical	36
3.1.2 EPR studies of the methyl radical.....	37
3.1.3 Theoretical calculations on the methyl radical.....	38
3.1.4 μ SR experiments and experimental approach.....	38
3.1.5 The reaction of hydrogen atoms with ketene	39
3.2 Experimental.....	40
3.3 Results	41
3.4 Radical identification.....	47
3.5 Temperature dependence of the hfcs of the CH ₂ Mu and CD ₂ Mu radicals	47

3.5.1	Vibrational motion of methyl radical isotopomers	48
3.5.2	Solvent effects	52
3.6	Relaxation of the CH ₂ Mu and CD ₂ Mu radicals	54
3.7	Discussion.....	58
3.8	Future Work.....	59
3.9	Conclusions.....	59
CHAPTER 4. STRUCTURE AND DYNAMICS OF THE MUONIUM ADDUCT OF DIKETENE		61
4.1	Introduction.....	61
4.2	Experimental.....	63
4.3	Results	63
4.4	Radical assignment.....	65
4.5	Calculations and discussion	67
4.6	Conclusions.....	72
CHAPTER 5. DIRECT FORMATION OF ALPHA-MUONIATED RADICALS: ADDITION OF MUONIUM TO STABLE SINGLET CARBENES		73
5.1	Introduction.....	73
5.2	Experimental.....	75
5.3	Results of μ SR experiments	76
5.3.1	Transverse field muon spin rotation	76
5.3.2	Avoided muon level crossing resonance.....	82
5.4	Radical identification.....	85
5.4.1	Comparison with previous μ SR and EPR experiments	85
5.4.2	Quantum calculations	86
5.4.3	Discussion	92
5.5	Vibrational motion of α -muoniated radicals.....	93

5.5.1	Inversion potentials of radicals 5.1a-3a	95
5.5.2	Angular variation of hfcs in radicals 5.1a-3a	96
5.5.3	Vibrational wavefunctions	97
5.6	Future work	100
5.7	Conclusions	100
CHAPTER 6. DETECTION OF MUONIATED ACYL AND THIOACYL RADICALS.....		101
6.1	Introduction.....	101
6.2	Experimental	105
6.3	Results	105
6.4	Assignment of observed radicals.....	108
6.5	Discussion and calculations	113
6.6	Conclusions.....	119
CHAPTER 7. SUMMARY		121
Bibliography		124

LIST OF FIGURES

Figure 1.1:	Decay of the positive pion (π^+). P_X is the momentum vector and S_X is the spin vector of particle X.....	5
Figure 1.2:	Decay of the positive muon (μ^+). P_X is the momentum vector and S_X is the spin vector of particle X.....	6
Figure 1.3:	TF- μ SR histogram of a diamagnetic muon in water in an applied field of 400 Gauss.....	8
Figure 1.4:	Breit-Rabi diagram for a two-spin-1/2 system. $B_c = 1590$ Gauss, the ratio of the hyperfine frequency of Mu to the gyromagnetic ratio of the electron. Of the four allowed transitions at low-fields, only the two denoted by solid lines are resolvable.	10
Figure 1.5:	TF- μ SR spectrum of the CH_2Mu radical at 184 K.	12
Figure 1.6:	μ LCR spectrum of the CH_2Mu radical at 184 K.	15
Figure 1.7:	a) β -muoniated radical b) α -muoniated radical.	16
Figure 1.8:	a) Formation of the muoniated-trimethylsilylmethyl radical. b) Formation of the N -muono-pyridinyl radical.	17
Figure 1.9:	Generalised scheme for indirect formation of α -muoniated radicals.....	18
Figure 2.1:	Schematic for TF- μ SR experiment.	26
Figure 2.2:	Schematic diagram of a μ LCR experiment.	28
Figure 3.1:	TF- μ SR spectrum of ketene at 184 K in an applied magnetic field of 14.5 kG.....	41
Figure 3.2:	Temperature dependence of the reduced muon hfc in CH_2Mu (\square) and CD_2Mu (\circ). The solid lines are a guide for the eyes only.	44
Figure 3.3:	μ LCR spectrum of ketene at 184 K.	45
Figure 3.4:	μ LCR spectrum of d2-ketene at 200 K.	46
Figure 3.5:	Relaxation rate of the radical signals in the TF- μ SR spectrum of CH_2Mu as a function of temperature.	54
Figure 3.6:	Relaxation rate of the radical signals in the TF- μ SR spectrum of CD_2Mu as a function of temperature.	55

Figure 4.1:	TF- μ SR spectrum of d2-ketene at 235 K and 14.5 kG. The truncated peak labelled "D" is due to muons in a diamagnetic environment and the peaks labelled "R1" are due to the CD ₂ Mu radical. The peaks labelled "R2" are attributed to a Mu adduct of diketene.	61
Figure 4.2:	Diketene (4-methylene-oxetan-2-one).	62
Figure 4.3:	TF- μ SR spectrum of a neat diketene sample at 298 K and 11.6 kG.	63
Figure 4.4:	μ LCR spectrum of diketene at 298 K.	65
Figure 4.5:	Possible radicals resulting from the reaction of Mu with diketene.	66
Figure 4.6:	a) Newman projection along the C _{β} -C _{α} bond of the minimum energy geometry of 4.2 showing the unpaired electron spin density. b) Definition of the dihedral angle (θ) in 4.2 (the carbonyl group is not shown for clarity).	69
Figure 4.7:	Muon (\square), methyl proton (\circ) and ring proton (Δ) hyperfine coupling constants and calculated values (lines) for the 4-muonomethyl-oxetan-2-yl radical. The error bars of the experimental values are smaller than the data points.	71
Figure 5.1:	Stable singlet carbenes (<i>i</i> -Pr = CH(CH ₃) ₂ , Mes = 2,4,6-trimethylphenyl, Ph = phenyl).	74
Figure 5.2:	Structures of radicals that could form by addition of Mu to the carbeneic carbons or the five-membered rings of carbenes 5.1-5.4	75
Figure 5.3:	TF- μ SR spectrum of 4,5-dimethyl-1,3-bis(isopropyl)imidazol-2-ylidene (5.1) at 298 K in an applied magnetic field of 14.5 kG.	77
Figure 5.4:	TF- μ SR spectrum of 1,3-bis(2,4,6-trimethylphenyl)imidazol-2-ylidene (5.2) at 298 K in an applied magnetic field of 14.5 kG.	77
Figure 5.5:	TF- μ SR spectrum of 1,3,4-triphenyl-4,5-dihydro-1 <i>H</i> -1,2,4-triazol-5-ylidene (5.3) at 298 K in an applied magnetic field of 14.5 kG.	78
Figure 5.6:	TF- μ SR spectrum of 1,3-bis(2,4,6-trimethylphenyl)imidazolin-2-ylidene (5.4) at 298 K in an applied magnetic field of 14.5 kG.	78
Figure 5.7:	Temperature dependence of the muon hfc in the Mu adduct of 4,5-dimethyl-1,3-bis(isopropyl)imidazol-2-ylidene (\circ), the Mu adduct of 1,3-bis(2,4,6-trimethylphenyl)imidazole-2-ylidene (\square) and the Mu adduct of 1,3,4-triphenyl-4,5-dihydro-1 <i>H</i> -1,2,4-triazol-5-ylidene (Δ). The lines are a guide for the eyes only.	81
Figure 5.8:	Avoided muon level crossing resonance spectrum of 4,5-dimethyl-1,3-bis(isopropyl)imidazol-2-ylidene (5.1).	83

Figure 5.9:	Additional resonance in the avoided muon level crossing resonance spectrum of 40% ^{13}C enriched 4,5-dimethyl-1,3-bis(isopropyl)imidazol-2-ylidene (5.1).....	83
Figure 5.10:	Avoided muon level crossing resonance spectrum of 1,3-bis(2,4,6-trimethylphenyl)imidazol-2-ylidene (5.2).....	84
Figure 5.11:	Avoided muon level crossing resonance spectrum of 1,3,4-triphenyl-4,5-dihydro-1 <i>H</i> -1,2,4-triazol-5-ylidene (5.3).....	84
Figure 5.12:	Reaction profile for the addition of Mu to the carbeneic carbon (\square) and the double bond (\circ) of 4,5-dimethyl-1,3-bis(isopropyl)imidazol-2-ylidene (5.1).....	90
Figure 5.13:	Calculated potential (UB3LYP/6-311G**) for the out-of-plane vibrational mode of 5.1a	96
Figure 5.14:	Square vibrational wavefunctions for symmetric double-welled potentials with different inversion barriers.	98
Figure 6.1:	Structure and unpaired electron spin density in the a) 2-muono-1-phenyl-1-ethenyl, b) 2-methyl-4-muono-but-2-en-3-yl and c) 1,2-bis(trimethylsilyl)-1-muono-2-ethenyl radicals. (UB3LYP/6-311G).....	104
Figure 6.2:	TF- μ SR spectrum of <i>tert</i> -butylisocyanate at 298 K and an applied magnetic field of 14.5 kG.....	106
Figure 6.3:	μ LCR spectrum of <i>tert</i> -butylisocyanate at 298 K.....	106
Figure 6.4:	TF- μ SR spectra of <i>tert</i> -butylisocyanate at 266 K and applied magnetic fields of a) 14.5 kG and b) 19.3 kG.	108
Figure 6.5:	Reactions relevant to the addition of Mu to <i>tert</i> -butylisocyanate (X = O) and <i>tert</i> -butylisothiocyanate (X = S).....	110
Figure 6.6:	Structure and unpaired electron spin density in radicals a) E6.3 , b) Z6.3 , c) E6.4 and d) Z6.4 obtained from quantum calculations.	114
Figure 6.7:	Relative internal energies for the reactions of a) H with <i>tert</i> -butylisocyanate and b) Mu with <i>tert</i> -butylisocyanate.....	117

LIST OF TABLES

Table 1.1:	Physical properties of the positive muon.	2
Table 1.2:	Selected properties of muonium.	3
Table 3.1:	Muon hfc and relaxation rate for the Mu adduct of ketene.	42
Table 3.2:	Muon hfc and relaxation rate for the Mu adduct of d2-ketene.	43
Table 3.3:	μ LCR resonance field, width and the proton hfc of the Mu adduct of ketene as a function of temperature.	45
Table 3.4:	μ LCR resonance field, width and the deuteron hfc of the Mu adduct of deuterated ketene as a function of temperature.	46
Table 3.5:	Vibrational modes of the methyl radical.	49
Table 3.6:	Calculated vibrational modes and frequencies for the CH ₂ Mu radical.	50
Table 3.7:	Calculated vibrational modes and frequencies for the CD ₂ Mu radical.	51
Table 3.8:	Hyperfine coupling constants and calculated out-of-plane vibrational frequencies (UB3LYP/6-311++G(2df,p)) for isotopomers of the methyl radical.	58
Table 4.1:	Muon hyperfine constants for the Mu adduct of diketene.	64
Table 4.2:	Analysis of muon avoided level-crossing resonance spectra.	65
Table 4.3:	Relative energies and hyperfine constants for the minimum energy conformations of the muoniated methyl group in 4-muonomethyl-oxetan-2-on-4-yl.	70
Table 4.4:	Comparison of the measured muon hfcs of the second radical observed in ketene and d2-ketene with calculated hfcs for the H and D isotopomers of the 4-muonomethyl-oxetan-2on-4-yl radical.	72
Table 5.1:	Muon hfc as a function of temperature for the Mu adduct of 4,5-dimethyl-1,3-bis(isopropyl)imidazol-2-ylidene (5.1).	79
Table 5.2:	Muon hfc as a function of temperature for the Mu adduct of 1,3-bis(2,4,6-trimethylphenyl)imidazol-2-ylidene (5.2).	80
Table 5.3:	Muon hfc as a function of temperature for the Mu adduct of 1,3,4-triphenyl-4,5-dihydro-1H-1,2,4-triazol-5-ylidene (5.3).	80

Table 5.4:	μ LCR fields, widths and corresponding ^{13}C hfc as a function of temperature for the Mu adduct of 4,5-dimethyl-1,3-bis(isopropyl)imidazol-2-ylidene (5.1)....	82
Table 5.5:	Calculated hyperfine coupling constants (MHz) for the possible radicals formed by Mu addition to the imidazole ring of carbene 5.1 , and the experimentally determined hfc at 298 K.	91
Table 5.6:	Calculated hyperfine coupling constants (MHz) for the possible radicals formed by Mu addition to the imidazole ring of carbene 5.2 , and the experimentally determined hfc at 298 K.	91
Table 5.7:	Calculated hyperfine coupling constants (MHz) for the possible radicals formed by Mu addition to the triazole ring of carbene 5.3 , and the experimentally determined hfc at 298 K.	92
Table 5.8:	Calculated hyperfine coupling constants (MHz) for the radical 5.4a and the experimentally determined muon hfc at 298 K.	92
Table 5.9:	Inversion barrier heights for the out-of-plane vibration at the radical centre for radicals 5.1a-3a	96
Table 5.10:	Fitted parameters for the lowest inversion-doubled pair of levels of radical 5.3a	98
Table 6.1:	Muon hfc (MHz) and relaxation rates (μs^{-1}) of the Mu adduct of <i>tert</i> -butylisocyanate between 274 and 322 K.	105
Table 6.2:	Muon hfc (MHz) and relaxation rates (μs^{-1}) for the Mu adducts of <i>tert</i> -butylisothiocyanate.	107
Table 6.3:	Hfc (MHz) of related radicals determined by EPR.	111
Table 6.4:	Calculated hfc (MHz) for all the possible radicals that could form by Mu addition to <i>tert</i> -butylisocyanate and <i>tert</i> -butylisothiocyanate.	112
Table 6.5:	The internal, zero point and total energy of the molecules and transition states of reactions 6.2, 6.3 and 6.4 for X = O and S.	116

LIST OF ABBREVIATIONS

DFT	density functional theory
EPR	electron paramagnetic resonance
GTO	Gaussian-type orbital
hfc	hyperfine coupling constant
NMR	nuclear magnetic resonance
SCF	self-consistent field
SFU	Simon Fraser University
TF- μ SR	transverse field muon spin rotation
TRIUMF	Tri University Meson Facility
TS	transition state
ZPE	zero point energy
μ LCR	avoided muon level crossing resonance
μ SR	muon spin rotation, resonance, relaxation spectroscopy

CHAPTER 1.

INTRODUCTION

1.1 The positive muon in chemistry

Chemists are very familiar with protons and neutrons, the components of nuclei, and with electrons. They are less familiar with other fundamental particles such as the positive muon (μ^+). The less informed chemist might be tempted to believe that studying the muon is the realm of particle physicists and provides no important chemical information. Views such as these are extremely misguided. Even though the muon lifetime is only two-millionths of a second, this is long enough for it to participate in many fundamental chemical processes. The muon has the same spin and charge as the proton but with one-ninth the mass, so in matter it behaves as if it is a very light proton. In particular, combination with an electron results in the formation of muonium (Mu), which is entirely analogous to the hydrogen atom. Spectroscopic techniques involving the positive muon have provided valuable information about kinetics, structure and dynamics of transient free radicals.

Anderson and Neddermeyer first detected the positive muon in 1937 as a component of cosmic rays [1]. The positive muon can be artificially produced at high-energy (≥ 450 MeV) particle accelerators. Some of the properties of the positive muon are listed in Table 1.1.

On entering a solid, liquid or gas, the muon loses kinetic energy through ionization and excitation of the medium. These processes take place in the first 10^{-9} s, well before real time detection is possible. There is still controversy over the exact nature of these events and several models have been developed. The "hot" model was the first to be developed [2,3,4] but recent experimental results suggest that it is best applied to the gas phase [5], while the "spur" model is of greater importance to condensed phases [6]. Recently, the "delayed" Mu formation model was introduced [7]. Whatever the exact mechanism, the overall radiolysis damage to the medium is insignificant due to the small number of muons in the sample at any one time and the short lifetime of the radiolytic species.

Once the muon has thermalized, it can exist in three different magnetic states: as a muon in a diamagnetic environment, as free muonium, or as a muoniated radical.

Table 1.1: Physical properties of the positive muon. ^a

Property	Values
Charge	+e
Spin	1/2
Mass	105.6595 MeV c ⁻²
	206.76835 m _e
	0.1126096 m _p
	0.7570 m _π
Magnetic moment	4.49048 x 10 ⁻²³ erg G ⁻¹
	3.1833452 μ _p
	0.004834 μ _e
g-factor (g _μ)	2.002331848
	1.000006 g _e
Gyromagnetic ratio (γ _μ /2π)	13.55342 kHz G ⁻¹
Mean lifetime (τ _μ)	2.19714 μs

^a Reference [8].

In a diamagnetic environment there are no unpaired electrons. The diamagnetic state includes free muons, solvated or trapped muons, and any diamagnetic molecule incorporating the muon, such as MuH, MuOH, C₆H₁₃Mu, etc. The small changes in the precession frequency due the different chemical environments (chemical shift) are generally too small to be measured, due to the resolution of the experiments, which is a consequence of the short lifetime of the muon. As a result, the chemical identity of the diamagnetic species cannot be ascertained, so it is of little interest to chemists. In contrast, diamagnetic muons are of great utility to solid-state physicists, who use them to probe local magnetic field distributions.

In 1957, Friedman and Telegdi proposed that the positive muon could form a bound state with an electron in order to explain the depolarization of muon spins in nuclear emulsions [9]. This one-electron atom was named muonium ($\text{Mu} = [\mu^+, e^-]$). The first direct experimental observation of muonium in matter was in 1960, when Hughes *et al.* reported the detection of the characteristic muonium signal in argon gas [10]. In most gases, liquids and solids, a μ^+ can capture an electron from the medium during the final stages of thermalisation to form Mu. Some of the properties of Mu are given in Table 1.2. Although muonium has one-ninth the mass of a hydrogen atom, its reduced mass is 0.996 that of hydrogen. Accordingly, the Bohr radius and ionization potential of H and Mu are essentially the same, so chemically Mu can be thought of as light isotope of hydrogen.

Table 1.2: Selected properties of muonium. ^a

Property	Values
Mass	$207.8 m_e$
	$0.1131 m_H$
Reduced mass	$0.9956 m_H$
Bohr radius	0.5315 \AA
	$1.0044 a_0$
Ionization potential	13.539 eV
	0.9956 of H
Gyromagnetic ratio (γ_M)	1.394 MHz G^{-1}
Hyperfine frequency	$4463 \text{ MHz in vacuum}$
de Broglie wavelength (300K)	$2.979 \times 10^{-8} \text{ cm}$
	2.967 of H
Mean thermal velocity (300K)	$0.75 \times 10^6 \text{ cm s}^{-1}$
	$2.967 v_H$

^a Reference [11]

In 1963, Brodskii suggested that muoniated radicals could be formed by the addition of Mu to unsaturated molecules [12]. Roduner *et al.* first observed muoniated radicals in the liquid phase in 1978 [13]. Given that Mu is a light isotope of hydrogen, muoniated radicals can be thought of in the same way as deuterated or tritiated radicals. Comparisons of the hyperfine coupling constants of different isotopomers often show deviations beyond the ratio of the magnetic moments. These differences are due to dynamic effects because the vibrational wavefunctions are mass dependent. The light mass of Mu can result in large changes and this makes it a more sensitive probe of vibrational motion than conventional labelling.

Several experimental techniques have been developed that are based on the anisotropic radioactive decay of the muon. These spectroscopic techniques are collectively known by the acronym μ SR, which was coined to highlight the similarities with more well known magnetic resonance techniques such as NMR and ESR (or EPR). Transverse field muon spin rotation (TF- μ SR) is used to measure the muon hyperfine coupling constant (A_μ). Avoided muon level crossing resonance (μ LCR) is a means of measuring the hyperfine coupling constants of other magnetic nuclei in muoniated radicals. Theoretical details of these techniques will be given later in this chapter and the experimental details will be given in Chapter 2. There have been several excellent reviews of muonium chemistry and the μ SR spectroscopic techniques by Walker [14], Schenck [8], Roduner [11], Cox [15] and Brewer [16].

1.2 Production and decay of the positive muon

Muons are produced by the radioactive decay of the positive pion (π^+). The pions are in turn produced by the collision of high energy protons with nuclei such as copper and beryllium.



The minimum proton kinetic energy for pion production is about 180 MeV. Positive pions decay with a mean lifetime of 26 ns to give the positive muon and a muon neutrino [8].

$$\pi^+ \rightarrow \mu^+ + \nu_\mu \quad (1.2)$$

The decay process of equation (1.2) produces 4.1 MeV muons and violates parity. The pion is a spin 0 particle but the muon neutrino is a spin 1/2 particle with zero rest mass and negative helicity. Because of the conservation of linear and angular momentum, the muons emitted from the decay process at the surface of the production target are 100% polarized with negative helicity (Figure 1.1).

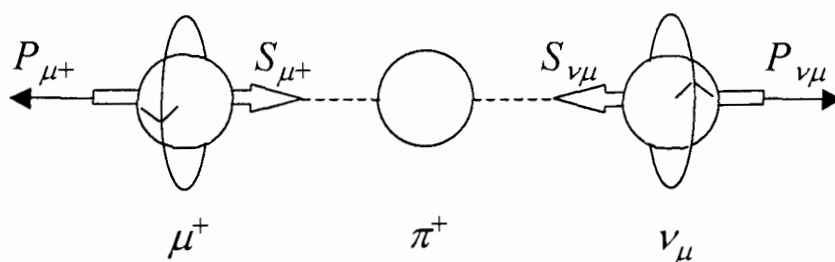


Figure 1.1: Decay of the positive pion (π^+). P_X is the momentum vector and S_X is the spin vector of particle X.

The muon decays with a lifetime of $2.2 \mu\text{s}$ and emits a positron, an electron neutrino and an anti-muon neutrino [17].

$$\mu^+ \rightarrow e^+ + \nu_e + \bar{\nu}_\mu \quad (1.3)$$

This decay process also violates parity. As a consequence of the conservation of energy, linear and angular momentum in this three-body decay, the positron is emitted preferentially along the direction of the muon spin [18]. This allows for the reconstruction of the muon polarization in a sample. Because of the three-body nature of the decay, the positron can have a range of kinetic energies from 0 to $E_{\text{max}} = 52.3 \text{ MeV}$.

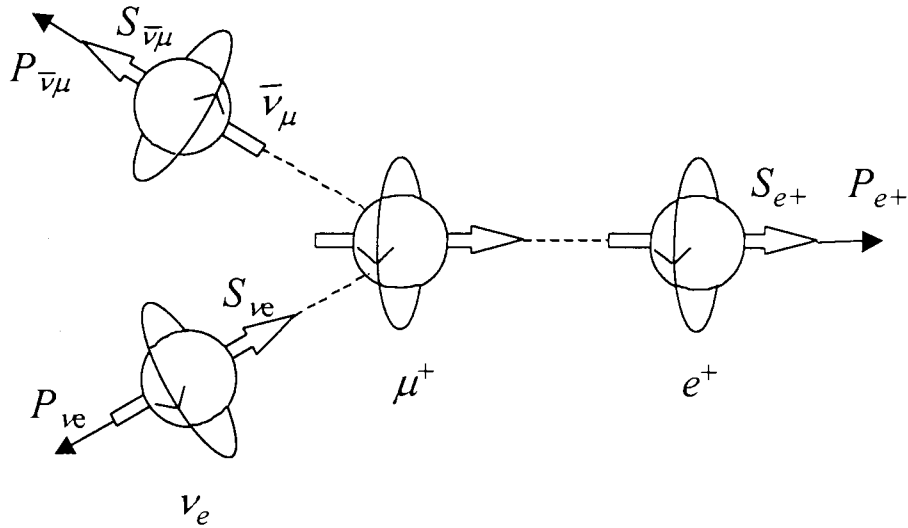


Figure 1.2: Decay of the positive muon (μ^+). P_X is the momentum vector and S_X is the spin vector of particle X.

The theoretical positron decay spectrum is given by [19]

$$\frac{dN}{d\varepsilon d\Omega} = \frac{C}{2\pi} [1 + A \cos\theta] \quad (1.4)$$

where N is the number of positrons with energy ε emitted at the angle θ with respect to the initial spin polarization of the muon, $\varepsilon = E/E_{\max}$ is the positron energy in terms of the maximum positron energy, Ω is the solid angle of the detector, $C = \varepsilon^2(3-2\varepsilon)$, and the muon asymmetry $A = (2\varepsilon-1)/(3-2\varepsilon)$.

The muon asymmetry has a maximum value when positrons are emitted with E_{\max} . The low energy positrons ($\varepsilon < 0.5$) are preferentially emitted in the direction opposite the muon spin. The average muon asymmetry over all positron energies is 1/3. The average asymmetry can be increased by removing the low energy muons with a degrader.

1.3 The transverse field muon spin rotation technique

The basis of this technique is the time-differential measurement of the asymmetric decay of a spin-polarized ensemble of positive muons precessing in a transverse magnetic field. A beam of spin-polarized muons is directed through a scintillator detector into the

sample. The passage of a muon through the scintillation detector generates an electronic pulse that starts a high precision clock. The muons thermalize in the sample, which is mounted in an external field that is transverse (or perpendicular) to the initial muon spin polarization. The muons stopped in the sample will precess in a plane perpendicular to the direction of the applied magnetic field, in which several positron detectors are arranged. The clock is stopped upon the detection of a decay positron. The TF- μ SR histogram has the following form:

$$N(t) = N_0 e^{-t/\tau_\mu} [1 + A(t)] + B_g \quad (1.5)$$

where N_0 is the normalization, B_g is the time-independent background, τ_μ is the muon lifetime (2.2 μ s) and $A(t)$ is the asymmetry spectrum. $A(t)$ represents the time evolution of the muon polarization, with the background subtracted and the exponential decay of the muon taken into account, and contains the information of interest to chemists.

Diamagnetic muon spins will precess at a muon Larmor angular frequency $\omega_\mu = \gamma_\mu B$, where γ_μ is the muon gyromagnetic ratio. For a sample containing only diamagnetic muons, the asymmetry is given by

$$A(t) = A_D e^{-\lambda t} \cos(\omega_\mu t + \phi_D) \quad (1.6)$$

where A_D contains information about the fraction of muon polarization in diamagnetic environments, λ is the decay rate (which is usually negligible for diamagnetic species) and ϕ_D is the initial phase. The probability of detecting positrons rises and falls as the precessing muon spin swings past the fixed positron detectors. A typical TF- μ SR time spectrum for a diamagnetic species is shown in Figure 1.3. The dominant feature of the spectrum is the exponential decay due to the muon lifetime on which is superimposed the oscillating muon asymmetry.

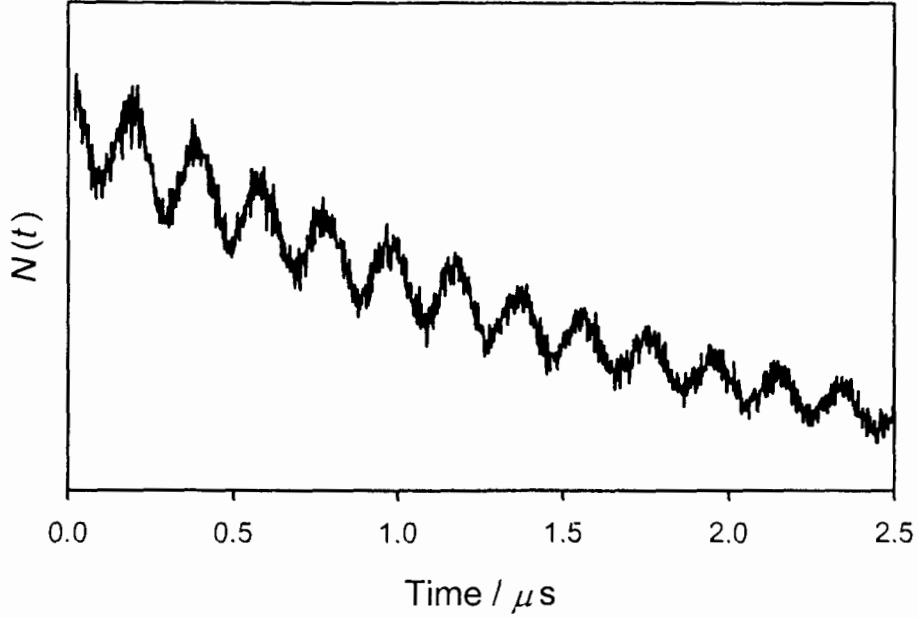


Figure 1.3: TF- μ SR histogram of a diamagnetic muon in water in an applied field of 400 Gauss.

1.4 Muonium

Muonium is a 'two-spin-1/2' system. The muon spin is not only coupled to the external magnetic field but also to the electron spin via the hyperfine interaction. Since the muons are polarized while the captured electrons are not, the initial spin states of Mu are assumed to be 50% $|\alpha_e \alpha_\mu\rangle$ and 50% $|\beta_e \alpha_\mu\rangle$, where the muon polarization direction defines the quantization axis. The spin Hamiltonian of Mu is given by:

$$\hat{H} = \omega_e S_z^e - \omega_\mu I_z^\mu + a_\mu \vec{S}^e \cdot \vec{I}^\mu \quad (1.7)$$

where S represents the electron spin operator, I the muon spin operator, ω_e and ω_μ are the Zeeman angular frequencies and a_μ is the muon hyperfine coupling constant in angular frequency units. The eigenstates of this Hamiltonian are [11]:

$$\begin{aligned}
|1\rangle &= |\alpha^e \alpha^\mu\rangle \\
|2\rangle &= s|\beta^e \alpha^\mu\rangle + c|\alpha^e \beta^\mu\rangle \\
|3\rangle &= |\beta^e \beta^\mu\rangle \\
|4\rangle &= c|\beta^e \alpha^\mu\rangle - s|\alpha^e \beta^\mu\rangle
\end{aligned}
\tag{1.8}$$

where

$$\begin{aligned}
c &= (1/\sqrt{2})\left(1 + \omega_+/\sqrt{\omega_+^2 + a_\mu^2}\right)^{1/2} \\
s &= (1/\sqrt{2})\left(1 - \omega_+/\sqrt{\omega_+^2 + a_\mu^2}\right)^{1/2} \\
\omega_+ &= 1/2(\omega_e + \omega_\mu)
\end{aligned}
\tag{1.9}$$

The variation of the four resulting energy levels as a function of field is displayed in the form of a Breit-Rabi diagram, shown in Figure 1.4. In the absence of a magnetic field, the four states form a triplet and a singlet system. When a magnetic field is applied, the degeneracy of the triplet is lifted.

There are four spectroscopic transitions that are magnetic dipole allowed. These are given by:

$$\begin{aligned}
\omega_{12} &= \omega_1 - \omega_2 = \omega_- - \Delta \\
\omega_{23} &= \omega_2 - \omega_3 = \omega_- + \Delta \\
\omega_{14} &= \omega_1 - \omega_4 = \omega_- + \Delta + a_\mu \\
\omega_{43} &= \omega_4 - \omega_3 = \omega_- - \Delta - a_\mu
\end{aligned}
\tag{1.10}$$

where

$$\begin{aligned}
\omega_- &= 1/2(\omega_e - \omega_\mu) \\
\Delta &= 1/2\left[\sqrt{\omega_+^2 + a_\mu^2} - a_\mu\right]
\end{aligned}
\tag{1.11}$$

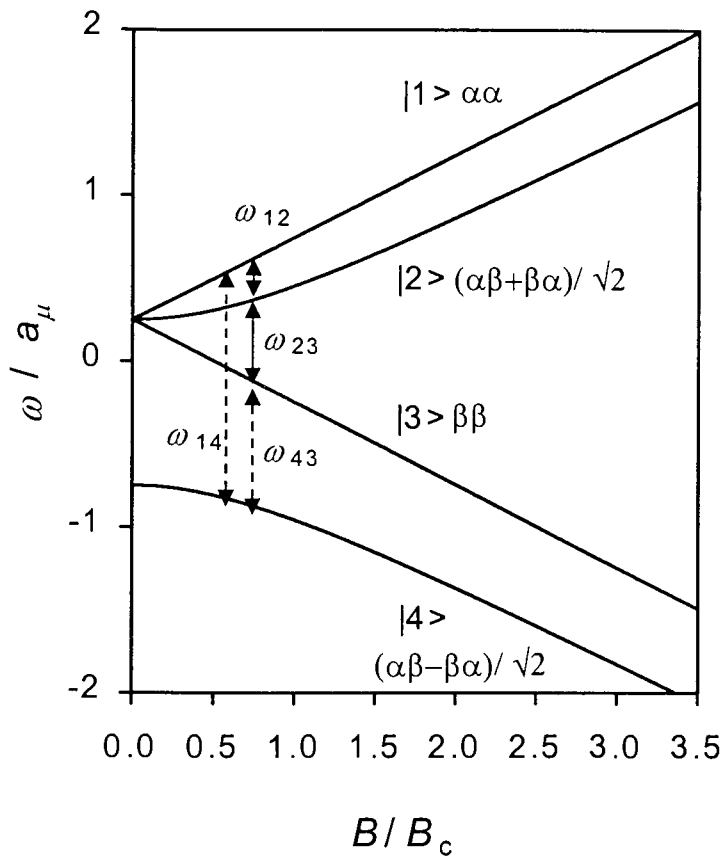


Figure 1.4: Breit-Rabi diagram for a two-spin-1/2 system. $B_c = 1590$ Gauss, the ratio of the hyperfine frequency of Mu to the gyromagnetic ratio of the electron. Of the four allowed transitions at low-fields, only the two denoted by solid lines are resolvable.

In low fields, two of the transitions (ω_{14} and ω_{43}) are at a frequency on the order of a_μ ($= 2.8 \times 10^{10} \text{ rad s}^{-1}$). Since the time resolution of a typical TF- μ SR experiment is approximately 2 ns, these transitions are not observable and this half of the muonium ensemble appears to be totally depolarized. For the other two transitions (ω_{12} and ω_{23}), the spins precess at the muonium Larmor frequency, $\omega_{\text{Mu}} = 103\omega_\mu$, in the sense opposite to free muon precession. The asymmetry is the sum of the muonium signal $A_M(t)$ and the diamagnetic signal $A_D(t)$ and takes the form:

$$A(t) = A_M e^{-\lambda_M t} \cos(\omega_{\text{Mu}} t + \phi_M) + A_D e^{-\lambda_D t} \cos(\omega_D t + \phi_D) \quad (1.12)$$

From the muonium decay rate λ_M , the pseudo-first order decay rates for chemical reactions of muonium can be determined [20,21].

1.5 Muonium-substituted free radicals

A radical is a molecular species that is paramagnetic due to an unpaired electron. The majority of radicals are very reactive. Measurements of the electron-nuclear hyperfine coupling constants are useful in determining the identity of the species, but also provide detailed information on the nature of the singly occupied molecular orbital and hence on molecular structure and dynamics.

In muoniated radicals, the unpaired electron spin couples to the muon and any other magnetic nuclei. The spin Hamiltonian for such a multi-spin system in a gas or non-viscous liquid is given by:

$$\hat{H} = \omega_e S_z^e - \omega_\mu I_z^\mu + a_\mu \vec{S}^e \cdot \vec{I}^\mu - \sum_k \omega_k I_z^k + \sum_k a_k \vec{S}^e \cdot \vec{I}^k \quad (1.13)$$

where ω_e , ω_μ and ω_k are the Zeeman angular frequencies, and a_μ and a_k are the isotropic Fermi contact hyperfine coupling constants (hfc) in angular frequency units for the muon and the nucleus k , respectively. For N nuclei with spin quantum numbers I_k there are $4\prod_k (2I_k+1)$ eigenstates. The selection rule for transitions between these states is that $\Delta M = \pm 1$ with:

$$M = m_\mu + m_e + \sum_k m_k \quad (1.14)$$

where m_i is the magnetic quantum number of particle i . The muon polarization oscillates between many of these eigenstates, and as a result the muon polarization is distributed over many frequencies. For low fields in particular, this makes detection of muoniated radicals difficult or impossible. However in sufficiently high fields, where the Zeeman energy is much larger than the hyperfine interactions ($\omega_e \gg a_\mu$ and a_k for all k), the frequency spectrum is considerably simplified. Under these conditions, the spin states are usually good approximations to eigenstates of the spin Hamiltonian and the selection rule becomes $\Delta m_\mu = \pm 1$, $\Delta m_e = 0$ and $\Delta m_k = 0$. The radical frequencies form two degenerate groups, independent of the number of coupled nuclei. These frequencies ($\omega = 2\pi\nu$) are:

$$\nu_{R1} = \nu_D - \frac{1}{2} A_\mu \quad (1.15)$$

$$\nu_{R2} = \nu_D + \frac{1}{2} A_\mu \quad (1.16)$$

where

$$\nu_D = \frac{1}{2} \left[\sqrt{A_\mu^2 + (\nu_e + \nu_\mu)^2} - \nu_e + \nu_\mu \right] \quad (1.17)$$

$$A_\mu = \frac{a_\mu}{2\pi} \quad (1.18)$$

The radical lines are equally spaced about ν_D , which is the muon Larmor frequency (ν_μ), shifted by a small amount dependent on the relative magnitudes of the electron Larmor frequency and the muon hfc. The muon hfc in units of frequency, A_μ , is calculated from the difference in the two precession frequencies. A typical TF- μ SR spectrum is shown in Figure 1.5.

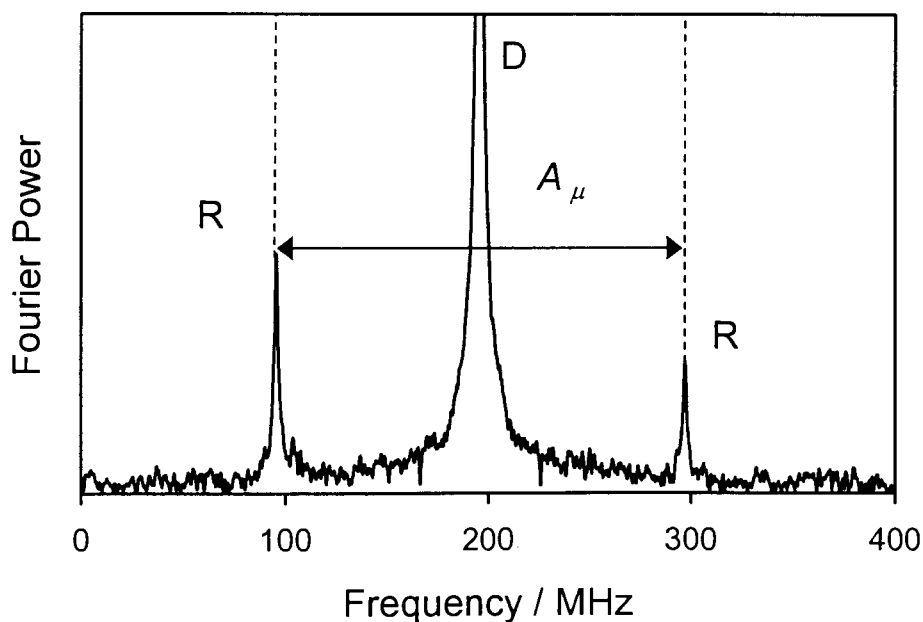


Figure 1.5: TF- μ SR spectrum of the CH_2Mu radical at 184 K.

1.6 Avoided muon level crossing resonance

Avoided muon level crossing resonance occurs at specific applied magnetic fields where a muon transition frequency is matched to that of some other nucleus in the coupled spin system. At the specific field, a nearly degenerate pair of levels, having different spin orientations for the muon and another nucleus, are mixed by the hyperfine interaction. This results in a resonant-like change in the muon polarization as the field is swept. The spin Hamiltonian for a muoniated radical in the gas phase or a non-viscous fluid is given by equation (1.13). In the high field limit, where ω_e is much greater than the hyperfine frequencies, the eigenstates can be expressed in terms of the basis of the product of individual eigenkets,

$$|m\rangle = \sum_i C_{im} |\chi_{ei}\rangle |\chi_{\mu i}\rangle \prod_k |\chi_{ki}\rangle \quad (1.19)$$

χ refers to the magnetic quantum numbers of the electron, muon and nucleus k , which are given the symbols m_e , m_μ and m_k , respectively. For a three-spin-1/2 system with an electron, a muon and one nucleus with spin-1/2, there are eight spin states. Due to the dominance of the electron Zeeman term, the energy levels form two well separated groups according to the sign of m_e . The selection rule of μ LCR for isotropic systems is $\Delta(m_\mu + m_k) = 0$. The 2x2 sub-secular determinant in this basis set in the high field limit after block diagonalization is [22]:

$$D = \begin{vmatrix} E_{11} + \frac{A_\mu^2}{4\omega_e} + \frac{b^2 A_k^2}{4\omega_e} - E & c \frac{A_\mu A_k}{4\omega_e} \\ c \frac{A_\mu A_k}{4\omega_e} & E_{22} + \frac{c^2 A_k^2}{4\omega_e} - E \end{vmatrix} \quad (1.20)$$

where

$$E_{ii} = m_e \omega_e - m_\mu \omega_\mu - m_k \omega_k + m_e m_\mu A_\mu + m_e m_k A_k \quad (1.21)$$

$$b^2 = I^k (I^k + 1) - M(M + 1) \quad (1.22)$$

$$c^2 = I^k(I^k + 1) - M(M - 1) \quad (1.23)$$

$$-I^k + 1 \leq M \leq I^k \quad (1.24)$$

Solving the eigenvalue problem and then integrating the muon polarization over t from 0 to ∞ with weight $\lambda e^{-\lambda t}$, produces the time-integrated μ LCR signal. The general expression for the muon polarization in a multi-spin system in the high field limit is given by [22]

$$P_z(B) = 1 - \frac{2}{N} \sum_i^{2I^k} \frac{\omega_{0i}^2}{\lambda^2 + \omega_{0i}^2 + [2\pi(B - B_{0i})(\gamma_\mu - \gamma_k)]^2} \quad (1.25)$$

where N is the dimension of the Hamiltonian matrix, γ_i 's are the gyromagnetic ratios, $\omega_{0i} = \pi c A_\mu A_k / B_{0i} \gamma_e$ is the transition frequency on resonance, λ is the damping rate and B_{0i} is the resonance field. The resonance field is given by:

$$B_{0i} = \left| \frac{A_\mu - A_k}{2(\gamma_\mu - \gamma_k)} - \frac{A_\mu^2 - 2MA_k^2}{2\gamma_e(A_\mu - A_k)} \right| \quad (1.26)$$

Near this field the off-diagonal terms of the spin Hamiltonian are no longer negligible and they mix the two spin states. The result is actually a non-crossing of the energy levels.

Measurement of the resonance field leads to an accurate determination of the magnitude of the hfc as well as the sign relative to the muon hfc. This is information that cannot easily be obtained by EPR. Another of the benefits of μ LCR is that at high fields the position and magnitude of each resonance is insensitive to the nuclei that are not on resonance. This makes μ LCR an exceptional technique to study complicated spin systems. The μ LCR technique also allows the observation of slowly formed radicals. Unlike TF- μ SR, where the radical must be formed within a nanosecond for sufficient spin polarization to be transferred to the radical, radicals observed by μ LCR can be observed when the lifetime of the muonium precursor is as much as a microsecond. An

example of a μ LCR spectrum is shown in Figure 1.6. The differential line-shape of the resonance in the μ LCR spectrum arises from the use of field modulation to minimize the effect of fluctuations in the incident muon beam intensity.

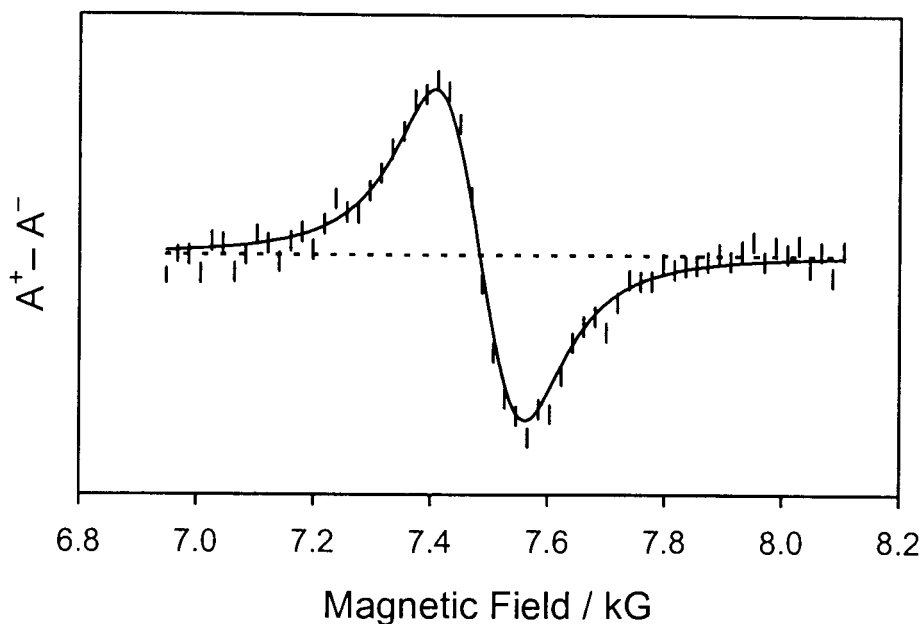


Figure 1.6: μ LCR spectrum of the CH_2Mu radical at 184 K.

1.7 Muoniated radicals

Muoniated radicals can be formed by the addition of Mu to an unsaturated bond. This results in the muon being attached adjacent (or β) to the radical centre (α). This type of radical is called a β -muoniated radical. These are the vast majority of radicals that have been observed by μ SR. Studies of these radicals have provided valuable information about the torsional motion in alkyl and cyclohexadienyl radicals. However, this field of research is not as active as it has been since the effects of the light mass of the muon on the vibrational motion of β -muoniated radicals are well understood. Studying radicals labeled with muonium at different positions would be extremely valuable as it would be possible to probe other types of vibrational motion, but unfortunately this has proved to be difficult because there is no way to alter the preferred direction of Mu addition to a given compound. Only four muoniated radicals have been observed with Mu attached directly to the radical centre (α -muoniated radicals). The aim of this research project was

to develop ways to produce α -muoniated radicals and to study the effect of Mu substitution on vibrational motion at the radical centre.

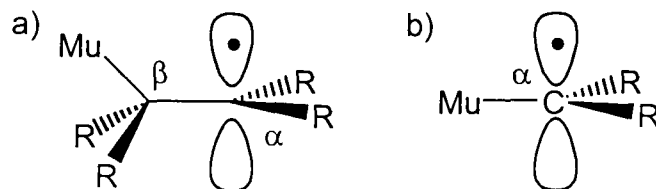


Figure 1.7: a) β -muoniated radical b) α -muoniated radical.

1.7.1 The muoniated trimethylsilylmethyl radical

The first reported α -muoniated radical was the trimethylsilylmethyl radical, which was produced by the reaction of Mu with trimethylsilyldiazomethane [23]. Mu added to the carbon atom of the diazo functional group to produce a nitrogen-centred- β -muoniated radical that rapidly dissociated by giving off N_2 to yield the α -muoniated radical. The involvement of an intermediate gave rise to this path being called indirect formation. The α -muon and α -proton hfc's were measured as a function of temperature and were used to conclusively identify the radical and to show that the configuration at the radical centre is non-planar [24]. The reduced muon hfc was found to be 2.2% larger than the proton hfc and was attributed to the differences in the zero-point energy of the anharmonic C-Mu and C-H stretches.

1.7.2 N-muono-pyridinyl radical

The N-muono-pyridinyl radical was formed by addition of Mu to the nitrogen atom of pyridine [25]. This has been referred to as direct formation due to the lack of a β -muoniated radical intermediate. Only the muon hfc was measured and there was a significant isotope effect compared with the proton isotopomer. The small magnitude of the muon hfc means that the amplitude of the proton resonances in the μ LCR spectrum will be so weak as to be practically undetectable.

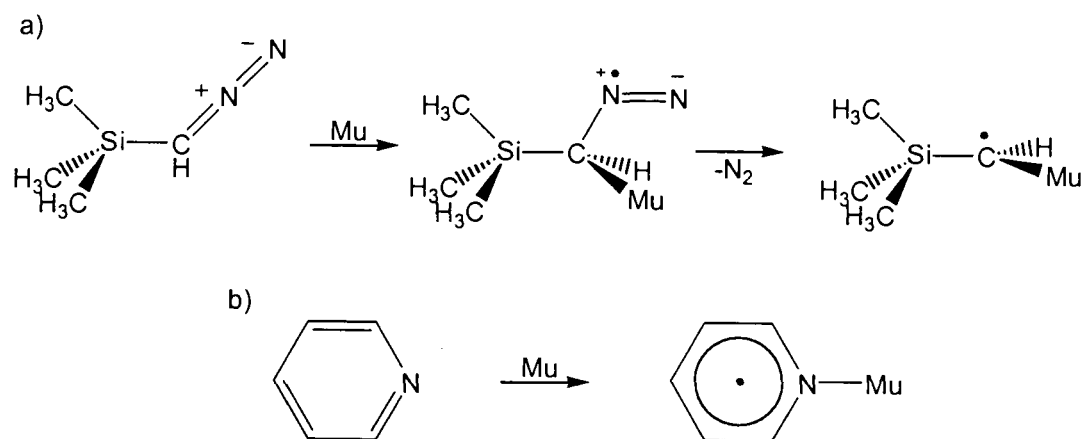


Figure 1.8: a) Formation of the muoniated-trimethylsilylmethyl radical. b) Formation of the *N*-muono-pyridinyl radical.

1.7.3 Inorganic α -muoniated radicals

There is evidence that suggests that muoniated radicals are formed upon μ^+ irradiation of sulphur and selenium. The data is not conclusive but seems to indicate that the observed species are the diatomic SMu and SeMu radicals.

Below 100 K there is a weak feature in the μ LCR spectrum of sulphur which has been interpreted as being a $\Delta M=1$ resonance [26]. The position of the resonance corresponds to a muon hfc with a magnitude of 233(5) MHz. The radical was not observed by TF- μ SR at any temperature between 20 and 300 K. Webster has provided two alternative explanations for the feature in the μ LCR spectrum, based on quantum calculations [27,28]. Webster and coworkers have determined the muon hfc for the muoniated sulphuranyl radical (SMu) to be -234 MHz. It was found that certain positions of Mu with respect to the S_8 rings could lead to ring opening and the formation of SMu radicals. The alternative explanation was that Mu could bridge between neighbouring sulphur atoms of the S_8 rings. The calculated muon hfc for this geometry was +229 MHz. It is necessary to measure the ^{33}S hfc's in order to determine conclusively which radical was formed. This has proved to be difficult due to the low isotopic abundance of ^{33}S .

The μ LCR spectrum of amorphous selenium is reported to exhibit a $\Delta M=1$ resonance near 0.85 T near 20 K [29]. This is much more intense than the corresponding resonance

in sulphur. The field position of the resonance corresponds to a muon hfc of 234 MHz. Nothing was seen in the TF- μ SR spectrum for samples of amorphous selenium, but short-lived radical signals were observed for crystalline samples of selenium [30]. The relaxation rate for the radical signals was approximately $20 \mu\text{s}^{-1}$, which made observation very difficult. The magnitude of the muon hfc was found to decrease with increasing temperature, going from 240 MHz at 5 K to 215 MHz at 200 K. The identity of the radical has not been confirmed and assignment will require measurement of the ^{77}Se hfc. There have been no quantum calculations to model the possible structures.

1.8 Routes to form α -muoniated radicals

The examples of the organic α -muoniated radicals in the literature demonstrate that there are at least two different routes to generate α -muoniated radicals. The essential features of the indirect and direct formation routes are discussed below and are used to predict suitable functional groups that could generate α -muoniated radicals.

1.8.1 Indirect formation

A generalised scheme for the indirect formation process is shown in Figure 1.9.

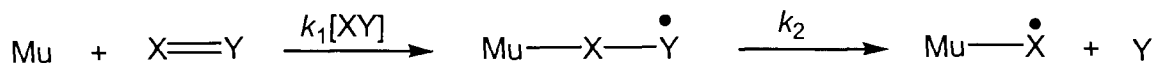


Figure 1.9: Generalised scheme for indirect formation of α -muoniated radicals.

In order for the α -muoniated radical to be observed by TF- μ SR there must be efficient transfer of spin polarization from Mu to the β -muoniated radical and then to the α -muoniated radical. The polarization (P_1) transferred from Mu to the β -muoniated radical is given by [31]

$$P_1 = \frac{\lambda_1^2}{\lambda_1^2 + \delta\omega_1^2} \quad (1.27)$$

where λ_1 is the first order muonium decay rate, which equals $k_1[XY]$ and $\delta\omega_1$ is the difference between the muon hfcs of Mu and the β -muoniated radical. The muon hfc of Mu is 4463 MHz while typical values for a β -muoniated radical range between approximately -200 and 500 MHz. Thus the lifetime of Mu must be less than 10^{-10} s for significant polarization to be transferred. The expression for the transfer of polarization (P_2) from the β -muoniated radical to the α -muoniated radical is similar to equation (1.27) and is given by

$$P_2 = \frac{k_2^2}{k_2^2 + \delta\omega_2^2} \quad (1.28)$$

where k_2 is the first-order rate constant for the decomposition of the β -muoniated radical and $\delta\omega_2$ is the difference in the muon hfcs of the β -muoniated and α -muoniated radicals. The $\delta\omega_2$ term is much smaller than the $\delta\omega_1$ term so the lifetime of the β -muoniated radical can be on the order of several nanoseconds for efficient transfer of spin polarization to occur. The total spin polarization transferred to the α -muoniated radical is given by the product of P_1 and P_2 . These conditions for efficient polarization transfer put severe restrictions on which target molecules can be used to generate α -muoniated radicals.

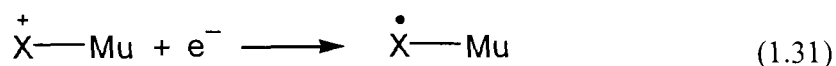
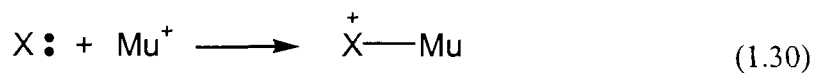
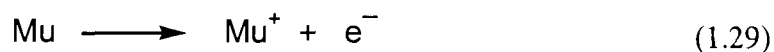
The experiments of Addison-Jones *et al.* [23,24] give an indication about which functional groups are suitable to generate α -muoniated radicals. In order for the β -muoniated radical to have a very short lifetime, the barrier to decomposition must be below the initial combined energy of Mu and the target molecule ($X=Y$). This occurs if the leaving group (Y) is a stable species such as N_2 . Apart from the diazo functional group, the only other suitable functional group that contains N_2 is an azide. The reaction of Mu with a molecule containing an azide functional group would likely generate a nitrogen-centred- α -muoniated radical. Another excellent leaving group is CO. The possible functional groups are ketene and isocyanate. Reaction of Mu with ketene could give a carbon-centred- α -muoniated radical and addition of Mu to an isocyanate could produce a nitrogen-centred- α -muoniated radical. There have been several experimental

and theoretical studies on the reactions of hydrogen atoms with azides, isocyanates and ketenes. The details of the experiments on the reactions of H with ketene and isocyanic acid (HNCO) will be discussed in detail in chapters 3 and 6, respectively.

Le Bras and Combourieu studied the reaction of hydrogen atoms with hydrazoic acid (HN₃) using mass spectrometry [32]. The hydrogen atom was assumed to add to the nitrogen bearing the hydrogen and produce the amidogen radical (NH₂) and N₂. This reaction was studied theoretically by Fueno and Takane [33]. They also found that addition of atomic hydrogen to the nitrogen already bearing the hydrogen was preferred. The combined energy of the hydrogen atom and hydrazoic acid was 222 kJ mol⁻¹ above the barrier to dissociation of the H₂N₃ radical. Accordingly, azides should be suitable molecules to produce nitrogen-centred- α -muoniated radicals. Unfortunately, azides are unstable and this makes them difficult to use as targets at TRIUMF. The reaction of Mu with azidotrimethylsilane was studied but no radicals were observed. It is possible that this compound reacted with the stainless steel sample cell and further studies are proposed using glass cells.

1.8.2 Direct formation

In order to understand the direct formation pathway, it is instructive to consider the sequential addition of μ^+ and e^- . There is evidence that the addition is concerted, but energetically there is no difference between sequential and concerted addition [34].



The overall reaction will proceed if the change in the Gibbs free energy is negative. Therefore, the overall reaction must be substantially exothermic, in order to counteract the negative entropy. This can occur if the proton (or muon) affinity of the target molecule (X) is high and if the muoniated cation has low-lying vacant orbitals for the

unpaired electron to occupy. This last requirement explains why there is long-lived Mu in water [35] and ammonia [36] and why radicals are formed by Mu addition to pyridine. The LUMO for H_3O^+ and NH_4^+ are extremely high-energy σ^* orbitals while the pyridinium cation has low-lying, vacant π orbitals.

N-heterocyclic carbenes have both a high proton affinity [37] and low-lying, vacant π orbitals that arise from the interaction of the p orbital at the carbene centre with the p orbitals on the neighbouring nitrogen atoms [38]. The carbenes are stable in oxygen and moisture-free environments and are suitable for studies at TRIUMF. The results of the studies on stable singlet carbenes are given in chapter 5.

1.9 Collaborative versus individual work

All of the μSR experiments were done in collaboration with the other members of the SFU muonium chemistry group (SFUMU). The TRIUMF facility operates 24 hours a day and beam time is allocated in blocks of typically one week, so members of the SFUMU group work in shifts to collect the μSR spectra. The stable carbenes used in Chapter 6 were provided by Prof. J. A. C. Clyburne and Prof. S. Nolan. Apart from the assistance listed above, I performed all of the work in this thesis. I conceived the experiments and used literature surveys and theoretical studies to examine the feasibility. I prepared the samples for TRIUMF and participated in the collection of the μSR spectra. I analyzed the spectra, used theoretical calculations to interpret the results and wrote the first draft of the papers, the content of which are presented in expanded form in chapters 3-6.

CHAPTER 2.

EXPERIMENTAL AND THEORETICAL METHODS

2.1 μ SR experiments

2.1.1 TRIUMF

The μ SR experiments described in this thesis were performed at TRIUMF, Canada's national meson facility. TRIUMF is an acronym for the TRI University Meson Facility. Five universities now manage the facility: Simon Fraser University, the University of Alberta, the University of British Columbia, the University of Victoria and Carleton University, and it is funded through the National Research Council of Canada. At the centre of the TRIUMF facility is an azimuthally varying field cyclotron that can accelerate negatively charged hydrogen ions, H^- , to a maximum energy of 520 MeV. Beams of energetic protons are extracted by removing the electrons of the hydride ions by means of a stripping foil. Four beams of protons can be extracted simultaneously, individually variable in energy. Beam line 1A delivers protons to the meson hall and Beam line 4 provides beam to experiments in the proton experimental hall. The energies of the protons in these beam lines can vary between 183 and 520 MeV. The intensity of these beams can reach a maximum of 150 μ A at 500 MeV. This high current qualifies TRIUMF as a 'meson factory'. Beam line 2C delivers a low-energy proton beam (70-100 MeV) for the production of radioisotopes. Beam line 2A provides protons to the ISAC (Isotope Separator and Accelerator) facility.

A great advantage of TRIUMF over other meson facilities is that the beam is delivered continuously on a macroscopic timescale (100% macroscopic duty cycle). The microscopic duty cycle is a 3 nanosecond burst of protons every 43 ns. Both the microscopic and macroscopic duty cycles can be altered.

Beam line 1A usually delivers up to 150 μ A of 500 MeV protons to two meson production targets. The first target, 1AT1, feeds three secondary beam lines; M11 (a medium-energy, 80 to 300 MeV, pion channel), M13 (a low energy pion and surface muon channel) and M15 (a dedicated surface muon channel). The second production

target, 1AT2, supplies beam to two secondary beam lines; M9 (a low energy pion and cloud muon channel) and M20 (a dedicated surface muon channel). The experiments detailed in this thesis were carried out on the M15 and M20 beam lines.

2.1.2 Surface muons

Surface or ‘Arizona’ muons are produced from pions decaying at rest within a few μm of the production target. The pion decay at rest is a two-body decay, which implies that the muon and the muon neutrino are collinearly emitted. Surface muons are nearly monoenergetic (4.1 MeV) and have a nominal momentum of 28.6 MeV/c. The spin of the pion is zero, so conservation of angular momentum requires that the total angular momentum of μ^+ and ν_μ must also be zero. The spin of ν_μ is antiparallel to its momentum (negative helicity) so the spin of the emerging muon must also be antiparallel to its momentum. If muons of a certain momentum direction are collected into a beam, this beam will have a spin polarisation of almost 100%.

Contamination of the muon beam with pions and protons is negligible but there are about 100 times more positrons than muons. Difficulties also arise in injecting surface muons into regions with strong transverse magnetic field, as the radius of curvature is less than 1 m/kG. The solution to both these problems is to use a dc separator to remove the positron contamination and to rotate the muon spin so that it is transverse to its momentum [39]. The spin rotator consists of a vertically oriented electric field (E_0) and a horizontally oriented magnetic field (B_0). B_0 affects both the spin and momentum of the muons while E_0 affects only the momentum. It is possible to select values of E_0 and B_0 that allow only particles with a certain mass to pass through the rotator without being deflected, and to rotate the spin by 90 degrees. This rotation permits injection of the surface muon beam into a strong magnetic field that is oriented longitudinally to the muon’s momentum but transverse to its spin. This allows for a single experimental apparatus to be used for both transverse field muon spin rotation and avoided level crossing resonance, using spin rotated and unrotated muons, respectively.

2.1.3 Scintillator detectors

Many substances scintillate (i.e. emit flashes of visible light) as a result of the action of ionizing radiation. Particle detection was provided by a set of plastic organic scintillators. The detector consists of a scintillator, a light guide and a photomultiplier tube. The light emitted from the scintillator is collected by the light guide and conducted towards the photomultiplier tube for amplification and conversion to an electrical signal. The high magnetic fields used in the experiments adversely affect the photomultiplier tubes so the light guides must be 1-2 m long in order that the photomultipliers can be located in a low magnetic field region. The length of the light guide limits the time resolution of μ SR experiments to 1 ns.

2.1.4 μ SR apparatus

All of the experiments detailed in this thesis were performed using the HELIOS superconducting spectrometer. This magnet can produce fields as high as 70 kG. Typical fields used in our experiments were in the range of 1 to 25 kG.

2.1.5 Temperature control

Two systems for controlling temperature were used in the experiments described in this thesis. For temperatures between approximately 263 and 373 K, the temperature was controlled by circulating fluid from a constant temperature bath through copper coils attached to a copper plate with the sample cell in contact. The temperature of the sample was measured with a type-K thermocouple that was embedded between the sample cell and the copper plate. It was found that this arrangement closely represented the temperature of the sample and the uncertainties in the temperature were estimated to be less than 1 K.

Sample temperatures between 20 and 270 K were obtained by using a helium-refrigerator cold-finger cryostat. The temperature of the sample was measured with either a silicon diode thermocouple or a carbon-glass thermocouple. The thermocouples were embedded in the cold head of the cryostat, next to the sample cells. The uncertainty of the sample temperature is estimated to be about 0.5 K.

2.1.6 TF- μ SR

A schematic diagram of a TF- μ SR experiment is shown in Figure 2.1. The sample (S) is placed in a magnetic field that is parallel to the muon's momentum. The muon's spin is rotated perpendicular to the momentum. The incident muons are detected by a thin scintillator counter (M) and the decay positrons are detected in one of four scintillator counters that are arranged in two sets of opposing pairs. Only the up (U) and down (D) pair are shown in Figure 2.2 for the sake of clarity. The other pair, which are designated left (L) and right (R) are perpendicular to the up-down pair. The advantage to using two sets of counters with this geometry is that it is possible to perform complex Fourier transforms and distinguish between positive and negative frequencies.

The signals from the muon and positron detectors are transformed into standard nuclear instrument and measurement (NIM) pulses of approximately 20 ns width. The pulses are routed through time-delay circuits for time synchronisation before being fed into various electronic units. An incident muon passing through the M counter triggers a ' μ -stop' signal to the 'start' input of a time digitizing converter (TDC). A good muon decay event requires that within a certain timer interval after the muon is stopped in the sample, a positron is detected. This period is called the data gate and usually extends over several muon lifetimes. The data gate is produced by a gate generator triggered by the muon stop signal. A good decay positron is identified by a coincidence of the positron signal with the data gate. This sends a signal to the 'stop' input of the TDC. The measured time then forms the address of a histogram memory and the content of the corresponding channel is increased by one. In this way the TF- μ SR histograms are formed, which typically have 10^6 - 10^7 events per histogram.

The electronics are designed to check for pile-up rejection. At high incident muon rates (current $> 1/\tau_\mu$), a second muon can enter the sample within the pile-up gate generated by a previous muon. With two muons in the sample, the subsequently emerging positron cannot be related unambiguously to the correct muon parent. This is referred to as 'pile-up' and the ill-defined event must be excluded. It is also necessary to exclude those

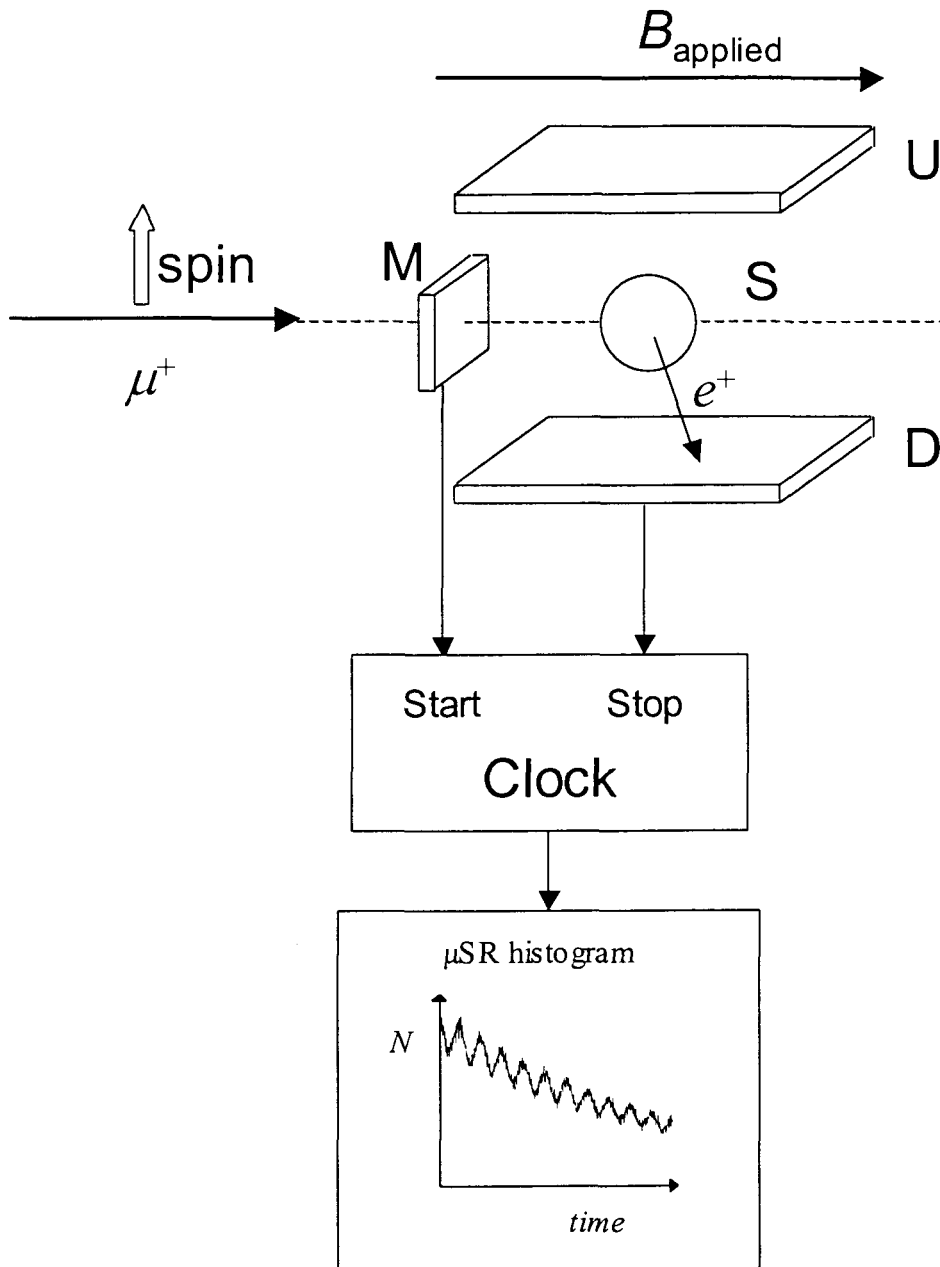


Figure 2.1: Schematic for TF- μ SR experiment.

events with the sequence muon(1)/positron/muon(2) all within the data gate set by muon(1). These events would otherwise result in distortion of the spectrum because the observation of long-lived muons has a larger probability of suppression by second muon events than short-lived muons. By excluding all pile-up events this bias is removed. It is impossible for the positron detectors to operate with 100% efficiency. If no positron is

detected within the period of the data gate, the TDC is cleared and made ready for another good muon event. In practice, the beam current is reduced with a set of lead collimators in order to reduce pile-up events.

2.1.7 μ LCR

The experimental setup for a μ LCR experiment is slightly different from that used in a TF- μ SR experiment although the similarities are such that the same apparatus can be used with only slight adjustments needed to switch between the two types of experiments. The main differences are the orientation of the muon spin, the layout of the counters and the use of field-modulation. A schematic diagram of a μ LCR experiment is shown in Figure 2.2.

The positron counters are positioned forwards (F) and backwards (B) of the sample, with respect to the muon beam. The muon spin is left unaltered, so it is parallel with the muon's momentum and the magnetic field. The process of finding the position of level crossing resonance fields involves measuring the time-integrated muon decay asymmetries as a function of the applied magnetic field. The raw integrated asymmetry is sensitive to systematic effects, such as deviations in the rate of the incoming muons. This is minimised by the use of a small square-wave field modulation. The signal is defined as $A^+ - A^-$, where A^+ and A^- are the muon asymmetries measured under opposite modulation phases. The muon decay asymmetries are defined as

$$A^\pm = \frac{N_F^\pm - N_B^\pm}{N_F^\pm + N_B^\pm} \quad (2.1)$$

where N_F^\pm and N_B^\pm are the total number of positrons detected in the forward and backward directions with respect to the incoming beam, respectively. When the resonance is wider than the field modulation width, the lineshape is approximately field-differential [40].

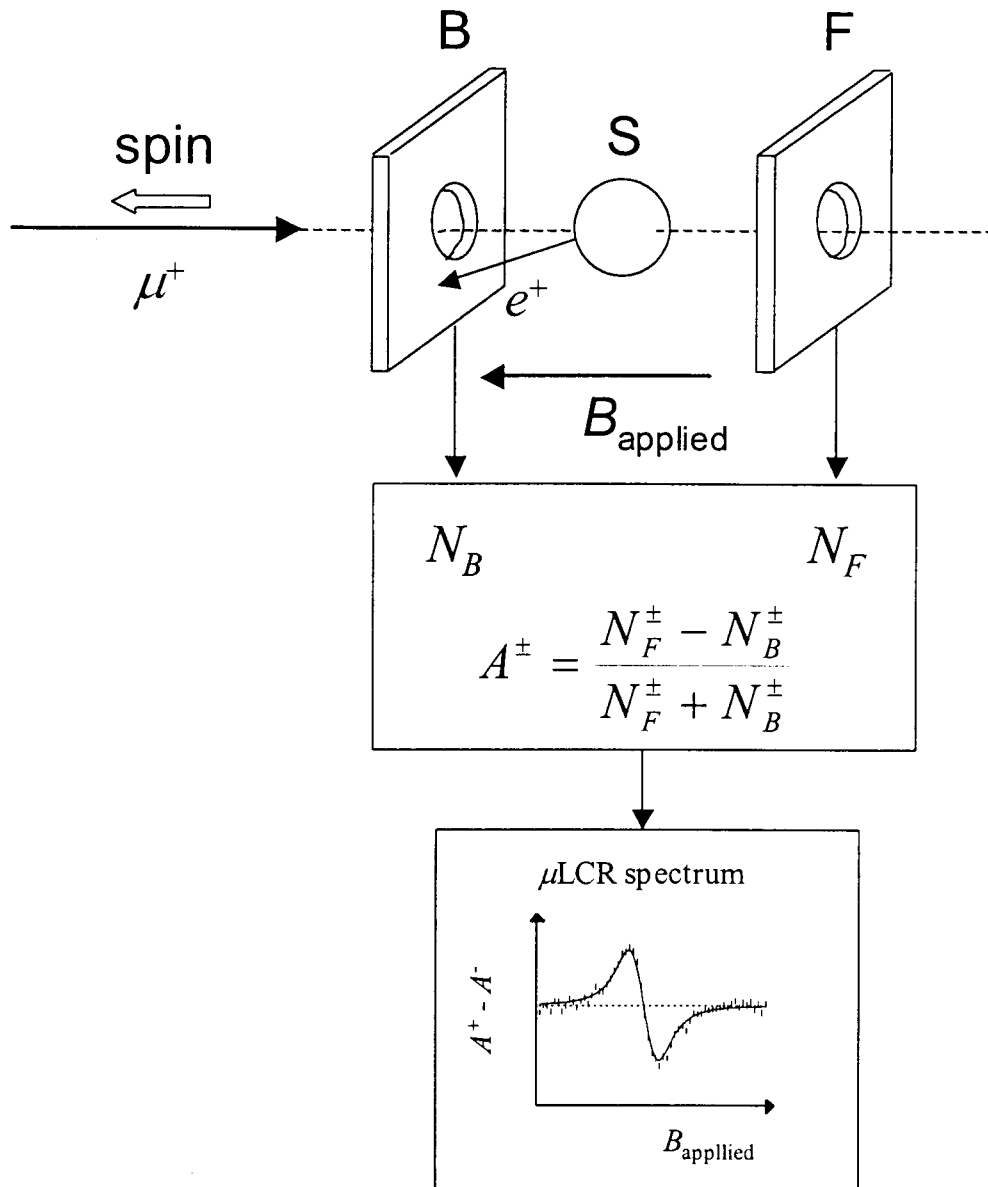


Figure 2.2: Schematic diagram of a μLCR experiment.

The experimental procedure involves accumulating a preset count (on the order of 10^6 events) detected by the sum of forward and backward detectors for each phase of the modulation field. Once the preset is reached, the scalars are read and stored in the computer. The number of modulation coil flips is typically 20 per field point. Once the desired count is reached, the main magnetic field is incremented. The usual size of the

increments is between 20 and 50 G. The data taking is inhibited if the beam current fluctuates by more than 5%.

2.1.8 Data analysis

The transverse field muon spin rotation spectra were analyzed using a computer program called JOMU that was written by a former SFUMU group member, Dr. J. Schüth. In this program, the four histograms are analyzed separately and a non-linear chi-squared minimization procedure is used to fit the histograms in the time domain. The JOMU program can fit up to ten peaks, each described by an amplitude, frequency, relaxation and a phase angle. The WIMDA program written by Dr. F. L. Pratt was used to generate some of the spectra displayed in later chapters but was not used to fit histograms as it could not handle more than three peaks [41,42].

Precise values of magnetic field are essential for the μ LCR experiments. The field is calibrated by measuring the diamagnetic frequencies from a TF- μ SR spectrum for different currents in the superconducting HELIOS magnet. The corresponding magnetic field (B) is obtained by dividing the diamagnetic frequency by the gyromagnetic ratio of the muon (13.55 kHz G⁻¹). The modulation field was also determined by this method.

The μ LCR resonances are fit to a theoretical expression that is the difference of two Lorentzian functions corresponding to the opposite directions of field modulation. This was done using the LCRPLOT program, written by Dr. J. H. Brewer and Dr. J.-C. Brodovitch, which makes use of the multi-parameter χ^2 minimization package, MINUIT, written by James and Roos [43].

2.2 Theoretical calculations

2.2.1 Introduction

Theoretical calculations were performed to assign the experimental μ SR data. The field of computational chemistry is a sub-discipline that is greatly increasing in importance and can provide insights into chemical systems that are not available from experiments. The goal of computational chemistry is to calculate chemical structures and properties from

first-principles. These properties are obtained from the wavefunction, ψ , which is in turn obtained by solving the time-independent, non-relativistic Schrödinger equation.

$$\hat{H}\psi = E\psi \quad (2.2)$$

where \hat{H} is the Hamiltonian operator and E is the energy. In the Born-Oppenheimer approximation, the Hamiltonian for a system with n electrons is given by

$$\hat{H} = \left\{ \sum_i^n \left[\frac{-\hbar^2}{2m} \nabla_i^2 + V_{\text{nuc}}(\vec{r}_i) \right] + \frac{1}{2} \sum_{i \neq j=1}^n \frac{e^2}{|\vec{r}_i - \vec{r}_j|} \right\} \quad (2.3)$$

where V_{nuc} is the electrostatic potential generated by the nuclei. The solution of equation (2.2) for the Hamiltonian given above is an intractable problem and approximations must be made to obtain solutions. There are two main approaches to solving the Schrödinger equation; by semi-empirical calculations and ab initio calculations [44,45]. They differ in the extent of the approximations that are made. Semi-empirical calculations use a simplified Hamiltonian and adjustable parameters with values obtained from experimental data. The advantage of semi-empirical calculations is that they are computationally inexpensive so it is possible to study large molecules. The drawback to this method is that there is a bias because of the reliance on previous experimental results. It is not necessarily true that parameters derived for one system will be applicable to another. Semi-empirical calculations were used to generate the input structures for the ab initio calculations. The approximations that are made for ab initio calculations are based on general physical principles and not on the results for a specific system. Hence, ab initio calculations can be applied with confidence to widely different systems. In ab initio calculations, a model is chosen for the wavefunction (basis set) and the Schrödinger equation is solved using only the coordinates of the nuclei as inputs.

The calculation of hyperfine coupling constants is a particularly difficult challenge for computational chemistry [46]. A survey of different ab initio methods has shown that electron correlation effects cannot be neglected [47]. The restricted open-shell Hartree-Fock method cannot take spin polarization into account while the unrestricted Hartree-

Fock method is strongly affected by spin contamination which lead to results that differ from experimental values by 100%. The quadratic configuration interaction and coupled cluster models have been found to give good results but these are limited to radicals with less than ten non-hydrogen atoms due to the computational expense. Methods based on the unrestricted Kohn-Sham approach to density functional theory (DFT) have been remarkably successful, even for large biological radicals. DFT calculations are less computationally expensive than other ab initio methods, which makes it possible to use large basis sets and include the effects due to the surrounding medium. Furthermore, DFT calculations inherently include electron correlation. There have been numerous reviews of density functional theory [48,49] and its application to radical systems [50,51].

2.2.2 Basis sets

The molecular orbitals can be written as linear combinations of atomic orbitals.

$$\psi = \sum_r c_r \phi_r \quad (2.4)$$

The atomic orbitals (ϕ_r) constitute the basis set for the calculation. In principle one needs an infinite basis set to represent the molecular orbitals exactly. This is not feasible so there is always basis-set contraction error. Accurate calculations require large basis sets in order to minimize this error but this results in an increase in the computation time. A balance must be found between these two competing requirements.

2.2.2.1 Gaussian-type orbitals

The atomic orbitals are represented mathematically by basis functions. The most commonly used type of basis function is a Gaussian-type orbital (GTO) that was first introduced by Boys [52]. The advantage to using GTOs is that they simplify the calculation of two-electron integrals over multiple centres, which results in a large computational savings. One drawback to the GTOs is that they do not accurately represent the behaviour of orbitals near nuclei. This can be overcome by grouping several 'primitive' Gaussian functions (g) together to give a contracted Gaussian function (χ).

$$\chi_j = \sum_i d_{ij} g_i \quad (2.5)$$

where d_{ij} are the contraction coefficients. The parameters that characterize the primitive Gaussian functions are fixed throughout a calculation. The molecular orbitals are given by a linear combination of contracted Gaussian functions.

$$\psi_i = \sum_j c_{ji} \chi_j \quad (2.6)$$

The use of contracted rather than primitive Gaussian functions reduces the number of unknown coefficients to be determined, which can lead to large savings in computation time.

The simplest basis set is the minimal basis set, in which one basis function is used to represent each atomic orbital. Calculations have shown that the minimal basis set leads to large basis-set contraction error. A significant improvement is obtained by using the double-zeta (DZ) basis set, where each atomic orbital is represented by two basis functions. A drawback to the DZ basis set is that it is very computationally demanding. A compromise between the minimal and DZ basis sets is the split valence basis set. An example of this is the 6-31G basis set. The numbers refer to the number of Gaussian functions used to describe the inner shell and valence electrons. In the 6-31G basis set, the inner shell atomic orbitals are represented by a contracted Gaussian function composed of six primitive Gaussian functions. The valence atomic orbitals are represented by two contracted Gaussian functions. The first is composed of three primitive Gaussian functions and the second is just one primitive Gaussian function.

2.2.2.2 Polarization functions

The shapes of the orbitals will be distorted from that of the free atom by interactions with neighbouring nuclei. This can be accounted for by adding extra basis functions that have larger angular momentum quantum numbers. The additional basis functions are called polarization functions. The polarization functions are listed in brackets following the name of the basis set. The first term refers to the polarization functions added to the first and second row elements and the second term refers to the polarization functions added

to hydrogens. For example, the 6-31G(2df,p) basis set has two d-type GTOs and one f-type GTO added to each first and second row element and one p-type orbital added to each hydrogen.

2.2.2.3 Diffuse functions

Diffuse functions are important to include in cases where the electron density is spread out over the molecule. Diffuse functions are GTOs with small exponents. Diffuse functions are written as + and ++. The + refers to adding diffuse s-type and p-type functions to the first and second row elements and ++ refers to adding s-type diffuse functions to hydrogen, in addition to the diffuse functions described by +.

2.2.2.4 Selection of basis set

The choice of a basis set for geometry optimization depends on the size of the molecule. For small radicals like the methyl radical, which is described in chapter 3, it is possible to use a very large basis set that includes polarization and diffuse functions. The calculations on the Mu adducts of stable carbenes, which are described in chapter 5, required much smaller basis sets. An appropriate basis set is one which results in the geometry optimization taking at most forty-eight hours. Most of the geometry optimizations were performed using the 6-31G and 6-311++G basis sets.

All of the calculations of the hyperfine interactions were performed using the EPR-II and EPR-III basis sets for carbon, hydrogen and nitrogen. These basis sets were specifically optimized for the calculation of isotropic hyperfine coupling constants [50].

2.2.3 Density functional theory

The basis of density functional theory is the Hohenberg and Kohn theorem, which states that any ground-state property, such as energy, and other properties are uniquely determined by the electron density [53]. The energy is said to be a *functional* of the electron density, hence the name ‘density functional theory’.

$$E = E[\rho] \tag{2.7}$$

Hohenberg and Kohn were not able to determine the form of the functional, just that it exists. Kohn and Sham determined that the energy of the functional could be written as

$$E[\rho] = T[\rho] + \int \rho(\vec{r}) \left[V_{\text{nuc}}(\vec{r}) + \frac{1}{2} V_{\text{C}}(\vec{r}) \right] d\vec{r} + E_{\text{XC}}[\rho] \quad (2.8)$$

The first term describes the kinetic energy of the system, which is a functional of the electron density. The integral describes the Coulomb interactions between the electrons and the nuclei (V_{nuc}) and the electron density as a functional of $\rho(\vec{r})$. The last term is the exchange-correlation energy functional. The form of E_{XC} is not known so there are several approximations for this term. Kohn and Sham found that the problem of calculating the total electronic energy as a functional of the electron density could be changed into solving a set of single-particle Schrödinger-like equations, which are known as Kohn-Sham equations [54].

$$\left\{ \frac{-\hbar^2}{2m} \nabla^2 + V_{\text{nuc}}(\vec{r}) + V_{\text{C}}(\vec{r}) + V_{\text{XC}}(\vec{r}) \right\} \psi_i(\vec{r}) = \varepsilon_i \psi_i(\vec{r}) \quad (2.9)$$

where ψ_i are the Kohn-Sham orbitals, ε_i are the Kohn-Sham orbital energies and V_{XC} is the exchange correlation potential, which is given by

$$V_{\text{XC}}(\vec{r}) = \frac{\delta E[\rho]}{\delta \rho} \quad (2.10)$$

The electron density of the system is given by

$$\rho(\vec{r}) = \sum_{i=1}^n |\psi_i(\vec{r})|^2 \quad (2.11)$$

The Kohn-Sham orbitals are obtained by solving equations (2.9-11) by the self-consistent field approach.

There are a number of different models for the exchange-correlation functional [55]. It has been shown that different functionals can generate highly different hfcs, although the reasons behind these differences are not well understood [56,57]. The various functionals

have been evaluated by comparing the calculated values with experimental data. There is no clear consensus on which functional is best, but most studies have found that the best agreement between theory and experiment for organic radicals is obtained with the B3LYP functional [50]. For this reason the B3LYP functional was used for all of the DFT calculations described in the subsequent chapters of this thesis.

2.2.4 Software packages for electronic structure calculation

There are numerous computer programs for calculating molecular structures and properties, such as the various versions of Gaussian [58,59], the Amsterdam Density Functional (ADF) package [60], and the General Atomic and Molecular Electronic Structure System (GAMESS) [61]. All of the calculations performed in this thesis were done with the Gaussian 98 package of programs.

For the first three years of this research, Gaussian 98 was run on a local personal computer, but since 2002 the calculations have been performed on the Simon Fraser University Bugaboo cluster. Use of the Bugaboo cluster allowed for a large increase in the number of calculations that could be performed due to both the higher speed of the cluster and the ability to run several calculations simultaneously.

CHAPTER 3.

THE MUONIATED METHYL RADICAL

3.1 Introduction

The methyl radical is the simplest organic π -radical and can be considered as a prototype for a wide class of hydrocarbon radicals. Consequently, it has been the subject of numerous experimental and theoretical studies that have provided valuable information about its structure and intramolecular dynamics.

3.1.1 UV and IR spectroscopy of the methyl radical

Optical spectroscopy of radicals is generally complicated by the coupling of the unpaired electron spin with other angular momenta of the molecule, which leads to splitting of previously degenerate levels and broad spectral lines [62]. There have been many spectroscopic investigations of the methyl radical due to its simple structure and symmetry. The methyl radical was first identified by Herzberg and Shoosmith using UV absorption spectroscopy [63]. IR spectroscopy has been used to study the methyl radical in several low-temperature matrices [64,65,66] and to measure the vibrational-rotational transitions in the gas phase [67,68]. The spectroscopic studies have shown that the methyl radical is an oblate symmetric top molecule with a planar equilibrium geometry.

In most of the spectroscopic experiments the rotational fine and hyperfine structure is obscured due to high temperatures and Doppler broadening. Davis *et al.* used the slit supersonic expansion technique coupled with pulsed electric discharges to generate methyl radicals with low rotational temperatures ($T_{\text{rot}} \sim 25$ K), under which conditions it was possible to resolve the spin rotation and hyperfine splittings [69]. The sign of the proton hyperfine coupling constant was confirmed to be negative based on the appearance of the spectra. The proton hyperfine coupling constant was found to be $-65.5(9)$ MHz in the ground state and $-65(2)$ MHz in the first excited state of the asymmetric C-H stretching mode. The spin rotation splittings were dominated by the spin rotation interaction about the perpendicular moments of inertia ($\epsilon_a = \epsilon_b \gg \epsilon_c$) [68]. The spin-rotation constant was found to be $-354(5)$ MHz in the ground state and $-353(2)$ MHz

in the first excited state of the asymmetric C-H stretching mode. Within the experimental uncertainties there is no dependence of either the proton hfc or the spin rotation interaction on the vibrational level of the asymmetric C-H stretching mode. The magnitude of the proton hfc in the gas phase is larger than any value measured in a condensed phase.

3.1.2 EPR studies of the methyl radical

Electron paramagnetic resonance (EPR) is one of the most versatile and useful techniques for studying free radicals [70,71,72]. EPR is a sensitive probe of the distribution of unpaired electron spin density throughout a radical, which in turn can provide valuable information about the electronic structure. The configuration and conformation of a radical can be probed by measuring the magnitude and sign of the hyperfine coupling constants (hfc), the temperature dependence of the hfc and observing the effect of isotopic substitution.

There have been dozens of EPR experiments on the methyl radical; the hyperfine coupling constants have been measured in a wide range of environments [73]. The magnitude of the proton and ^{13}C hfc of the methyl radical is consistent with a planar radical centre. The proton hfc are negative due to polarization of the C-H bonds by the unpaired electron [74]. The temperature dependence of the hfc has been measured over limited temperature ranges and the magnitude of A_p was observed to decrease with increasing temperature [75,76,77,78]. This is the result of population of the first excited state of the out-of-plane vibrational mode. The decrease in the magnitude of the proton hfc is due to the overlap of the protons with the singly occupied molecular orbital, which gives a contribution of positive spin density that partially counteracts the negative spin density due to spin polarization.

The effect of isotopic substitution on the structure of the methyl radical has been studied by experiments on the CH_2D , CHD_2 and CD_3 isotopomers [79,80]. After correcting for the different magnetic moments of the proton and the deuteron, there are differences in the unpaired spin density due to differences in vibrational averaging. These effects will be discussed in greater detail in a later section.

The EPR experiments on the methyl radical in the solid state revealed that the hyperfine interactions are slightly anisotropic. The principal values of the A_p tensor are 61.4, 63.3 and 63.3 MHz at 77 K. The g-factor is also slightly anisotropic with the principal components of the tensor being 2.0024, 2.0027 and 2.0027 [81].

3.1.3 Theoretical calculations on the methyl radical

The calculation of hyperfine coupling constants is a significant challenge for theoretical chemistry [50]. The methyl radical is often considered to be a benchmark for theoretical calculations because its small size allows for extensive calculations that can include vibrational averaging and solvent effects. There are numerous theoretical studies of the methyl radical but the common factor that was found by all of the ab initio calculations was that the methyl radical is planar and that vibrational averaging by the out-of-plane mode can greatly affect the hfcs [82,83,84,85].

3.1.4 μ SR experiments and experimental approach

Studying isotopomers of the muoniated methyl radical (CH_2Mu and CD_2Mu) could provide information about the effect of isotopic substitution on the vibrational motion at the radical centre, and the very light mass of the muon may possibly lead to the observation of effects that cannot be seen upon deuterium substitution.

The isotopomers of the muoniated methyl radical have not been previously studied because it is difficult to generate these species. Addison-Jones *et al.* attempted to produce the muoniated methyl radical by the reaction of Mu with diazomethane but were unsuccessful [23]. The failure of this approach to generating the CH_2Mu radical was due to the extreme instability of diazomethane at the high concentrations required for TF- μ SR experiments (typically 1 M or greater). They were successful in producing a substituted muoniated methyl radical by the reaction of Mu with a diazo compound, trimethylsilyldiazomethane [23,24].

The approach taken in this research was to generate the CH_2Mu radical by the reaction of Mu with a molecule that is structurally similar to diazomethane but is more easily handled. The compound that was chosen was ketene ($\text{H}_2\text{C}=\text{C}=\text{O}$).

3.1.5 The reaction of hydrogen atoms with ketene

There have been several experimental and theoretical studies on the reaction of hydrogen atoms with ketene. The experiments in the gas phase measured the rate of addition. The results were consistent with the formation of methyl radicals and carbon monoxide. Carr *et al.* [86] and Slemr and Warneck [87] used a discharge flow system coupled with mass spectrometric detection to study this reaction. The rate constant for the reaction at 298 K was found to be $7.8 \times 10^7 \text{ M}^{-1} \text{ s}^{-1}$ by Carr *et al.* and $7.2(6) \times 10^7 \text{ M}^{-1} \text{ s}^{-1}$ by Slemr and Warneck. Slemr and Warneck also measured the rate constant as a function of temperature between 218 K and 313 K and found that the rate constant could be expressed as $k(T) = 3.6(13) \times 10^9 \exp[-1179(100)/T] \text{ M}^{-1} \text{ s}^{-1}$. Michael *et al.* studied the reaction of H with ketene using flash-photolysis-resonance fluorescence (FP-RF) and discharge flow-resonance fluorescence (DF-RF) [88]. The rate constant at 298 K was found to be $3.7(10) \times 10^7 \text{ M}^{-1} \text{ s}^{-1}$ by FP-RF and $4.4(8) \times 10^7 \text{ M}^{-1} \text{ s}^{-1}$ by DF-RF. The temperature dependence of the rate constant was measured by the FP-RF technique and can be expressed as $k(T) = 1.13(67) \times 10^9 \exp[-1726(190)/T] \text{ M}^{-1} \text{ s}^{-1}$ between 298 K and 500 K. Umemoto *et al.* studied the reactions of hydrogen and deuterium atoms with ketene by pulse radiolysis-resonance absorption [89]. The rate constant for the addition of hydrogen atoms between 240 K and 440 K could be expressed as $k(T) = 3.9 \times 10^9 \exp[-4082/T] \text{ M}^{-1} \text{ s}^{-1}$. The addition of hydrogen atoms to ketene was faster than the analogous reaction of deuterium atoms. At 298 K the ratio of rate constants for hydrogen and deuterium addition is 1.32 and this difference could be explained by the differences in the collision frequencies. Frank *et al.* studied the reaction of H with ketene between 1650 K and 1850 K in a shock tube experiment [90]. The hydrogen atom and carbon monoxide concentrations were determined by optical absorption spectroscopy. The rate constants could be expressed as $k(T) = 4.54 \times 10^6 T^{1.28} \exp[-1591/T] \text{ M}^{-1} \text{ s}^{-1}$. The rate of this reaction is sufficiently fast that muoniated methyl radicals ought to be detected in the gas phase by TF- μ SR spectroscopy.

The results are quite different in condensed phases. Bennett and Mile used EPR in combination with the rotating cryostat technique to study the reaction of hydrogen and

deuterium atoms with ketene in water, benzene and adamantane matrices at 77 K [91]. The species that were formed were the methyl, acetyl and formylmethyl (CH_2CHO) radicals, and their yields strongly depended on the composition of the matrix. This is unlike the gas phase, where addition to the terminal carbon was the dominant reaction pathway. In water matrices the major product was the acetyl radical, of which a considerable portion was found to undergo scission to form the methyl radical. In benzene matrices the addition occurred primarily at the central carbon of ketene and there was no evidence of methyl radicals being formed, while in adamantane matrices addition occurred at both carbons. The reason for this pattern in reactivity is not known. There have been no studies of the reaction of hydrogen atoms with ketene in the liquid phase, so it was uncertain how the reaction would proceed.

Sung and Tidwell [92] and Lee and Bozzelli [93] have studied the reaction of H with ketene using quantum calculations. Hydrogen atom addition to the methylene carbon of ketene has the lowest energy barrier, compared with addition to the central carbon or the oxygen. The acetyl radical that is formed is highly vibrationally excited and will rapidly decompose to form the methyl radical and carbon monoxide. These calculations did not take solvent interactions into account and so are only directly applicable to the gas phase measurements.

3.2 Experimental

Ketene was produced by the pyrolysis of acetone in a 'Hurd' lamp or ketene generator. The design was based on a description of a ketene generator given in Vögel [94]. Acetone was used rather than diketene [95] or acetic anhydride [96] due to the lower cost of the starting material and the availability of deuterated samples. The ketene was trapped at 196 K and then purified by vacuum distillation, the middle third fraction being retained. The liquid ketene was de-oxygenated by the freeze-pump-thaw technique and sealed in a non-magnetic stainless-steel cell with a 25 μm thick window to allow penetration of the muons. The sample was stored in dry ice until needed to prevent dimerization. The μSR experiments were performed on the M15 and M20 beam lines with the HELIOS

spectrometer at the TRIUMF cyclotron in Vancouver, Canada. Details of the experimental apparatus and techniques were described in chapter 2.

3.3 Results

The TF- μ SR spectrum obtained upon irradiation of liquid ketene at 184 K with positive muons is shown in Fig. 3.1. The pair of lines symmetrically placed about the muon Larmor frequency (labeled 'D') shows that only one radical is present. The muon hfc (A_μ) was determined from the difference of these two radical precession frequencies (labeled 'R'). This technique does not provide the sign of the hfc, just its magnitude. The muon hfc was measured over a wide temperature range for both ketene and deuterated-ketene and the values are listed in Tables 3.1 and 3.2, respectively. An additional set of radical frequencies was observed above 200 K for both ketene and deuterated ketene. The identity of this radical is discussed in Chapter 4.

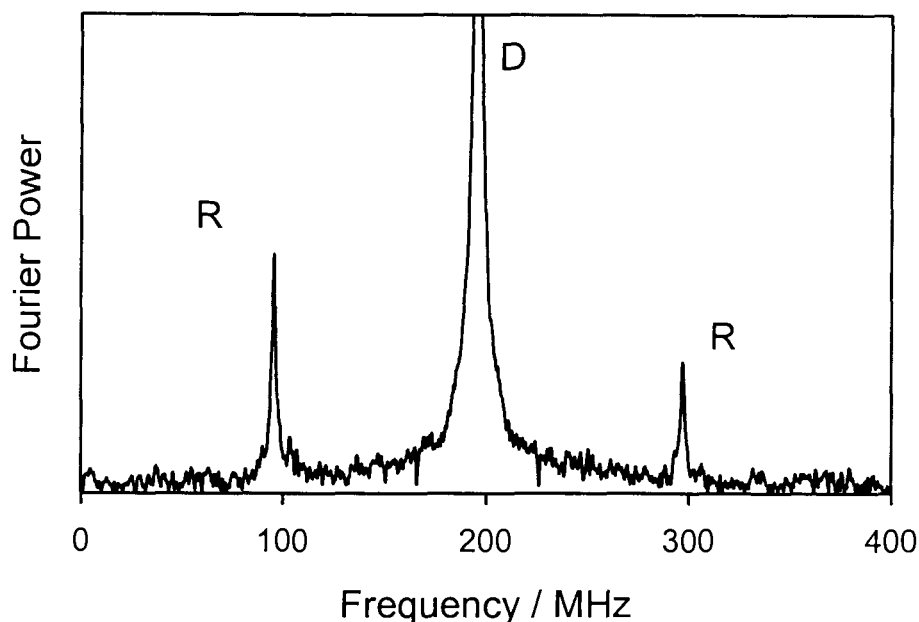


Figure 3.1: TF- μ SR spectrum of ketene at 184 K in an applied magnetic field of 14.5 kG.

Table 3.1: Muon hfc and relaxation rate for the Mu adduct of ketene. ^a

Temperature / K	$ A_\mu $ / MHz	λ / μs^{-1}
73	201.30(10)	3.57(12)
88	201.27(6)	2.30(14)
109	201.28(3)	1.19(10)
131	201.36(4)	1.46(10)
152	201.37(4)	1.66(11)
173	201.44(6)	2.20(14)
184	201.55(4)	2.14(13)
205	201.57(7)	3.03(20)
212	201.62(6)	2.89(15)
223	201.54(8)	3.14(24)

^a Statistical uncertainties given in parentheses.

Table 3.2: Muon hfc and relaxation rate for the Mu adduct of d2-ketene. ^a

Temperature / K	$ A_\mu $ / MHz	λ / μs^{-1}
81	202.29(5)	2.69(17)
93	202.37(2)	1.28(5)
105	202.42(2)	1.47(5)
113	202.42(2)	1.59(5)
125	202.43(2)	2.07(7)
137	202.45(3)	2.35(8)
140	202.45(3)	2.44(10)
150	202.39(4)	2.51(11)
160	202.44(4)	2.84(12)
170	202.48(4)	2.92(12)
180	202.42(4)	3.37(13)
190	202.51(5)	3.32(14)
200	202.53(5)	3.63(16)
210	202.68(5)	3.78(15)
220	202.66(8)	2.53(25)
225	202.35(7)	2.01(19)
235	202.01(12)	1.50(37)

^a Statistical uncertainties given in parentheses.

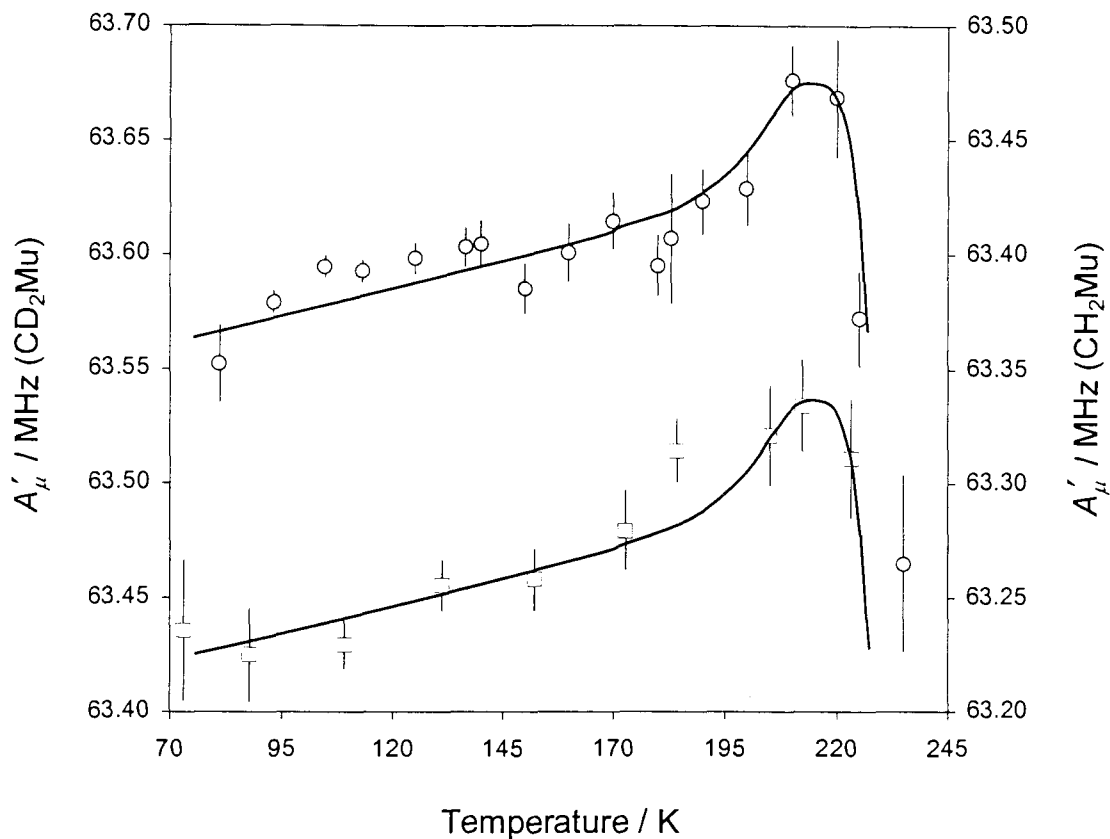


Figure 3.2: Temperature dependence of the reduced muon hfc in CH₂Mu (□) and CD₂Mu (○). The solid lines are a guide for the eyes only.

There is a single resonance in the μ LCR spectrum of both ketene (Figure 3.3) and deuterated-ketene (Figure 3.4). The deuterium resonance is much weaker than the proton resonance because the amplitude of a μ LCR resonance is directly related to the hfc and the gyromagnetic ratio of the nucleus. The hfc value was calculated from the resonance field position (B_{LCR}) by using eq (3.1):

$$B_{LCR} = \frac{1}{2} \left[\frac{(A_\mu - A_p)}{(\gamma_\mu - \gamma_p)} - \frac{(A_\mu + A_p)}{\gamma_e} \right] \quad (3.1)$$

where γ_μ , γ_p and γ_e represent the gyromagnetic ratios of the muon, proton and electron, respectively. The position of the resonances indicates that the proton and deuteron hfcs have the same sign as the muon hfc. The values of the proton and deuteron hfcs are given in Tables 3.3 and 3.4, respectively.

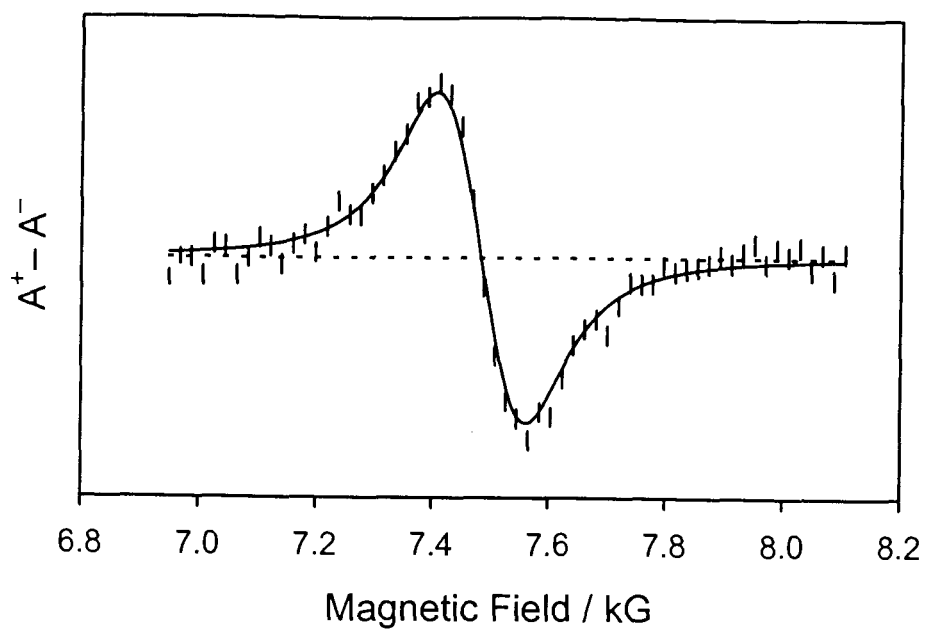


Figure 3.3: μ LCR spectrum of ketene at 184 K.

Table 3.3: μ LCR resonance field, width and the proton hfc of the Mu adduct of ketene as a function of temperature. ^a

Temperature / K	$ A_\mu ^b$ / MHz	B_{res} / G	Width / G	$ A_p $ / MHz	A_μ' / A_p^c
132	201.33(2)	7488.7(20)	75.6(47)	61.23(4)	1.033(1)
152	201.38(2)	7491.1(18)	90.2(44)	61.23(4)	1.033(1)
162	201.41(2)	7485.9(15)	80.1(37)	61.35(3)	1.031(1)
184	201.47(2)	7485.2(15)	90.2(36)	61.44(3)	1.030(1)
192	201.50(2)	7486.2(26)	97.0(66)	61.44(5)	1.030(1)
204	201.54(2)	7491.9(11)	102.5(27)	61.38(3)	1.032(1)
212	201.57(3)	7490.8(17)	104.3(40)	61.43(4)	1.031(1)
223	201.61(4)	7493.3(34)	110.0(80)	61.42(7)	1.031(1)

^a Statistical uncertainties given in parentheses. ^b Fitted muon hfc. ^c $A_\mu' = A_\mu / 3.183$.

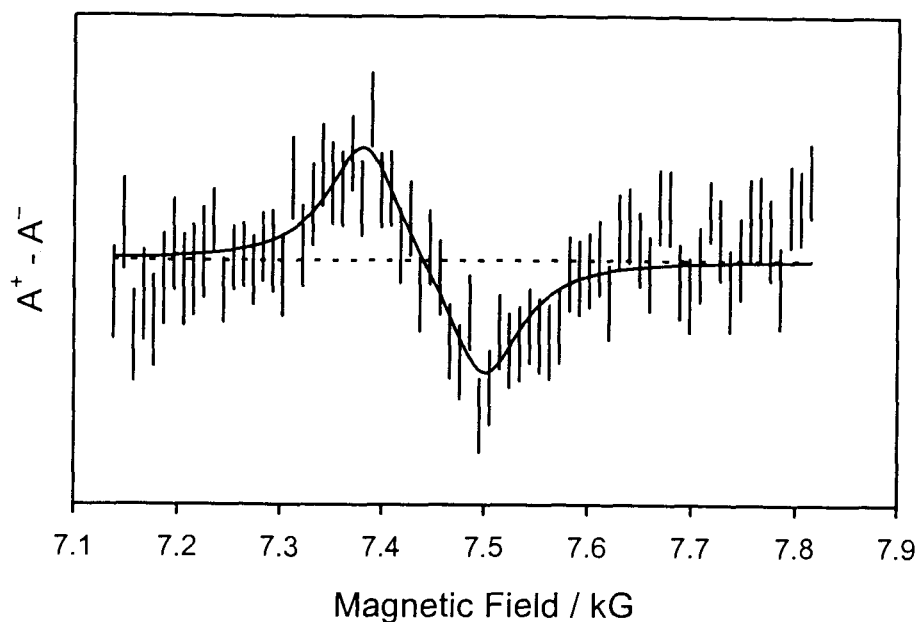


Figure 3.4: μ LCR spectrum of d2-ketene at 200 K.

Table 3.4: μ LCR resonance field, width and the deuteron hfc of the Mu adduct of deuterated ketene as a function of temperature. ^a

Temperature / K	$ A_\mu ^b / \text{MHz}$	$B_{\text{res}} / \text{G}$	Width / G	$ A_d / \text{MHz}$	A_μ' / A_d^c
120	202.42(2)	7438.0(20)	19.7(29)	9.55(6)	1.023(6)
140	202.44(2)	7443.0(58)	21.1(84)	9.44(15)	1.035(16)
160	202.46(2)	7445.2(60)	21.6(86)	9.40(16)	1.039(16)
180	202.48(2)	7438.0(49)	28.6(68)	9.60(13)	1.018(13)
200	202.49(3)	7440.4(42)	45.1(85)	9.55(11)	1.023(12)

^a Statistical uncertainties given in parentheses. ^b Fitted muon hfc. ^c $A_\mu' = A_\mu / 3.183$

3.4 Radical identification

The radical can be identified by comparing the measured hfc's with EPR data on the possible radicals. To aid in comparison with ESR data, it is convenient to refer to the reduced muon hfc ($A_{\mu}' = A_{\mu} / 3.183$) and the reduced deuteron hfc ($A_{\text{d}}' = 6.514 A_{\text{d}}$) to account for the different magnetic moments. The reduced muon, proton and reduced deuteron hfc's for the observed radicals are almost equal, with values that range between approximately 61 and 64 MHz.

There are four possible radicals that could form from the reaction of Mu with ketene; the muoniated methyl radical, the muoniated acetyl radical, the muoniated formylmethyl radical, and the muoniated hydroxyvinyl radical. The conventional isotopomers of the methyl, acetyl and formylmethyl radicals have been studied by EPR spectroscopy. The acetyl radical (H_3CCO) has a proton hfc of 11.2 MHz at 170 K [97], while the formyl methyl radical (CH_2CHO) has two α protons with hfc's of 53.8 and 52.4 MHz and a β proton with an hfc of 1.4 MHz at 260 K [98]. Neither of these radicals would produce the spectra that were observed experimentally, and can therefore be discounted. The hydroxyl vinyl radical can be discounted as Bennett and Miles found no evidence of addition of hydrogen atoms to the oxygen atom of ketene [91]. The methyl radical has three equivalent protons with A_{p} equal to $-64.56(3)$ MHz at 170 K [79], which agrees well with what we have observed. The observed radicals are undoubtedly the muoniated isotopomers of the methyl radical, CH_2Mu and CD_2Mu .

3.5 Temperature dependence of the hfc's of the CH_2Mu and CD_2Mu radicals

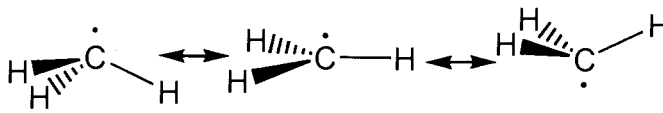
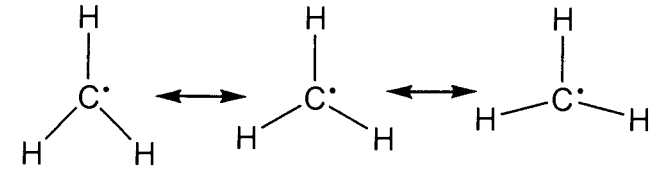
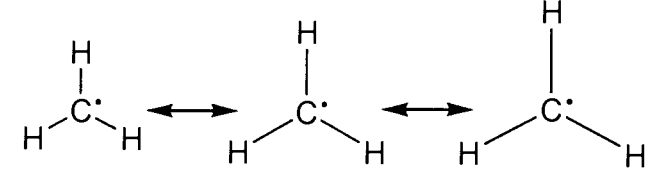
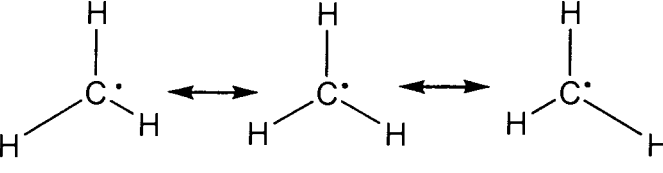
The absolute value of the muon and proton hfc's of CH_2Mu and the muon hfc of CD_2Mu were found to increase with temperature over the liquid range of ketene. The uncertainty in the deuteron hfc's is so large that it is not possible to tell whether there is a small temperature dependence of A_{d} . There is a maximum in the muon hfc's at approximately 220 K, which is close to the boiling point of ketene (b.p. 217 K). Above 220 K the muon hfc's for both isotopomers were observed to fall rapidly. The temperature dependence of the hfc's observed for the muoniated methyl radical isotopomers is unlike that seen for

any of the other isotopomers of this radical. There are two possible explanations for the different behaviour of the hyperfine coupling constants. The first possibility is that Mu substitution greatly alters the vibrational motion of the radical, and the second is that the temperature dependence of the hfcs arises from a temperature dependent interaction of the methyl radical with the ketene solvent molecules. It is also possible that both mechanisms play a role.

3.5.1 Vibrational motion of methyl radical isotopomers

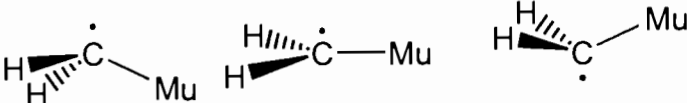
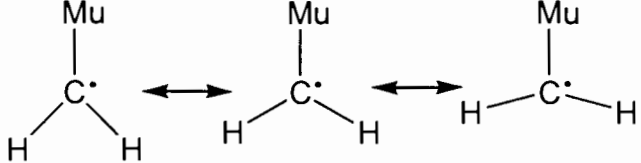
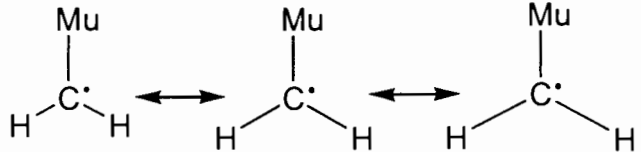
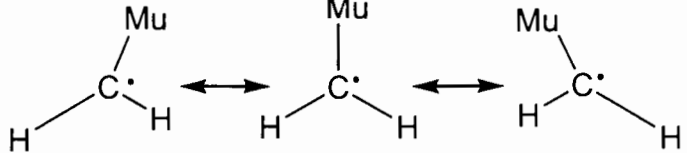
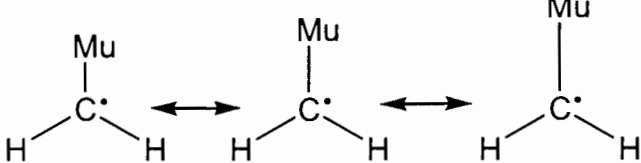
The effect of the light mass of Mu on the vibrational motion of the methyl radical was investigated using quantum calculations. The methyl radical was optimized at the UB3LYP/6-311++G(2df,p) level of theory. Performing the calculations with such a large basis is possible due to the small size of CH₃. The calculations were performed using the Gaussian 98 package of programs [59]. The calculated bond length was 1.0795 Å and the H-C-H bond angle was 120°. These values are in excellent agreement with the experimental values [99]. The vibrational frequencies of CH₃, CH₂D, CHD₂, CD₃, CH₂Mu and CD₂Mu were calculated at the UB3LYP/6-311++G(2df,p) level using the optimized geometry for CH₃. The calculated vibrational frequencies for CH₃ and the muoniated isotopomers are listed in Tables 3.5-7. The calculated frequencies for CH₃ are in general agreement with the experimental values. The worst agreement between the calculated and experimental vibrational frequencies is for the out-of-plane vibrational mode. This is because the potential surface for this vibrational mode is best described as quartic potential rather than a harmonic potential, which was assumed in the calculation of the vibrational frequencies.

Table 3.5: Vibrational modes of the methyl radical. ^a

Mode	ν / cm^{-1} (Calculated)	ν / cm^{-1} (Literature) ^b
 <p>Out-of-plane bend, singly degenerate</p>	539.6	606
 <p>Symmetric in-plane bend, doubly degenerate</p>	1407.3	1383
 <p>Symmetric C-H stretch, singly degenerate</p>	3107.3	3077
 <p>Asymmetric C-H stretch, doubly degenerate</p>	3283.4	3161

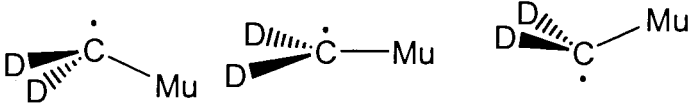
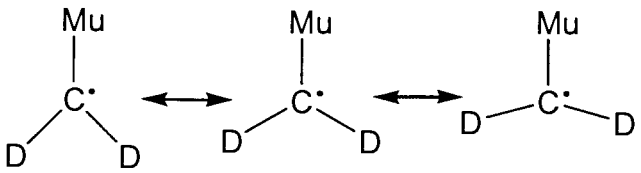
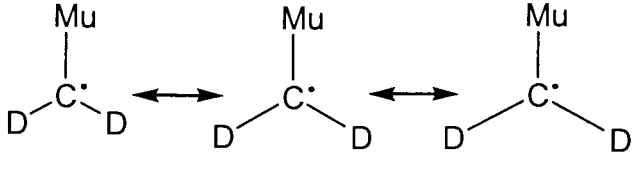
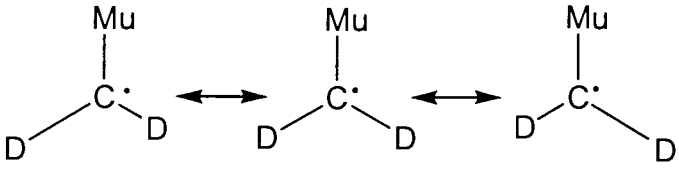
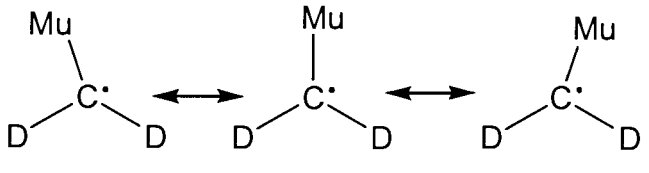
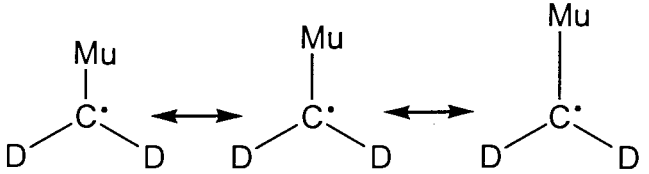
^a UB3LYP/6-311++G(2df,p). ^b Reference [99].

Table 3.6: Calculated vibrational modes and frequencies for the CH₂Mu radical. ^a

Mode	ν / cm^{-1}
 <p>Out-of-plane bend</p>	959.9
 <p>In-plane symmetric bend</p>	1410.1
 <p>Symmetric C-H stretch</p>	3166.6
 <p>Asymmetric C-H stretch + C-Mu wag</p>	3248.1 and 3254.1
 <p>C-Mu stretch</p>	9381.4

^a UB3LYP/6-311++G(2df,p).

Table 3.7: Calculated vibrational modes and frequencies for the CD₂Mu radical. ^a

Mode	ν / cm^{-1}
 <p>Out-of-plane bend</p>	920.2
 <p>In-plane symmetric bend</p>	1045.8
 <p>Symmetric C-D stretch</p>	2283.7
 <p>Asymmetric C-D stretch</p>	2446.7
 <p>C-Mu wag</p>	3353.6
 <p>C-Mu stretch</p>	9380.9

^a UB3LYP/6-311++G(2df,p).

The substitution of Mu into the methyl radical results in large changes to the vibrational motion, due to the light mass of Mu. The most important change is that the vibrational frequencies for the out-of-plane modes of CH₂Mu and CD₂Mu are approximately 50% larger than that of CH₃. It is the population of the first excited state of this mode that results in the large decrease in A_p with increasing temperature for CH₃. In contrast, the large vibrational frequencies for the muoniated isotopomers means that there will be negligible population of the excited vibrational level at the temperatures studied experimentally. Population of other vibrational levels was also considered as a source of the observed temperature dependence, but was quickly discounted as the large vibrational frequencies of these levels would require the hfc in the excited vibrational levels to have physically unrealistic values. For example, if the temperature dependence observed for CH₂Mu was due to the population of the in-plane symmetric bending mode (1410.1 cm⁻¹), the hfc in the first excited state of this mode would have to be approximately -4200 MHz, which is physically unrealistic.

Over the temperature range studied experimentally, the hfc for the muoniated methyl radical isotopomers should be nearly independent of temperature. This suggests that the observed positive temperature dependence for both isotopomers is the result of interactions between the methyl radical and the surrounding ketene molecules.

3.5.2 Solvent effects

The hyperfine coupling constants of a radical depend on the properties of the solvent. Solvent parameters such as dielectric constant, density or hydrogen-bonding ability can affect the hfc by causing small changes in the structure of the radical or by modification of the interactions between the radical and the solvent. There have been several EPR studies on the effect of solvent polarity on the hyperfine couplings of nitroxide radicals [100,101,102]. When there was no hydrogen-bonding between the radical and the solvent the ¹⁴N hyperfine coupling constants were found to depend linearly on a solvent parameter that describes polarity. Al-Bala'a and Bates found that the ¹⁴N hfc were linearly correlated with $(\epsilon-1)/(\epsilon+1)$, where ϵ is the dielectric constant of the solvent [101].

The effect of different dielectric constants on the hfc of the methyl radical was investigated theoretically by Fernandez *et al.* [103]. The magnitude of the proton hfc increased with decreasing dielectric constant, with A_p of CH_3 in methane ($\epsilon = 1.700$) being 0.3 MHz larger than A_p of CH_3 in water ($\epsilon = 78.540$). For the muoniated methyl radical this would correspond to a change in A_μ of 0.9 MHz. The calculated hfc varied linearly with $(\epsilon-1)/(\epsilon+1)$. This dependence of A_p on the term $(\epsilon-1)/(\epsilon+1)$ means that significant changes in A_p can occur for small changes in the dielectric constant if ϵ is close to 1, and negligible changes in A_p if the dielectric constant is large. The range of muon hfc was 0.33 MHz and 0.29 MHz for CH_2Mu and CD_2Mu , respectively, which is small enough that it could be due to a decrease in the dielectric constant of ketene with increasing temperature. Unfortunately the dielectric constant of ketene has not been measured, so it is not possible to determine whether this effect is responsible for the observed behaviour.

Davis *et al.* noticed that the hyperfine coupling constants of the methyl radical were loosely correlated with the inverse of the heat of vaporization of the medium [69]. The heat of vaporization can be thought of as related to the strength of the methyl radical–medium interactions. They speculated that the solvent could modify the out-of-plane bend potential for CH_3 by stabilizing non-planar configurations of the umbrella bend coordinate. This would cause the magnitude of the proton hfc to be smaller as the averaged geometry of the radical would be non-planar. This possibility was also raised by Stratt and Desjardins [104]. If the strength of the radical–solvent interaction decreases as the temperature increases, the methyl radical would become more planar on average, and the magnitude of the proton (or muon) hfc would increase. This possibility could be tested theoretically using the ab initio/molecular mechanics technique that Tachikawa and co-workers have used to model $\text{CH}_3\text{--HF}$ [105] and $\text{CH}_3\text{--H}_2\text{O}$ complexes [106].

The maximum in the muon hfc for both CH_2Mu and CD_2Mu near 220 K is likely related to changes in the density of the sample that result from the phase change of ketene and the formation of diketene. As ketene nears the boiling point (b.p. 217 K) the density of the sample will likely decrease. This should result in an increase in radius of the solvent cavity around the methyl radical. Fernandez *et al.* found that an increase in the radius of

the solvent cavity resulted in a small increase in the magnitude of the proton hfc. The decrease in the magnitude of A_μ above 220 K is possibly due to an increase in the density of the sample which results from the formation of diketene, which is a solid at this temperature.

3.6 Relaxation of the CH₂Mu and CD₂Mu radicals

The relaxation rate of the radical signals in the TF- μ SR spectrum of both CH₂Mu and CD₂Mu was found to vary significantly with temperature. The relaxation rate of the radical signals is the inverse of the transverse, or spin-spin, relaxation time (T_2). Below 90-100 K the relaxation rate increased with decreasing temperature, while above this temperature the relaxation increased linearly with increasing temperature. The relaxation of CD₂Mu was observed to decrease above the boiling point of ketene. The rate of the increase in the relaxation rate for CD₂Mu is approximately 1.22 times larger than that of CH₂Mu.

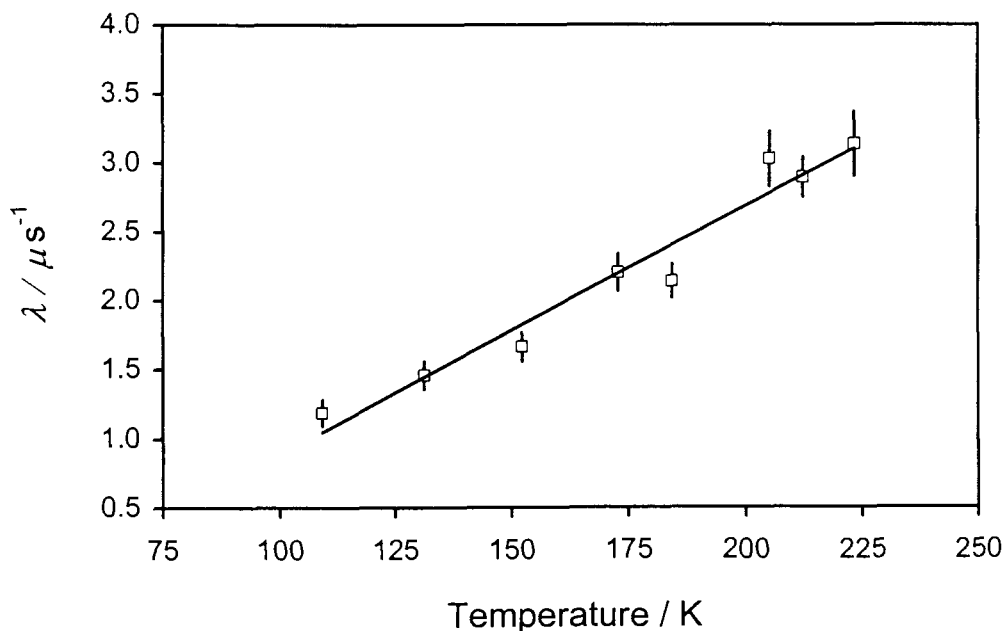


Figure 3.5: Relaxation rate of the radical signals in the TF- μ SR spectrum of CH₂Mu as a function of temperature.

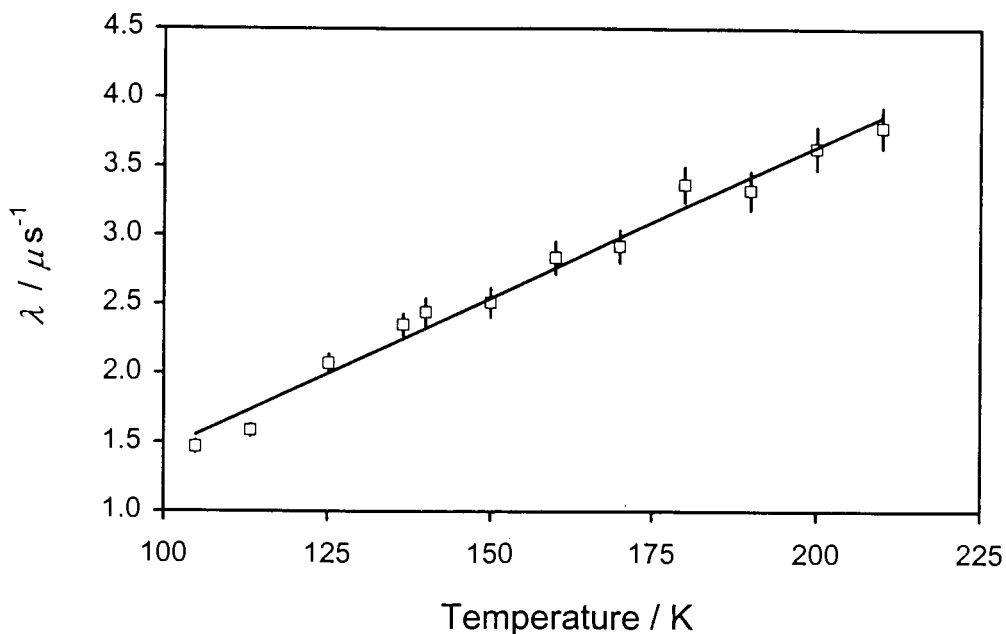


Figure 3.6: Relaxation rate of the radical signals in the TF- μ SR spectrum of CD₂Mu as a function of temperature.

The relaxation rate of the radical signals is the sum of the relaxation due to chemical reactions of the radical (λ_{chem}), random tumbling of the radical that modulates the anisotropic g-value and the hyperfine interactions (λ_{hf}) and spin-rotational interactions (λ_{SR}).

$$\lambda = \lambda_{\text{chem}} + \lambda_{\text{hf}} + \lambda_{\text{SR}} \quad (3.2)$$

Each of these processes depends on temperature in a unique manner, so it is possible to determine which mechanism is dominant from the experimental temperature dependence of the relaxation rate.

Chemical processes involve a reaction or an isomerization that modulates the precession frequency. The relaxation rate is related to the rate of reaction by

$$\lambda_{\text{chem}} = \lambda_0 + k_2[X] \quad (3.3)$$

where λ_0 is the relaxation due to other processes, k_2 is the second-order rate constant and $[X]$ is the concentration of the species with which the radical is reacting. If the process is

an isomerization then the term $k_2[X]$ is replaced by the first-order rate constant, k_1 . It is possible that the methyl radical isotopomers are reacting with the surrounding ketene molecules, but this was considered to be a minor contribution to relaxation based on the theoretical calculations of Sung and Tidwell [92]. Their study on the reaction of methyl radicals with ketene found that addition to both the terminal and central carbon of ketene is exothermic, but there is a significant barrier of approximately 40 kJ mol^{-1} for both reactions. Such a high activation energy cannot account for the variation in the relaxation rates observed experimentally, which would need a barrier of only $2\text{-}3 \text{ kJ mol}^{-1}$.

Tumbling of a radical in the liquid phase can result in relaxation of the electron spin by modulation of the anisotropic g -value (Δg) and hyperfine interactions (ΔA). The relaxation rate of the electron spin is known to be proportional to the rotational correlation time (τ_c), which is given by [107]

$$\tau_c = \frac{4\pi\eta r_0^3}{3kT} \quad (3.4)$$

where η is the viscosity of the solvent and r_0 is the radius of the molecule. The relaxation of the electron spin will indirectly cause relaxation of the muon spin through the hyperfine interaction. Since the rotational correlation time is proportional to η/T , the relaxation rate should decrease with temperature if this mechanism dominates. This is at odds with the experimental results and allows for this mechanism to be discounted. This mechanism is likely responsible for the increase in the relaxation rate with decreasing temperature, below $90\text{-}100 \text{ K}$.

In the liquid phase the spin-rotation relaxation mechanism is only important for small radicals, such as HCO [108]. This mechanism was proposed by Atkins *et al.* to account for the variation of the linewidths of the ClO_2 radical in a variety of solvents [109]. Generally, the linewidths of the radical signals in the TF- μ SR spectrum are narrowed by rapid collisions [11]. For small radicals in non-viscous solvents, several rotations can occur between collisions. A rotating molecule can acquire a magnetic moment because the electrons lag slightly behind the motion of the nuclei. This magnetic moment can couple to the spin of the unpaired electron. Relaxation occurs due to fluctuations of the

angular momentum (J). The fluctuations of J are characterized by the angular momentum correlation time (τ_J), which is much faster than the rotational correlation time (τ_c) for small radicals. McClung calculated that in the limit of extreme motional narrowing the linewidth contribution from the spin rotational interaction for a symmetric top molecule is given by [110]

$$\lambda_{\text{SR}} = \left(\frac{2kT}{3\hbar^2} \right) [\varepsilon_a^2 I_a + \varepsilon_b^2 I_b + \varepsilon_c^2 I_c] \tau_J \quad (3.5)$$

Where ε_a , ε_b and ε_c are the principal values of the spin-rotational coupling tensor and I_a , I_b and I_c are the moments of inertia of the radical. The angular momentum correlation time is given by [111]

$$\tau_J = \frac{I}{8\pi r_0^3 \kappa \eta} \quad (3.6)$$

where r_0 is the radius of the molecule, η is the viscosity, I is the average moment of inertia and κ is a dimensionless parameter between 0 and 1 that describes the solute-solvent interactions and must be determined empirically. The result predicts that the relaxation rate of the radical signal should be proportional to T/η . The viscosity of the sample depends on temperature, generally decreasing with increasing temperature. There is no information on the viscosity of ketene or on its temperature dependence, so the assumption was made that it behaves like acetone, for which this information is known. T/η is proportional to T over most of the liquid range of acetone. This means that the relaxation rate of the radical signal should be proportional to temperature. This is exactly what was seen experimentally, so it can be concluded that the relaxation of the methyl radicals isotopomers is dominated by the spin-rotational interaction. The relaxation rate increases more rapidly for CD_2Mu than for CH_2Mu because of the larger moment of inertia of CD_2Mu .

3.7 Discussion

Table 3.8: Hyperfine coupling constants and calculated out-of-plane vibrational frequencies (UB3LYP/6-311++G(2df,p)) for isotopomers of the methyl radical.

Radical	A_{μ}' / MHz	A_p / MHz	A_d' / MHz	Isotope effect	ν / cm^{-1}
$\text{CD}_3^{a,b}$	—	—	-65.28	—	418.1
$\text{CHD}_2^{a,c}$	—	-65.05	-64.84	0.997 ^d	462.5
$\text{CH}_2\text{D}^{a,c}$	—	-64.74	-64.46	0.996 ^d	501.9
$\text{CH}_3^{a,b}$	—	-64.56	—	—	539.6
CD_2Mu^e	-63.61	—	-62.21	1.022 ^f	920.2
CH_2Mu^g	-63.31	-61.49	—	1.030 ^h	959.9

^a Reference [79]. ^b In liquid methane at 96 K. ^c In krypton matrix at 85 K. ^d Defined as A_d' / A_p . ^e In liquid d2-ketene at 180 K. ^f Defined as A_{μ}' / A_d' . ^g In liquid ketene at 184 K. ^h Defined as A_{μ}' / A_p .

Table 3.8 includes the hfcs and the calculated out-of-plane vibrational frequencies for several isotopomers of the methyl radical. There is a significant variation in the values of the reduced muon, proton and reduced deuteron hfcs which is due to vibrational averaging in the ground vibrational states. The reduced muon, proton and reduced deuteron hfcs appear to be inversely correlated with the magnitude of the out-of-plane vibrational frequency. The ground state vibrational wavefunction for the out-of-plane mode is more localized for heavier isotopomers, like CD_3 , than for lighter isotopomers, like CH_2Mu , due to the differences in the zero-point energy. The magnitude of the hfcs in the methyl radical isotopomers decrease with increasing out-of-plane angle. The CH_2Mu isotopomer has a larger contribution from non-planar configurations than CD_3 , which results in the averaged hfcs for CH_2Mu being smaller than the averaged hfc in CD_3 . This also explains why the magnitude of the muon hfc in CD_2Mu was larger than the corresponding value in CH_2Mu .

The reduced muon hfc is approximately 3% larger than the proton hfc in CH₂Mu, while in CH₂D and CHD₂ the reduced deuterium hfcs are approximately 0.5% smaller than the proton hfc. These differences are in accord with expectations based on anharmonicity in the C-H bond stretch and the zero-point energy. The higher zero-point energy in the C-Mu bond results in the C-Mu bond being slightly longer than the C-H bond. Roduner and Reid estimated the increase in bond length to be on the order of 4.9% [112]. The longer bond length results in the reduced muon hfc being slightly more positive than the proton hfc. Conversely, the lower zero-point energy in the C-D bond results in the C-D bond being slightly shorter than the C-H bond and leads to the reduced deuteron hfc being slightly smaller than the proton hfc. A similar comparison between the muon and deuteron hfcs in CD₂Mu is not applicable due to the large uncertainty in A_d .

3.8 Future Work

Although it has been demonstrated that the muoniated methyl radical can be produced by the reaction of Mu with ketene, the vibrational motion of the methyl radical isotopomers has not been probed. The temperature dependence that was observed at low temperatures is due to interactions of the methyl radical with the solvent molecules. It is the effect of Mu substitution on the vibrational motion that is of greatest interest and this can be studied by measuring the temperature dependence of the hfcs at higher temperatures and in the gas phase. The high temperatures are necessary to have a significant population in the excited vibrational levels and a measurable temperature dependence of the hyperfine coupling constants. Performing the experiments in the gas phase will minimize the dimerization of ketene at the higher temperatures [113] and will provide information about the electronic structure of the methyl radical free from solvent effects.

3.9 Conclusions

The CH₂Mu and CD₂Mu isotopomers were produced by the reaction of muonium with ketene and d₂-ketene, respectively. The radicals were identified by a comparison of the experimental hfcs with values determined by EPR for the possible radicals. The temperature dependence of the hfcs is unlike that of any other methyl isotopomer in that the magnitude of the hfc increases with increasing temperature. This is due to the out-of-

plane bending mode being much higher in energy due to the light mass of the muon, which means that there is negligible population of the first excited state at the low temperatures studied in these experiments. As a result, it is the interaction of the methyl radical with the surrounding solvent molecules that results in the temperature dependence of the hfc's. The differences in the magnitudes of the muon hfc's for CH_2Mu and CD_2Mu are due to the different zero-point energies of the out-of-plane vibrational mode. The reduced muon hfc is 3% larger than the proton hfc in CH_2Mu due to the difference in the zero-point energy of the C-Mu/H stretching vibration. The relaxation of the radical signals in the TF- μSR spectrum is consistent with the spin-rotation relaxation mechanism based on the temperature dependence of the relaxation rate.

CHAPTER 4.

STRUCTURE AND DYNAMICS OF THE MUONIUM ADDUCT OF DIKETENE

4.1 Introduction

In the previous chapter it was demonstrated that muonium adds exclusively to the terminal carbon of ketene to produce the methyl radical at temperatures below 220 K. Once the sample was heated above 220 K, the intensity of the methyl radical signals was greatly diminished and a second set of radical frequencies was observed (Figure 4.1). The methyl radical signals disappeared entirely by 235 K. The second radical was observed in both ketene and d₂-ketene and the muon hyperfine coupling constant was found to range between 267 MHz and 283 MHz (Table 4.4).

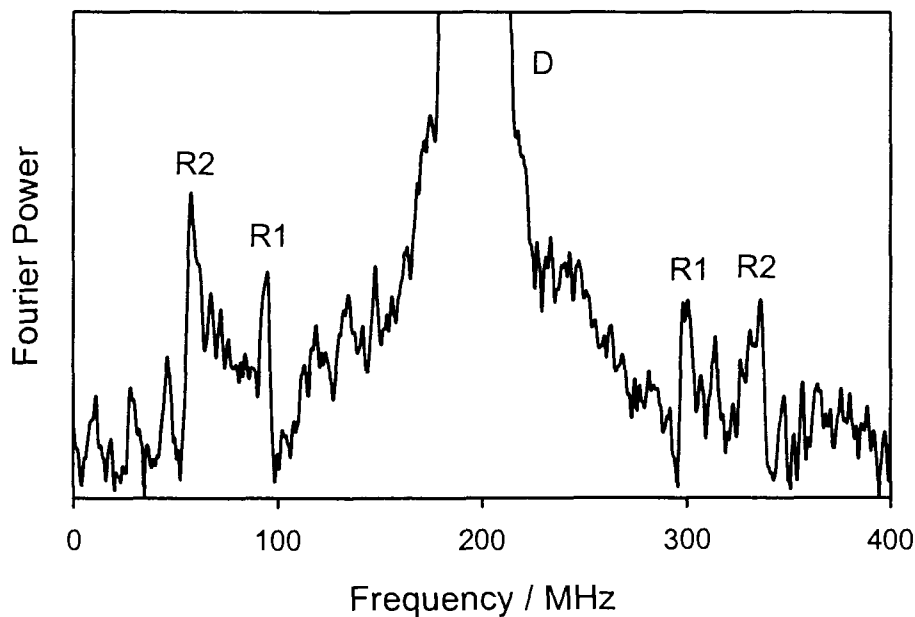


Figure 4.1: TF- μ SR spectrum of d₂-ketene at 235 K and 14.5 kG. The truncated peak labelled “D” is due to muons in a diamagnetic environment and the peaks labelled “R1” are due to the CD₂Mu radical. The peaks labelled “R2” are attributed to a Mu adduct of diketene.

One possible structure for R2 is the muoniated formyl methyl radical, which is formed by the addition of Mu to the central carbon of ketene. The addition of hydrogen atoms to the central carbon of ketene has been observed in a benzene matrix at 77 K [91] but the muon

hfc for the muoniated formyl methyl radical would be much smaller than the observed hfc, based on values obtained from EPR experiments [98].

Addition of Mu to the oxygen of ketene is also unlikely, as the addition of hydrogen atoms to the oxygen was not observed in either water or benzene matrices at 77 K [91]. The addition of H to the oxygen would generate the hydroxyvinyl radical (CH_2COH), which has not been observed by EPR. Sung and Tidwell calculated that the barrier for addition of H to the oxygen of ketene lies 33.5 kJ mol^{-1} and 28.5 kJ mol^{-1} above the in-plane and out-of-plane barriers for addition of H to the central carbon of ketene, respectively [114]. This result suggests that the rate of formation of the hydroxyvinyl radical is much slower than the rate of formation of the formyl methyl radical. Since the muoniated formyl methyl radical was not observed, observation of the more slowly formed hydroxyvinyl radical is very unlikely.

The second radical could be the result of Mu reacting with diketene (4-methylene-oxetan-2-one), whose structure is shown in Figure 4.2. Diketene is formed by the dimerization of ketene. Ketene can be stored for several days at temperatures below 190 K. At this temperature only 0.8% of a sample dimerized in one week. Above this temperature the dimerization is rapid [115]. At 273 K the second order rate constant for dimerization in diketene has a value of $1.4 \times 10^{-4} \text{ M}^{-1} \text{ s}^{-1}$ [116]. A sealed sample of ketene will polymerize completely within 1.5 hours if it is allowed to warm to 273 K [115].

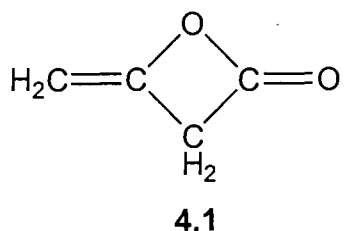


Figure 4.2: Diketene (4-methylene-oxetan-2-one).

The reaction of Mu with a pure sample of diketene was studied in order to determine what radicals are formed, their structure and whether this reaction could account for the second radical that was observed in ketene above 220 K.

4.2 Experimental

Diketene (b.p. 382-383 K) was purchased from Aldrich Chemicals and used without further purification. The diketene contained a small amount of copper sulfate to prevent polymerization. The sample was sealed in a stainless steel cell with a glass stem and subjected to several freeze-pump-thaw cycles to remove dissolved oxygen, at which point the cell was flame sealed. The μ SR experiments were performed on the M20 beam line at TRIUMF with the HELIOS spectrometer.

4.3 Results

An example of a TF- μ SR spectrum is shown in Figure 4.3. The pair of lines symmetrically placed about the muon Larmor frequency (at 157 MHz) shows that only one type of radical is present. Muon hfc (A_μ) were determined from the difference of these two radical precession frequencies and are listed in Table 4.1.

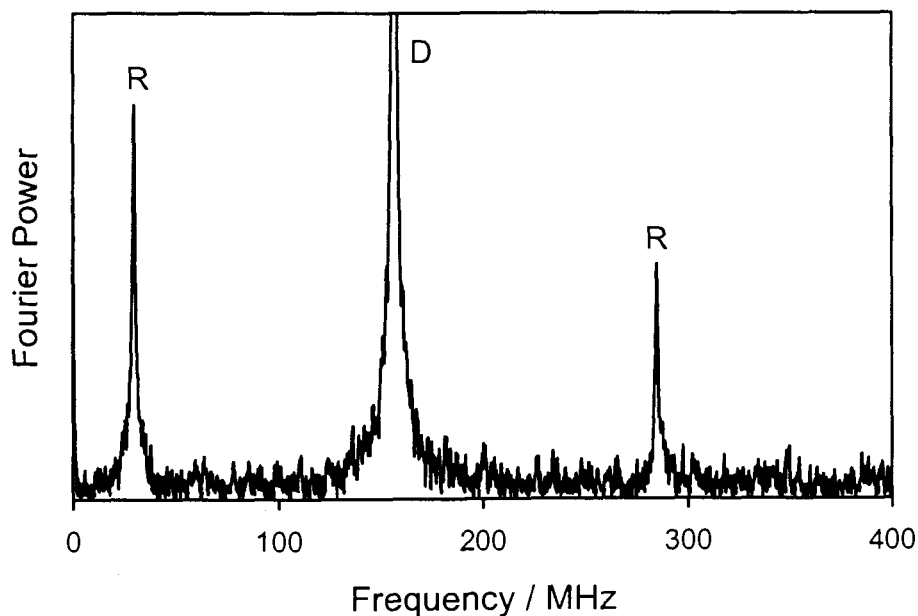


Figure 4.3: TF- μ SR spectrum of a neat diketene sample at 298 K and 11.6 kG.

Table 4.1: Muon hyperfine constants for the Mu adduct of diketene

Temperature/K	A_μ/MHz^a
279.9	259.08(7)
297.0	255.19(4)
322.5	250.31(10)
331.7	248.87(5)
350.6	245.88(4)
362.5	244.12(5)

^a Statistical uncertainties are shown in parentheses

There are two resonances in the μLCR spectrum, as evident from the example shown in Figure 4.4. They are assigned to two groups of protons with different hfc (A_{p1} and A_{p2}). The hfc values were calculated from the resonance field positions (B_{LCR}) by using equation 4.1:

$$B_{\text{LCR}} = \frac{1}{2} \left[\frac{A_\mu - A_p}{\gamma_\mu - \gamma_p} - \frac{A_\mu + A_p}{\gamma_e} \right] \quad (4.1)$$

where γ_μ , γ_p and γ_e represent the magnetogyric ratios of the muon, proton and electron, respectively. Since the TF- μSR and μLCR spectra were not taken at exactly the same temperatures, values of A_μ at the desired temperatures were interpolated from a fit of the Table 4.1 data before substitution into equation 4.1. The results of the analysis are listed in Table 4.2.

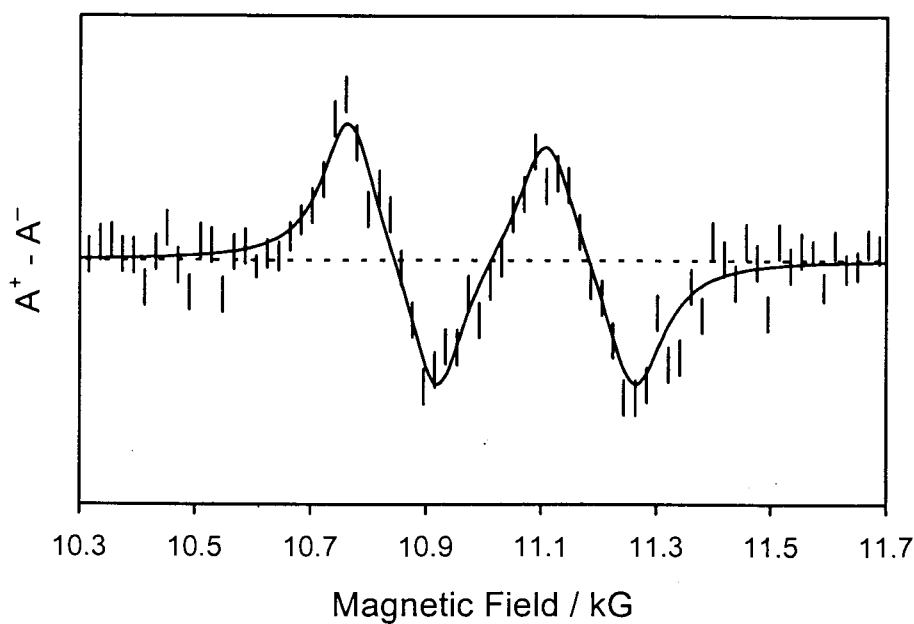


Figure 4.4: μ LCR spectrum of diketene at 298 K.

Table 4.2: Analysis of muon avoided level-crossing resonance spectra.^a

Temperature/K	A_{μ} /MHz ^b	B_{LCR} /kG	A_{p1} /MHz	B_{LCR} /kG	A_{p2} /MHz
281.8	258.61	11.036(3)	52.40(8)	11.348(3)	46.62(8)
297.0	255.19	10.826(3)	52.88(6)	11.168(2)	46.56(5)
320.9	250.65	10.579(3)	52.95(6)	10.943(2)	46.21(5)
343.5	246.98	10.342(2)	53.70(5)	10.727(3)	46.56(6)
362.5	244.11	10.180(2)	53.85(7)	10.571(3)	46.60(7)

^a Statistical uncertainties are shown in parentheses. ^b Interpolated from the data of Table 4.1.

4.4 Radical assignment

There are four sites in diketene to which Mu could add, generating the radicals whose structures are shown in Figure 4.5. The assignment of the radical was based on empirical data from other muoniated radicals. Addition of Mu to either of the carbons on the lactone ring is unlikely as it has been shown that Mu will add preferentially to the less substituted end of the double bond, yielding the more stable radical [117]. Addition of

Mu to the carbonyl oxygen can also be discounted, as this type of radical typically has a much smaller muon hfc [118]. Furthermore, none of these possibilities gives two sets of protons with similar hyperfine constants. The only radical that fits the observations is the 4-muonomethyl-oxetan-2-on-4-yl radical (4.2), which was formed by Mu addition to the methylene carbon of the carbon-carbon double bond. This radical has two pairs of protons adjacent (beta) to the radical centre: one pair in the ring and the other pair in the muoniated methyl group.

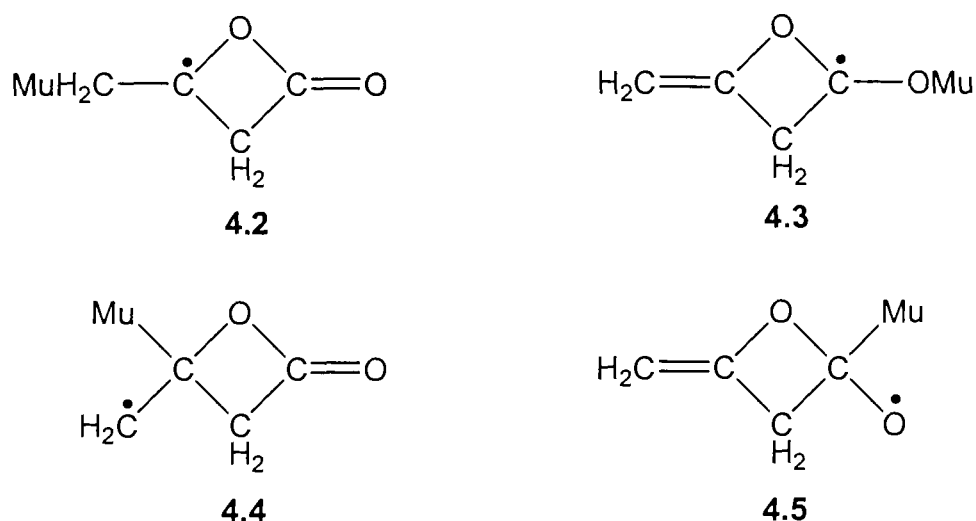


Figure 4.5: Possible radicals resulting from the reaction of Mu with diketene.

The hfc's of beta nuclei in alkyl radicals generally satisfy the McConnell equation [119],

$$A = L + M \langle \cos^2(\theta - \theta_0) \rangle \quad (4.2)$$

where L and M are constants ($M \gg L$) and θ is the dihedral angle between the axis of the p-orbital centred on C_α and the $\text{C}_\beta\text{-H}(\text{Mu})$ bond. The observed hfc is a Boltzmann weighted average over the various torsional states. In muoniated radicals, the $\text{C}_\beta\text{-Mu}$ bond aligns preferentially with the orbital containing the unpaired electron ($\theta = 0$) [117]. This preference causes the muon hfc to decrease and the proton hfc's to increase as the temperature is raised [120]. This is just the behaviour that we have observed for the muon hfc and the proton with the larger hfc. They both have magnitudes typical for the CH_2Mu

group. The protons with the nearly temperature independent hfc are attributed to the ring CH₂.

4.5 Calculations and discussion

The temperature dependence of the hyperfine coupling constants of 4.2 were modeled in order to predict the values of the hfc below the temperatures that were studied, and thereby compare these values with those of the second radical observed in ketene. Unfortunately, theoretical modeling of the temperature dependence of hyperfine coupling constants in a pseudo-methyl group has traditionally been a very involved process. The temperature dependence arises from the thermal population of quantized torsional levels [120, 121]. Expressions for the torsional wavefunctions and their energies can be obtained by solving the appropriate torsional Hamiltonian, which is given by

$$\hat{H} = -\frac{\hbar^2}{2I} \frac{\partial^2}{\partial \theta^2} + V(\theta) \quad (4.3)$$

where θ is the dihedral angle, $V(\theta)$ is the rotational potential and I is the reduced moment of inertia. The torsional Hamiltonian has to be solved numerically. $V(\theta)$ can be obtained by performing quantum calculations as a function of the dihedral angle, but a major drawback is that this is very computationally demanding as it requires numerous calculations. An alternative approach is to use a simple model for the rotational potential (such as the three-fold potential $V(\theta) = (V_2/2)(1-\cos 2\theta) + (V_3/2)(1-\cos 3\theta)$ that was used for the muoniated *tert*-butyl radical [120, 121]) and obtain the parameters for the rotational potential by fitting the experimental data. A drawback to this approach is that it is difficult to fit for more complicated potentials, which would need to be defined using several parameters, especially if data is available for only a small temperature range.

The temperature dependence of hyperfine coupling constants in radical 4.2 has been modelled using a method that was recently reported by Shiotani *et al* [122]. Their method of calculation was successful in modelling the temperature dependence of proton and deuteron hfc in several isotopomers of the dimethyl ether radical cation in CCl₃F matrices at low temperatures. The basis of their method was to assume that the values of

the hfc's in the lowest torsional wavefunctions can be approximated by the values in the minimum energy geometry and that the energies of the torsional levels can be obtained by assuming that the rotational potential is harmonic near the minimum energy geometry. The only calculations that are required are the optimisation of the radical's geometry and the calculation of the zero point energy for the different conformations of the pseudo-methyl group, which makes this method computationally inexpensive. The averaged hfc for a given temperature can be expressed by the following equation.

$$A(T) = \sum_i p_i A_i \quad (4.4)$$

where p_i is the probability of finding the radical in the i^{th} torsional state and A_i is the corresponding hfc. The probabilities, p_i , are calculated from the differences in the zero point energies for the different conformations of the pseudo-methyl group. The approximation is not valid at elevated temperatures, where higher energy torsional states would be significantly occupied.

The zero point energies for the conformations of the pseudo-methyl group were calculated from frequency calculations on the minimum energy geometry obtained from density functional calculations at the UB3LYP/6-31G** level of theory. Muonium was treated as an isotope of hydrogen with a mass of 0.114 u, and a scaling factor of 0.8929 was used for all the frequency calculations. The frequency calculations were also performed for the deuterated isotopomer. The hfc's of radical **4.2** were obtained using the minimum energy geometry from UB3LYP/6-311+G(2df,p) calculations. The single point calculations were performed at the UB3LYP/EPR-III level and included the effect of the medium (*i.e.* solvent effect), which was estimated using the polarized continuum model of Tomasi *et al.* [123] and the dielectric constant for acetone ($\epsilon = 20.7$). The dielectric constant for acetone was used for the quantum calculations since the corresponding value for diketene is not known and acetone and diketene both contain the C=O functional group.

The minimum energy structure at the UB3LYP/6-31G** level was found to have a non-planar radical centre, similar to the *tert*-butyl radical [124, 125, 126]. The angle between

the $C_{\alpha}-C_{\beta}$ bond and the $O-C_{\alpha}-CH_2$ plane is 31.8° , compared to 22° for the corresponding angle in the *tert*-butyl radical. The larger degree of non-planarity can be attributed to strain in the β -lactone ring. The presence of only two resonances in the LCR spectrum indicates that inversion of the radical centre occurs rapidly. It is likely that inversion is coupled with rotation of the methyl group, as deduced from calculations on *tert*-butyl [125, 126]

In the minimum energy conformation the methyl group of **4.2** is staggered with respect to the four-membered ring, with the C_3-Mu bond eclipsing the orbital containing the unpaired electron (see Figure 4.6a). The potential for rotation of the methyl also has minima at dihedral angles of 120° and 240° . These three conformations have identical electronic energies (on the Born–Oppenheimer surface); it is only with inclusion of the zero-point vibrational energy contributions that the conformations are distinguished. Their relative energies are listed in Table 4.3.

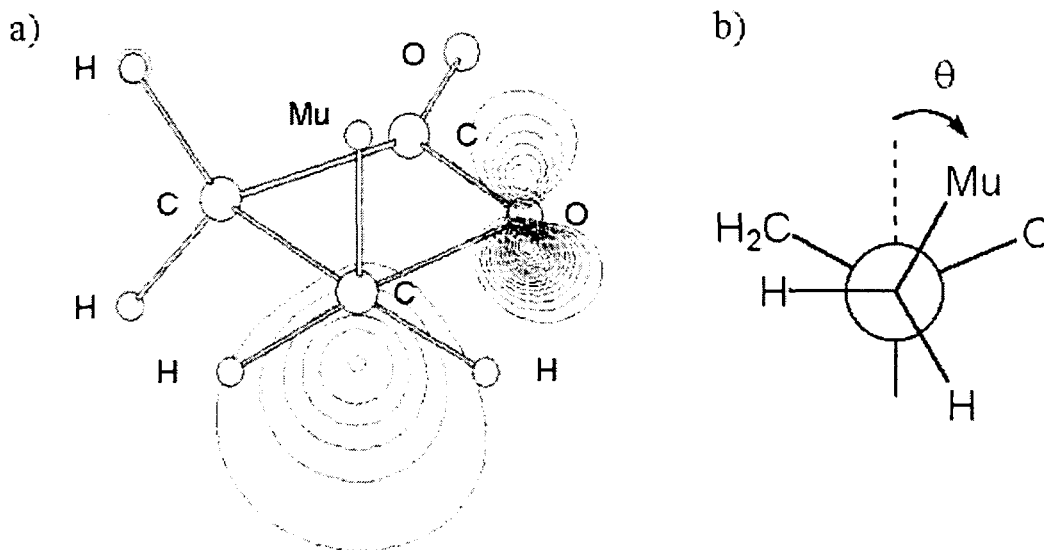


Figure 4.6: a) Newman projection along the $C_{\beta}-C_{\alpha}$ bond of the minimum energy geometry of **4.2** showing the unpaired electron spin density. b) Definition of the dihedral angle (θ) in **4.2** (the carbonyl group is not shown for clarity).

Table 4.3: Relative energies and hyperfine constants for the minimum energy conformations of the muoniated methyl group in 4-muonomethyl-oxetan-2-on-4-yl.

Dihedral angle / degrees ^a	hfc / MHz ^b			H ^c	D ^c
	A_p (1)	A_p (2)	A_p (3)	ΔE / kJ mol ⁻¹	
0	135.28	13.80	35.60	0	0
120	35.60	135.28	13.80	1.79	2.02
240	13.80	35.60	135.28	1.74	2.21

^a The dihedral angle is defined in Figure 4.6b. ^b Multiply A_p by 3.183 to convert to A_μ and divide by 6.514 to convert to A_d . ^c The H and D labels refer to the proton and deuteron isotopomers of 4.2, respectively.

Using the above procedures results in the hfcs denoted by the lines in Figure 4.7. For ease of comparison of muon and proton data, the reduced muon hfc is used in the plot; $A_\mu' = A_\mu/3.183$ corrects for the different magnetic moments of the muon and proton. Considering the simplicity of the model, there is surprisingly good agreement between the calculations and the experimental data. Presumably one reason is the relatively high barrier to rotation for the methyl group, so that only the lowest torsional levels are significantly occupied.

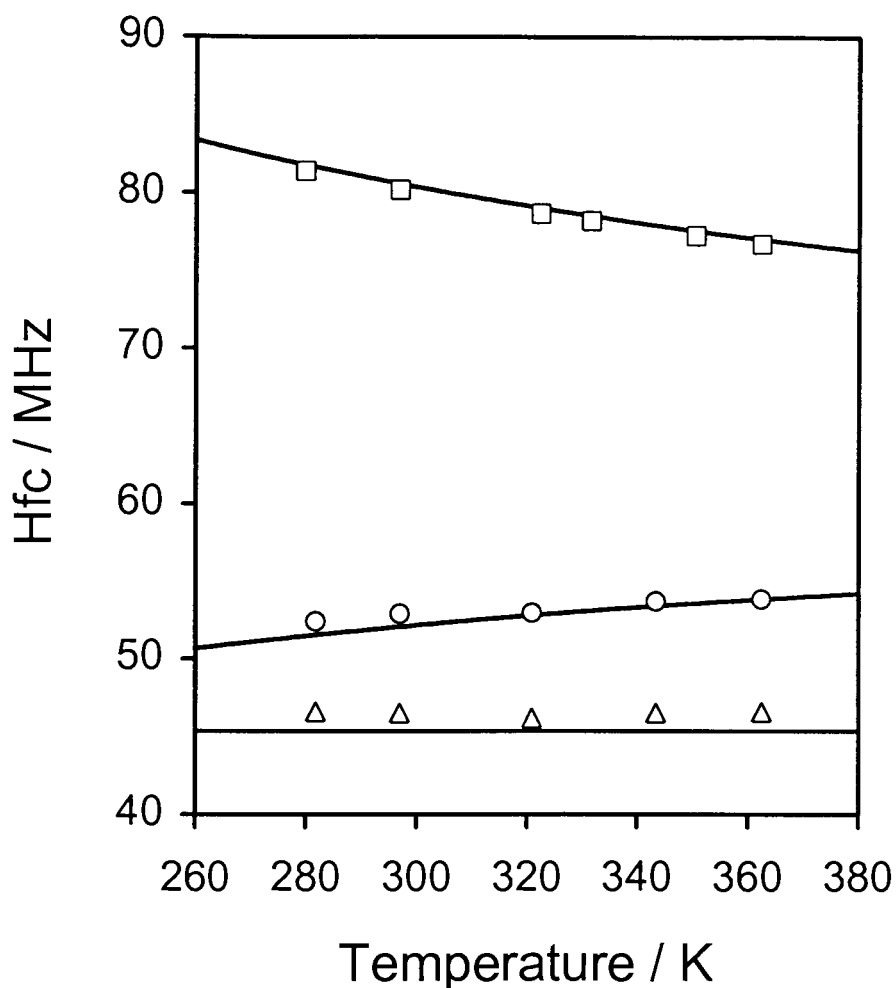


Figure 4.7: Muon (□), methyl proton (○) and ring proton (Δ) hyperfine coupling constants and calculated values (lines) for the 4-muonomethyl-oxetan-2-on-4-yl radical. The error bars of the experimental values are smaller than the data points.

Quantum calculations were performed using a variety of different basis sets. The basis sets reported in this chapter were the combination that gave the closest agreement with the experimental values. Inclusion of the solvent effects was necessary as calculations performed without the solvent model gave values that were consistently below the experimental values by approximately 5 MHz.

The hyperfine coupling constants of the second radical observed in ketene and deuterated ketene and the theoretical values for the two isotopomers of the 4-muonomethyl-oxetan-2-on-4-yl radical at these temperatures are listed in Table 4.4.

Table 4.4: Comparison of the measured muon hfcs of the second radical observed in ketene and d2-ketene with calculated hfcs for the H and D isotopomers of the 4-muonomethyl-oxetan-2-on-4-yl radical.

Isotopomer ^a	Temperature / K	A_{μ} / MHz (Experiment)	A_{μ} / MHz (Calculated)
H	223	273.52(13)	277.19
D	225	282.90(13)	293.20
D	230	280.49(13)	291.13
D	235	279.72(24)	289.14
D	255	273.74(11)	281.88
D	275	267.78(11)	275.59

^a The H and D labels refer to the isotopomer of ketene and radical 4.2.

The calculated hfcs for the appropriate isotopomer of radical 4.2 are within 4% of the hfcs for the second radical observed in ketene. This close agreement between calculated and experimental hfcs allows us to conclude that the 4-muonomethyl-oxetan-2-on-4-yl radical was the second radical observed in ketene at temperatures above 220 K.

4.6 Conclusions

Muonium adds exclusively to the terminal carbon of the C=C bond in diketene to produce the 4-muonomethyl-oxetan-2-on-4-yl radical. The assignment of the radical was based on the number of different hyperfine coupling constants, their magnitude and their temperature dependence behaviour. The temperature dependence of the hfcs was successfully modelled by calculating the relative energies of the minimum energy conformations for rotation of the pseudo-methyl group. The second radical observed in ketene above 220 K was confirmed to be the 4-muonomethyl-oxetan-2-on-4-yl radical.

CHAPTER 5.

DIRECT FORMATION OF ALPHA-MUONIATED RADICALS: ADDITION OF MUONIUM TO STABLE SINGLET CARBENES

5.1 Introduction

Carbenes ($R_2C:$) are molecules that possess a neutral dicoordinate carbon atom with six valence electrons, which results in high reactivity for these carbon centres. This high reactivity was, in part, the reason for their elusive nature. Until recently carbenes were only observed as intermediates or trapped in an inert matrix at cryogenic temperatures [127,128].

The first stable molecule that could be formulated as a carbene, [bis(diisopropylamin)phosphino]-trimethylsilylcarbene [129], was produced by Bertrand in 1988 but its reactivity indicated that it was more like a phosphacetylene. The first true stable singlet carbene was 1,3-bis(adamantyl)imidazol-2-ylidene, which was produced by Arduengo in 1991 [130]. Imidazol-2-ylidenes have been prepared with a large variety of substituents (such as **5.1** and **5.2**). Subsequent to the discovery of the imidazol-2-ylidenes, other types of stable carbenes were produced. Notable molecules are 1,3,4-triphenyl-4,5-dihydro-1*H*-1,2,4-triazol-5-ylidene (**5.3**) [131], which was the first carbene to be commercially available, and 1,3-dimesitylimidazolin-2-ylidene (**5.4**) which has a saturated five-membered ring [132]. The structures of selected stable carbenes are shown in Figure 5.1. The stability of carbenes **5.1-5.4** is the result of the π -donating nitrogen atoms adjacent to the carbeneic centre. The energy of the p orbital at the carbeneic carbon is raised by interacting with the nitrogen lone pairs, and this results in a singlet ground state rather than a highly reactive triplet state [133,134]. There have been numerous studies on the reactivity and electronic structure of carbenes as a result of the impact that the isolation of these highly reactive molecules has had on synthetic chemistry. Reviews have covered the quest for isolable carbenes [135], main group element carbenes and carbene analogues [136], transition metal carbene complexes and catalysts [137,138] and main group element carbene complexes [139].

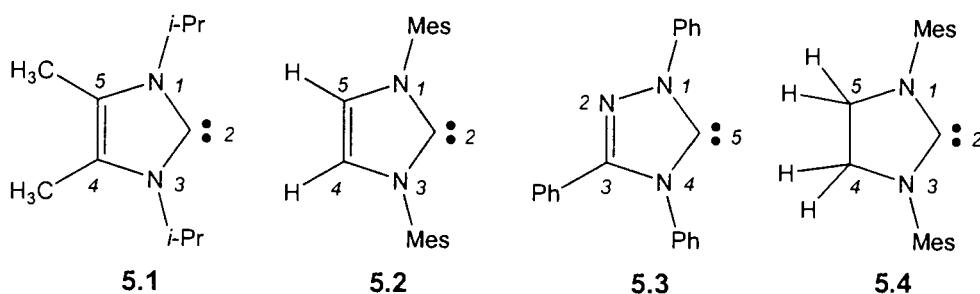


Figure 5.1: Stable singlet carbenes (*i*-Pr = CH(CH₃)₂, Mes = 2,4,6-trimethylphenyl, Ph = phenyl).

Given the importance of stable carbenes, the lack of reports on their reactivity with *any* free radical species is very surprising. The only example of a radical generated from a stable carbene is the radical anion of 1,3,4-triphenyl-4,5-dihydro-1*H*-1,2,4-triazol-5-ylidene (**5.3**) (which can formally be viewed as the product of the reaction between a carbene and the simplest radical, the electron). This radical was produced electrochemically and studied by electron spin resonance (ESR), cyclic voltammetry and theoretical calculations [140,141]. The magnitude of the proton coupling in the ESR spectrum of the radical anion of **5.3** implies that about 2/3 of the unpaired spin density is delocalized onto one of the substituent phenyl rings. There is also a small nitrogen coupling. Thus, at most 1/4 of the unpaired electron density remains at the nominal radical centre (the original carbene). In a formal sense the H atom adduct may be viewed as the protonated radical anion, but this can not be used to predict the preferred site of radical attack on the carbene, which depends on both the reactivity of the various sites and the geometry of the transition state. The transfer of a hydrogen atom to a dinitroxide carbene was recently reported as part of a much larger study. The nitronyl nitroxide carbene abstracted a H atom from the solvent and this was seen as indicative of partial radical character at the radical centre, unlike the imidazole-2-ylidenes [142].

It is not obvious how muonium will react with stable singlet carbenes, particularly given recent theoretical evidence for π -electron delocalization around the ring of imidazole-2-ylidenes [143,144], the large number of possible sites of addition, and that hydrogen and deuterium atoms abstract a hydrogen atom from ³CH₂ and don't add to the carbenic carbon in the gas phase [145]. The radicals that can possibly form by addition

of Mu to the stable singlet carbenes can be grouped into three different categories: (a) α -muoniated radicals that result from Mu addition to the carbeneic carbon (**5.1a** – **5.4a**), (b) those formed by Mu addition to the five-membered ring (**5.1b**, **5.2b** and **5.3b-c**) and (c) cyclohexadienyl radicals originating from Mu addition to the aromatic substituents. The structures of the α -muoniated radicals and those resulting from addition of Mu to the unsaturated bond in the five-membered ring are shown in Figure 5.2.

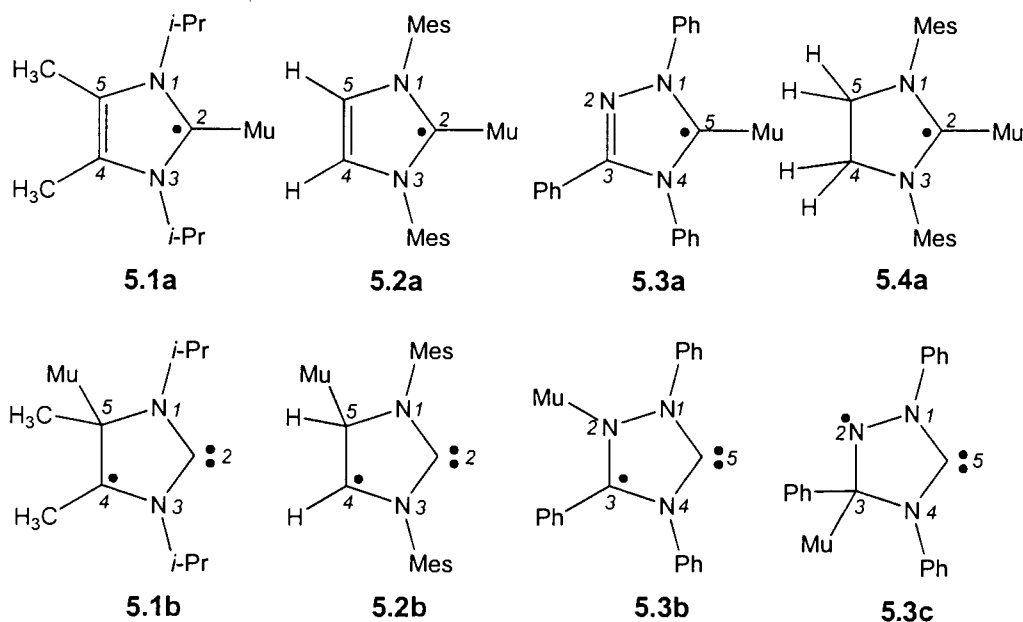


Figure 5.2: Structures of radicals that could form by addition of Mu to the carbeneic carbons or the five-membered rings of carbenes **5.1-5.4**.

5.2 Experimental

The carbenes 1,3-bis(isopropyl)-4,5-dimethylimidazole-2-ylidene (**5.1**) and 1,3-dimesitylimidazole-2-ylidene (**5.2**) were prepared by the research group of Dr. J. A. C. Clyburne following the established literature procedures [146]. A ¹³C labeled sample of **5.1** (40% enriched at C2) was prepared starting from ¹³CS₂. 1,3,4-triphenyl-4,5-dihydro-1H-1,2,4-triazol-5-ylidene (**5.3**) was purchased from Acros Organics and used without further purification. **5.4** was provided by Dr. S. Nolan from the University of New Orleans and used without further purification.

The samples used at TRIUMF were solutions of the carbenes in tetrahydrofuran (THF). Due to the sensitivity of carbenes towards oxygen and moisture, the solutions were

prepared in a glove-box using pre-degassed and distilled THF and dried glassware. The concentrations of each solution depended on the solubility of the carbene in THF and on the amount of material available. The following concentrations were prepared: 1.0 M for **5.1**, 0.5 M for **5.2**, 0.25 M for **5.3** and 0.25 M for **5.4**. The total volume of each sample was 5 mL. Prior to use, the solutions were subjected to several freeze-pump-thaw cycles to remove any dissolved oxygen, and then sealed in non-magnetic stainless-steel cells. Details of the apparatus and the muon spectroscopic techniques are given in chapter 2.

5.3 Results of μ SR experiments

5.3.1 Transverse field muon spin rotation

Muon hyperfine coupling constants were determined by transverse field muon spin rotation (TF- μ SR). The spectra produced by muon irradiation of carbenes **5.1-4** at 298 K are shown in Figures 5.3-6, respectively. In all cases, only one type of radical was found, as evident from the characteristic pair of frequencies (labeled R) above and below the muon Larmor frequency (labeled D). The muon hfc was determined from the difference in the two radical precession frequencies. The temperature dependence of the muon hfc was measured over a wide temperature range for carbenes **5.1-3**. The muon hfcs of the radicals generated from carbenes **5.1** and **5.2** decreased with increasing temperature while the muon hfc of the radical generated from carbene **5.3** increased with increasing temperature. The measured muon hfcs as a function of temperature are given in Tables 5.1-3 and displayed in Figure 5.7. The muon hfc of the radical formed by Mu addition to carbene **5.4** was only measured at 298 K, at which temperature the value was 114.43(4) MHz.

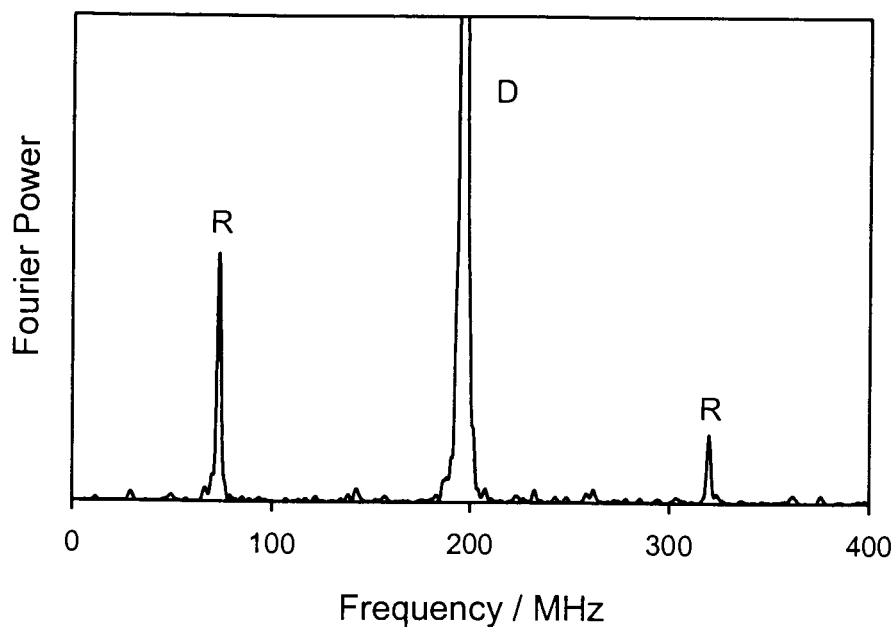


Figure 5.3: TF- μ SR spectrum of 4,5-dimethyl-1,3-bis(isopropyl)imidazol-2-ylidene (**5.1**) at 298 K in an applied magnetic field of 14.5 kG.

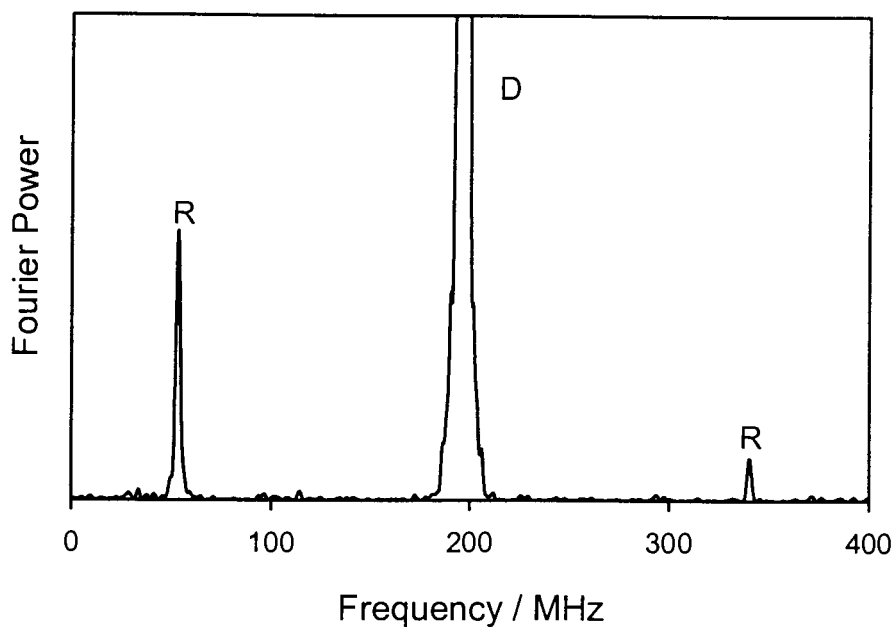


Figure 5.4: TF- μ SR spectrum of 1,3-bis(2,4,6-trimethylphenyl)imidazol-2-ylidene (**5.2**) at 298 K in an applied magnetic field of 14.5 kG.

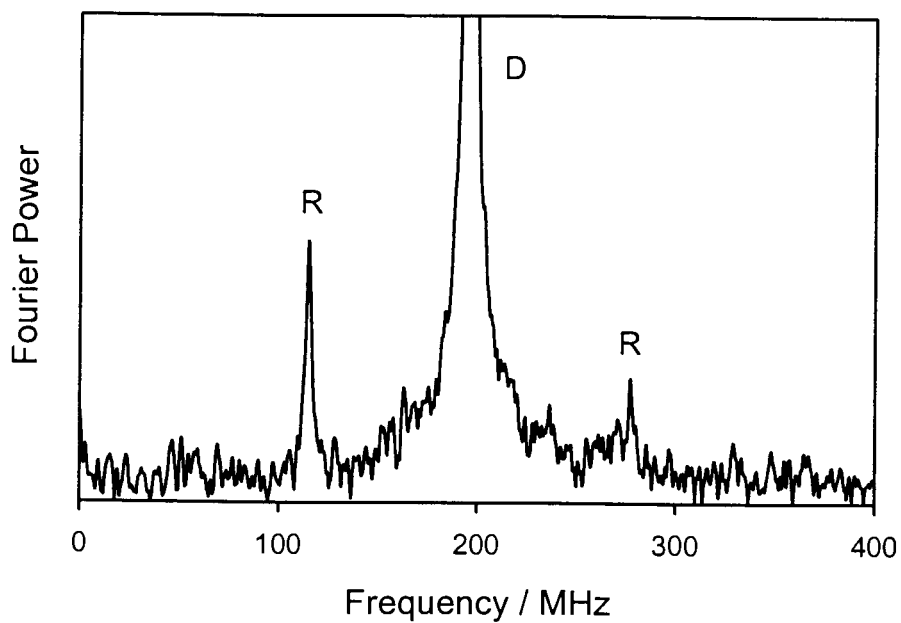


Figure 5.5: TF- μ SR spectrum of 1,3,4-triphenyl-4,5-dihydro-1*H*-1,2,4-triazol-5-ylidene (5.3) at 298 K in an applied magnetic field of 14.5 kG.

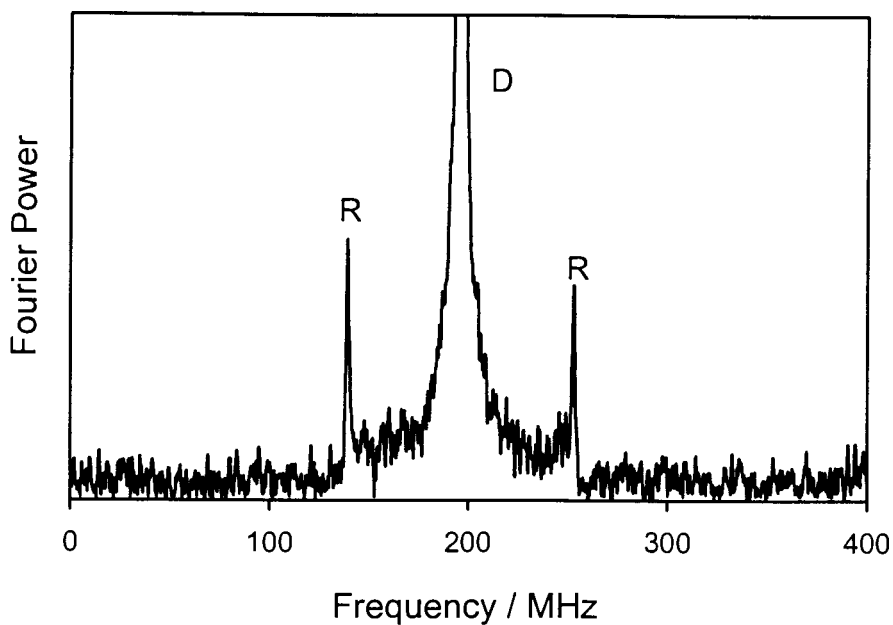


Figure 5.6: TF- μ SR spectrum of 1,3-bis(2,4,6-trimethylphenyl)imidazolin-2-ylidene (5.4) at 298 K in an applied magnetic field of 14.5 kG.

Table 5.1: Muon $h\nu c^a$ as a function of temperature for the Mu adduct of 4,5-dimethyl-1,3-bis(isopropyl)imidazol-2-ylidene (**5.1**).

Temperature / K	A_μ / MHz
245.6	248.63(3)
250.8	248.39(3)
260.9	248.05(3)
273.9	247.28(3)
278.2	247.07(2)
288.9	246.71(2)
294.7	246.50(2)
297.7	246.43(2)
307.2	246.11(2)
316.9	245.82(1)
326.6	245.44(2)

^a Statistical uncertainties are shown in parenthesis.

Table 5.2: Muon hfc^a as a function of temperature for the Mu adduct of 1,3-bis(2,4,6-trimethylphenyl)imidazol-2-ylidene (**5.2**).

Temperature / K	A_μ / MHz
256.0	291.21(8)
261.1	290.31(9)
273.2	289.35(8)
278.7	288.69(7)
289.1	287.52(11)
298.1	286.69(7)
307.2	285.68(7)
316.8	284.62(7)
326.6	283.42(8)

^a Statistical uncertainties are shown in parenthesis.

Table 5.3: Muon hfc^a as a function of temperature for the Mu adduct of 1,3,4-triphenyl-4,5-dihydro-1*H*-1,2,4-triazol-5-ylidene (**5.3**).

Temperature / K	A_μ / MHz
280.0	161.32(6)
288.0	162.72(24)
298.0	164.26(15)
318.0	166.63(23)
334.0	168.55(12)

^a Statistical uncertainties are shown in parenthesis.

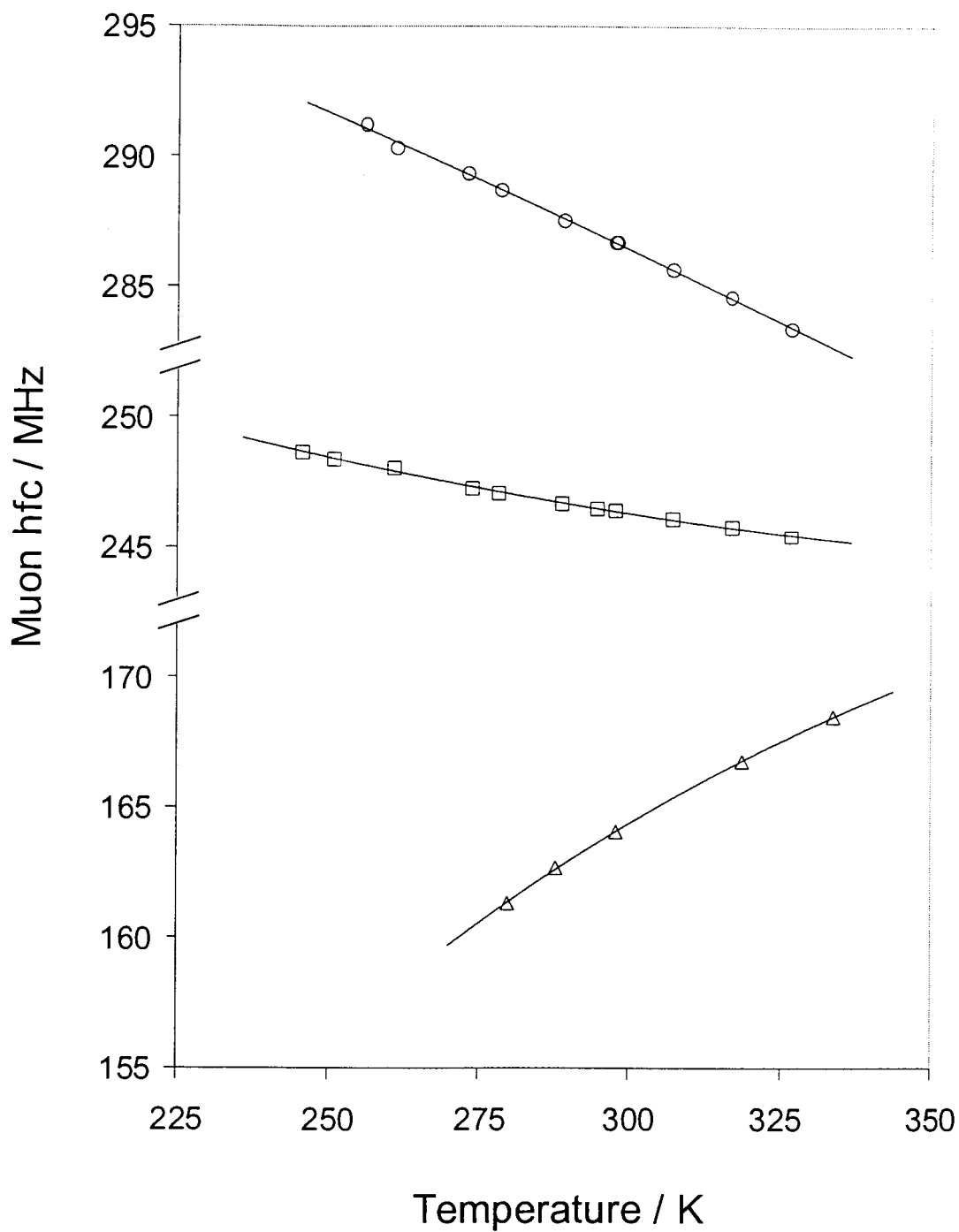


Figure 5.7: Temperature dependence of the muon hfc in the Mu adduct of 4,5-dimethyl-1,3-bis(isopropyl)imidazol-2-ylidene (\circ), the Mu adduct of 1,3-bis(2,4,6-trimethylphenyl)imidazole-2-ylidene (\square) and the Mu adduct of 1,3,4-triphenyl-4,5-dihydro-1*H*-1,2,4-triazol-5-ylidene (Δ). The lines are a guide for the eyes only.

5.3.2 Avoided muon level crossing resonance

Hyperfine coupling constants for other nuclei in the radicals were determined by muon avoided level-crossing resonance. A single resonance was found in the μ LCR spectrum obtained from **5.1** (Figure 5.8). The field position at 298 K was 8736.4(1.2) G, which corresponds to either ^{14}N nuclei with $A_{\text{N}} = +13.73(4)$ MHz or protons with $A_{\text{p}} = +82.88(3)$ MHz. It is believed to be due to the ^{14}N nuclei because of the amplitude of the resonance. An additional resonance was observed for the ^{13}C labeled sample of **5.1** (Figure 5.9), which is undoubtedly due to the ^{13}C nucleus (C2). The μ LCR spectrum was obtained at 274, 298 and 322 K and the data is listed in Table 5.4. A single resonance was also found in the μ LCR spectrum obtained by muon irradiation of carbene **5.2** at 298 K (Figure 5.10). In principle the resonance field position, 10276.6(3.1) G, could be due to either ^{14}N nuclei with $A_{\text{N}} = +13.01(10)$ MHz or protons with $A_{\text{p}} = +94.53(8)$ MHz. The amplitude of the resonance suggests that it is due to ^{14}N nuclei.

Table 5.4: μ LCR fields^a, widths^a and corresponding ^{13}C hfc^a as a function of temperature for the Mu adduct of 4,5-dimethyl-1,3-bis(isopropyl)imidazol-2-ylidene (**5.1**).

T / K	B_{res} / kG	FWHM/ G	A_{C} / MHz
274	4.337(25)	215(54)	137.33(53)
298	4.208(11)	127(20)	139.64(21)
322	4.081(13)	99(31)	141.99(29)

^a Statistical uncertainties shown in parentheses.

A very weak resonance was observed in the μ LCR spectrum upon irradiation of carbene **5.3** (Figure 5.11). The resonance was observed at 5836.1(8.2) G and corresponds to a ^{14}N hfc of 8.65(23) MHz. The extremely low amplitude of the resonance strongly suggests that the resonance is due to a ^{14}N nucleus and not a proton.

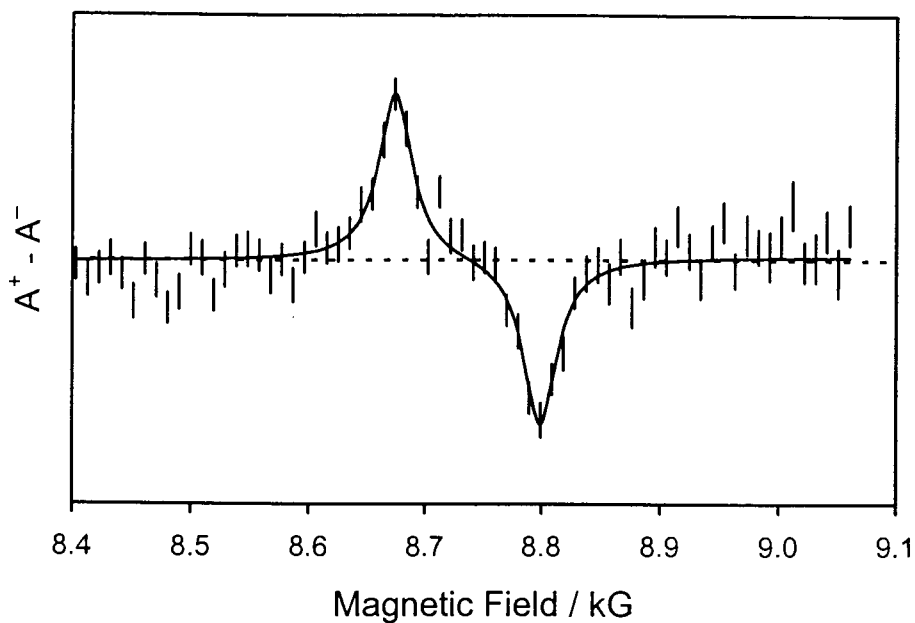


Figure 5.8: Avoided muon level crossing resonance spectrum of 4,5-dimethyl-1,3-bis(isopropyl)imidazol-2-ylidene (**5.1**).

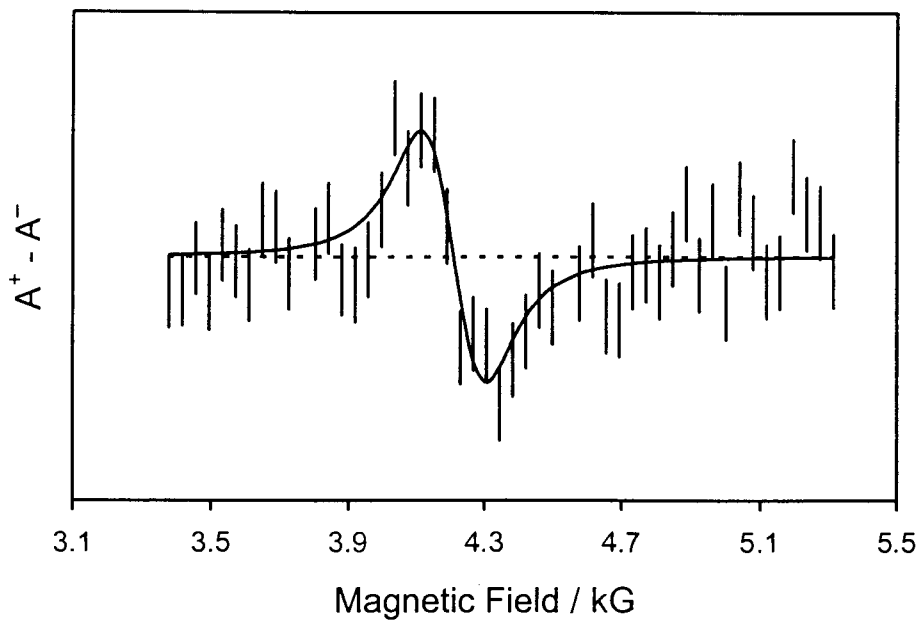


Figure 5.9: Additional resonance in the avoided muon level crossing resonance spectrum of 40% ^{13}C enriched 4,5-dimethyl-1,3-bis(isopropyl)imidazol-2-ylidene (**5.1**).

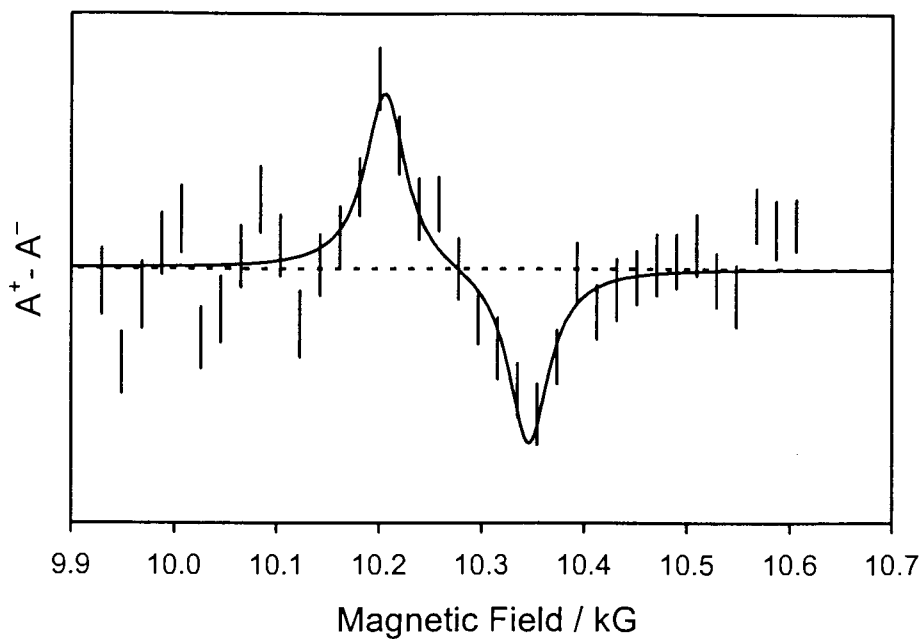


Figure 5.10: Avoided muon level crossing resonance spectrum of 1,3-bis(2,4,6-trimethylphenyl)imidazol-2-ylidene (**5.2**).

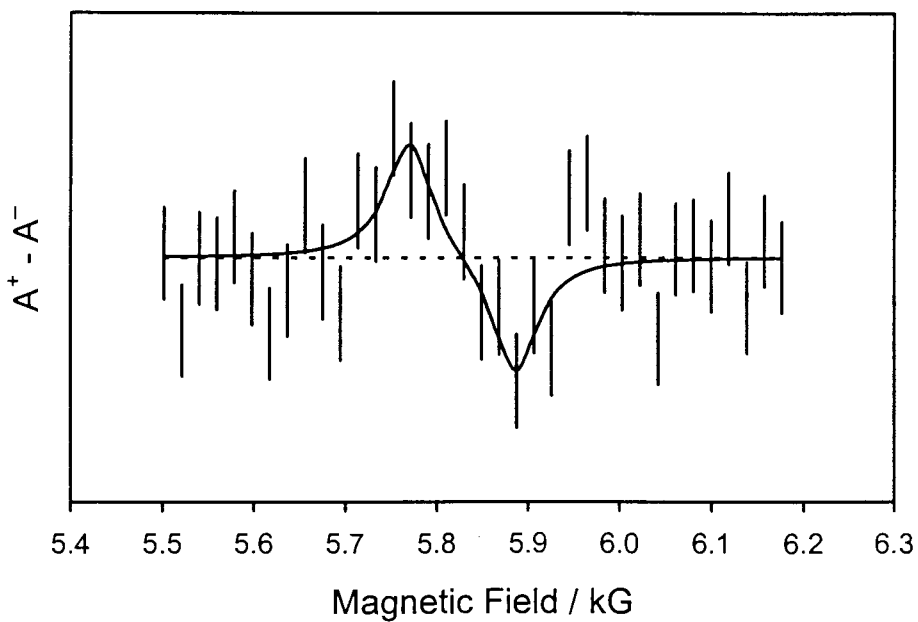


Figure 5.11: Avoided muon level crossing resonance spectrum of 1,3,4-triphenyl-4,5-dihydro-1*H*-1,2,4-triazol-5-ylidene (**5.3**).

No definite resonance was observed in the μ LCR spectrum obtained by muon irradiation of carbene **5.4** at 298 K between approximately 2800 G and 8800 G. TF- μ SR spectra were obtained both before and after the μ LCR spectrum, confirming that the sample did not degrade during the experiment. The lack of a resonance means that the unpaired electron in the radical only interacts very weakly with any magnetic nuclei in the molecule, or that the resonance is broadened beyond detection by some motion of the molecule.

5.4 Radical identification

Determining the structures of the observed radicals is not a trivial process, particularly in this experiment where there are numerous possible structures. There are 15 different radicals that could form by the addition of Mu to carbene **5.3**! The structure of a radical was assigned by comparing the measured hfc's with values obtained from previous μ SR and EPR experiments on similar radicals, or with values calculated by theoretical methods, and from calculations of the relative energies of the possible products and the barriers to addition.

5.4.1 Comparison with previous μ SR and EPR experiments

The majority of the possible radical structures result from addition of muonium to the phenyl or mesityl rings, which generates substituted cyclohexadienyl radicals. Substituted cyclohexadienyl radicals have been extensively studied by μ SR [11]. Addition of muonium to mesitylene (1,3,5-trimethylbenzene) produces two radicals, the 1-muono-2,4,6-trimethylcyclohexadienyl and the 1-muono-1,3,5-trimethylcyclohexadienyl radicals, whose muon hfc's are 453.1 and 483.9 MHz, respectively [147]. Addition to toluene (a model for a phenyl ring with one substituent) resulted in the formation of three types of radicals. The muon hfc is 489.6 MHz for the *ortho* carbon adduct, 509.3 MHz for the meta carbon adduct and 496.4 MHz for the *para* carbon adduct [147]. The muon hfc's for the radicals formed by addition of Mu to the aromatic rings of **5.2-4** are expected to be of similar magnitude. The large difference in the muon hfc values for cyclohexadienyl radicals and the measured muon hfc's for the unknown radicals means that all of these possible structures can be discounted. In addition, cyclohexadienyl

radicals have a strong resonance in the μ LCR spectrum corresponding to a proton with an hfc of approximately $A_{\mu}/3.183$. No such resonances were observed. From this we can conclude that the radical observed upon Mu irradiation of carbene **5.4** was not a substituted cyclohexadienyl radical and therefore must be the α -muoniated radical **5.4a**.

A survey of the μ SR and EPR literature revealed that there are no radicals with structures that are sufficiently similar to **5.1a-b**, **5.2a-b** and **5.3a-c** for a comparison to be meaningful and convincing. While numerous radicals with five-membered rings have been studied, the presence of hetero-atoms at different positions in the ring could have a large effect on the hyperfine coupling constants. Lacking suitable comparisons, the assignment of the observed radical had to be based on quantum calculations.

5.4.2 Quantum calculations

5.4.2.1 Computational details

Theoretical calculations on the parent carbenes and the radicals resulting from Mu addition to the five-membered rings were performed using the Gaussian 98 package of programs [59]. The calculation of the hfcs of open shell systems has been a considerable challenge and it is only recently that density functional theory (DFT) calculations have been successful in reproducing the geometry and magnetic properties of free radicals at moderate computational cost, relative to other appropriate methods [148,149] Accurate calculation of the hfcs also requires inclusion of solvent effects and averaging over large amplitude modes [150].

Geometry optimizations and calculation of hyperfine coupling constants (hfcs) was performed using the B3LYP functional [150], which has been well validated for calculations on free radicals [151]. The geometries of molecules **5.1**, **5.1a** and **5.1b** were optimized using the 6-311G** basis set, and the magnetic properties of **5.1a** and **5.1b** were found using the EPR-III basis set. Molecules **5.2**, **5.2a**, **5.2b**, **5.3**, **5.3a**, **5.3b**, **5.3c**, **5.4** and **5.4a** were optimized using the 6-31G basis set and the hyperfine coupling constants were calculated using the EPR-II basis set. The EPR-II and EPR-III basis sets were specifically optimized for computing isotropic hfcs [151]. Solvent effects were

included in the single-point calculations by using the polarized continuum model (PCM) with the solvent parameters for THF ($\epsilon = 7.58$) [123].

The molecular geometry for each H adduct radical is also valid for the muoniated species, within the Born–Oppenheimer approximation. Similarly, electron distributions should be identical for isotopomers. However, zero-point vibrational effects are larger for normal modes involving Mu, and this can result in considerable isotope effects on vibrationally averaged hyperfine interactions. These effects have been investigated in the cyclohexadienyl [152] and fullerenyl radicals [153, 154]. For the purpose of identifying the radicals the vibrational averaging effects were treated empirically. The C-Mu bond is estimated to be 4.9% longer than the corresponding C-H bond due to this vibrational averaging [112]. Accordingly, the C-Mu bond was artificially lengthened by this amount for the calculation of the hfc.

It is essential to include the averaging due to the out-of-plane vibrational mode for the α -muoniated radicals (**5.1a-4a**) as this has been demonstrated to be equally as important as a good quality basis set [150]. The effect of this mode has been investigated extensively for non-planar radicals such as the fluoromethyl [84], cyclopropyl [155,156] and oxiranyl radicals [157]. For radicals with a non-planar radical centre, the effect of vibrational averaging is to change the hfc of the α -proton (or muon) and the α -carbon to values that correspond to a single-point calculation for a structure with a smaller out-of-plane angle compared to the minimum energy geometry [155]. The geometries of the α -muoniated radicals were optimized for several out-of-plane angles θ (defined as the angle between the C_α -Mu bond and the N- C_α -N plane) between approximately 25° and 45°, and the angular variation of the hfc was fitted with a cubic function. The vibrationally averaged radical structures were then found empirically by adjusting θ to give the best agreement with the experimental hfc.

5.4.2.2 Geometric Structures

The structures of carbenes **5.1-4** were calculated and compared to values obtained by X-ray crystallography [131,132,158] in order to verify the reliability of the chosen computational methods. Carbene **5.1** was compared with the closely related 1,3,4,5-

tetramethylimidazol-2-ylidene because X-ray data on **5.1** was not available. The calculated geometrical parameters of the five-membered rings of **5.1-4** are in good agreement with the corresponding experimental value although the DFT calculations tended to overestimate the bond-lengths by 0.01-0.02 Å, on average. Given the close agreement between the theoretical and experimental values, it was concluded that the computational methods used generated accurate geometries and would be suitable for calculating the geometries of the radical species.

The minimum energy structures of the α -muoniated radicals (**5.1a-4a**) have non-planar radical centres. This is the first reported addition to a carbene that does not produce a planar tri-coordinate carbon. The out-of-plane angle (θ) is quite large for these molecules: 40.1° for **5.1a**, 41.4° for **5.2a**, 39.6° for **5.3a** and 36.6° for **5.4a**. The carbon-nitrogen bonds adjacent to the radical centre and the N-C $_{\alpha}$ -N bond angle were found to be larger than in the parent carbene. This increase in bond lengths and angles at the radical centre has been noted for the cyclopropyl and oxiranyl radicals [155,157]. The increase in these parameters is due to the unpaired electron occupying an orbital with significant anti-bonding character. The addition of Mu causes the five-membered rings of **5.1a-3a** to distort from planarity.

The orientation of the aromatic rings in the radicals can have a large effect on the calculated hyperfine coupling constants. For carbenes **5.2** and **5.4** the mesityl rings were found to be perpendicular to the N1-C2-N3 plane. This is in agreement with the structures obtained by X-ray crystallography. The reason for this geometry is that it minimizes the steric interactions of the *ortho*-methyl groups of the mesityl ring with the five-membered rings. In the minimum energy geometry of **5.2a** the mesityl rings were found to be at an angle of 61.9° with the N1-C2-N3 plane and in **5.4a** the rings were at angles of 54.5 and 63.3°. This configuration would allow unpaired electron spin density to delocalize onto the mesityl rings but steric interactions should prevent this overlap. To model this the hfc's were calculated using structures with the mesityl rings fixed perpendicular to the N1-C2-N3 plane but all other parameters were optimized.

The situation is quite different for **5.3** and **5.3a**. There are fewer steric interactions that would prevent the π -systems of the imidazole and phenyl rings from overlapping. In the minimum energy of **5.3** and **5.3a** the phenyl ring on N1 is nearly coplanar with the imidazole ring. This is in agreement with the structure of **5.3** obtained by X-ray crystallography [140]. The orientations of the phenyl rings were not constrained for the calculation of the hfcs.

5.4.2.3 Energetics

Quantum calculations were performed to determine the energetics of Mu addition to the carbeneic carbon and the unsaturated bond in the five-membered ring of **5.1** (UB3LYP/6-311G**) and **5.2-5.3** (UB3LYP/6-31G). Both reactions are exothermic (-182.74 and -122.29 kJ mol⁻¹, respectively) for **5.1**, with radical **5.1a** (addition to the carbeneic site) being favoured. The same result was found for carbene **5.2**: the carbeneic site is favored over the double bond (the energies of reaction are -213.76 and -134.60 kJ mol⁻¹, respectively). Addition to the carbeneic carbon of **5.3** (-230.70 kJ mol⁻¹) is preferred over addition to either the carbon or the nitrogen of the double bond in the triazole ring (-140.73 kJ mol⁻¹ and -110.94 kJ mol⁻¹, respectively). Addition to the carbeneic carbon is more exothermic because this reaction only involves the redistribution of electrons, whereas addition to other sites on the five-membered rings results in considerable changes in the structure. This type of behaviour was seen in the Mu adducts of C₇₀ [159], pyrene [160] and fluoranthene [161].

The barriers to addition at the carbeneic carbon as well as to the double bond of carbene **5.1** have been calculated. The distinguished coordinate paths for addition of Mu to the carbeneic carbon and the alkeneic carbon of **5.1** were obtained by partially optimizing the geometry as a function of the distance between Mu and the site of addition, and are shown in Figure 5.12. There is a discernible transition state for addition to the double bond, with a C-Mu distance of ~1.92 Å and an activation barrier of 4.5 kJ mol⁻¹. This value is similar to the barrier for the H + C₂H₄ reaction [162]. There is no clear transition state for reaction at the carbeneic carbon. While it well known that DFT calculations have difficulty in locating transition states [163], the fact that one was located for addition to the double bond suggests that the lack of a transition state is not due to problems with the

theoretical model but reflects the behaviour of the system. The non-existent activation barrier for addition at the carbeneic carbon suggests that this should be the dominant pathway, and that the observed radicals were the α -muoniated radicals **5.1a-4a**.

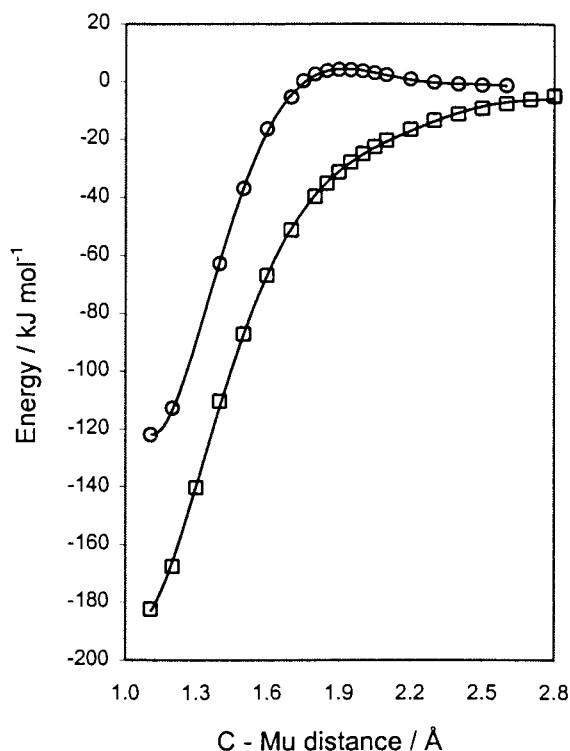


Figure 5.12: Reaction profile for the addition of Mu to the carbeneic carbon (\square) and the double bond (\circ) of 4,5-dimethyl-1,3-bis(isopropyl)imidazol-2-ylidene (**5.1**).

5.4.2.4 Hyperfine Coupling Constants

The theoretical calculations on **5.1a-4a** showed that most of the unpaired electron spin density is localized on the α -carbon with some delocalized onto the adjacent nitrogen atoms. There is a small amount of negative spin density on the atoms of the double bond in **5.1a-3a**. The muon, ^{13}C and ^{14}N hfc's of **5.1a-4a** depended almost linearly on the out-of-plane angle between 25° and 45° . There is also very little delocalization in the β -muoniated radicals (**5.1b**, **5.2b** and **5.3b-c**). The calculated hfc's for the α - and β -muoniated radicals are listed in Tables 5.5-8 and compared with the experimental values.

Table 5.5: Calculated hyperfine coupling constants^{a,b,c} (MHz) for the possible radicals formed by Mu addition to the imidazole ring of carbene **5.1**, and the experimentally determined hfcs at 298 K.

	5.1a ^d	5.1a ^e	5.1b	Expt.
A_{μ} ^f	278.84	246.43	402.75	246.43(2)
A_C (C2)	136.01	119.07	7.35	139.64(21)
A_N (N1)			3.96	
	8.32	8.17		13.73(4)
A_N (N3)			0.42	
A_p (CH ₃ C4) ^g			52.37	(82.88(3)) ^h
	0.75	0.80		
A_p (CH ₃ C5) ^g			-0.73	-

^a Proton hfc's for the isopropyl substituents are not reported. ^b UB3LYP/6-311G**//UB3LYP/EPR-III. ^c C-Mu bond length increased by 4.9%. ^d Minimum energy structure. ^e $\theta = 35.3^\circ$ to simulate vibrational averaging. ^f $A_{\mu} = A_p (\gamma_{\mu}/\gamma_p)$. ^g Average proton hfc in methyl group. ^h Rejected alternative assignment.

Table 5.6: Calculated hyperfine coupling constants^{a,b,c} (MHz) for the possible radicals formed by Mu addition to the imidazole ring of carbene **5.2**, and the experimentally determined hfcs at 298 K.

	5.2a ^{d,e}	5.2a ^{e,f}	5.2b	Expt.
A_{μ} ^g	340.05	286.69	422.35	286.69(7)
A_C (C2)	220.01	203.42	6.22	-
A_N (N1)			0.17	
	10.63	10.58		13.01(10)
A_N (N3)			3.70	
A_p (HC4)			132.69	(94.53(8)) ^h
	-1.48	-0.94		
A_p (HC5)			-43.6	-

^a Proton hfc's for the mesityl substituents are not reported. ^b UB3LYP/6-31G//UB3LYP/EPR-II. ^c C-Mu bond length increased by 4.9%. ^d Minimum energy structure. ^e Mesityl rings fixed perpendicular to the N1-C2-N3 plane. ^f $\theta = 35.3^\circ$ to simulate vibrational averaging. ^g $A_{\mu} = A_p (\gamma_{\mu}/\gamma_p)$. ^h Rejected alternative assignment.

Table 5.7: Calculated hyperfine coupling constants^{a,b,c} (MHz) for the possible radicals formed by Mu addition to the triazole ring of carbene **5.3**, and the experimentally determined hfcs at 298 K.

	5.3a ^d	5.3a ^e	5.3b	5.3c	Expt.
A_{μ} ^f	244.97	164.08	333.20	380.01	164.08(8)
$A_C(C5)$	199.87	169.66	-2.67	1.72	-
$A_N(N1)$	8.87	8.60	3.28	3.67	8.65(23) ^g
$A_N(N2)$	1.45	1.39	13.30	27.86	
$A_N(N4)$	6.86	5.66	0.50	2.86	

^a proton hfcs for the phenyl rings are not reported. ^b UB3LYP/6-31G//UB3LYP/EPR-II. ^c C-Mu bond length increased by 4.9%. ^d minimum energy structure. ^e $\theta = 34.1^\circ$ to simulate vibrational averaging. ^f $A_{\mu} = A_p(\gamma_{\mu}/\gamma_p)$. ^g Possibly two overlapping resonances.

Table 5.8: Calculated hyperfine coupling constants^{a,b,c} (MHz) for the radical **5.4a** and the experimentally determined muon hfc at 298 K.

	5.4a ^{d,e}	5.4a ^{e,f}	Expt.
A_{μ} ^g	258.78	114.43	114.43(4)
$A_C(C2)$	228.81	170.66	-
$A_N(N1)$	9.12 ^h	9.18 ^h	-
$A_N(N3)$			
$A_p(H_2C4)$	12.61 ^h	12.05 ^h	-
$A_p(H_2C5)$			

^a Proton hfc's for the mesityl substituents are not reported. ^b UB3LYP/6-31G//UB3LYP/EPR-II. ^c C-Mu bond length increased by 4.9%. ^d Minimum energy structure. ^e Mesityl rings fixed perpendicular to the N1-C2-N3 plane. ^f $\theta = 27.35^\circ$ to simulate vibrational averaging. ^g $A_{\mu} = A_p(\gamma_{\mu}/\gamma_p)$. ^h Averaged hfc due to rapid inversion.

5.4.3 Discussion

A comparison of the experimental and calculated hyperfine coupling constants shows that the observed radicals were undoubtedly the α -muoniated radicals **5.1a-4a**. The calculated

muon hfcs for the α -muoniated radicals matched the experimental values, once vibrational averaging at the radical centre was taken into account, while the calculated muon hfcs for the β -muoniated radicals were much larger than the experimental values. The calculated nitrogen hfcs of **5.1a-3a** were in reasonable agreement with the experimental nitrogen hfcs, whereas the alternate assignment of the relevant μ LCR resonances gives proton hfcs that are completely unacceptable. Furthermore, the ^{13}C resonance that was observed for the 40% isotopically enriched sample of **5.1** could only arise from radical **5.1a**. The assignment of the observed radicals was supported by the theoretical calculations that found that the α -muoniated radicals are the lowest energy products and that there is no activation barrier for addition of Mu to the carbeneic carbon. The calculated nitrogen hfc for **5.4a** should have fallen into the range that was studied in the μ LCR experiment but the reason for its elusiveness is not known.

5.5 Vibrational motion of α -muoniated radicals

As is evident from the preceding sections, hyperfine coupling constants are very sensitive to the geometry of a radical. Vibrational motion can affect the hfc so measurement of the temperature dependence of hfcs is a powerful way to probe the internal dynamics of a radical [70], information that generally cannot be obtained by any other experimental technique. Studies of the temperature dependence of the hyperfine coupling in the muoniated isotopomers of the *tert*-butyl [120] and cyclohexadienyl radicals [152] has provided valuable information about torsional motion and the effects due to the light mass of the muon.

Often the relationship between the temperature dependence of hfcs and the vibrational motion of the radical is complex and difficult to interpret. Structurally similar radicals can in some cases exhibit substantially different behaviour [164]. The greatest success has been for radicals in which a single vibrational mode dominates in altering the hfcs. In the case of the muoniated ethyl and *tert*-butyl radicals, it was rotation about the C-C bond that had the largest effect. The temperature dependence of α -protons is generally assumed to be dominated by the out-of-plane or inversion vibration at the radical centre [70]. Barone and coworkers have had considerable success in modeling vibrational

averaging effects on the hfc's of small organic radicals [155,157,165,166]. The potential for the out-of-plane vibrational mode is constructed by optimizing the geometry of the radical as a function of the out-of-plane angle, θ . The potential ($V(\theta)$) is used to obtain the vibrational wavefunctions and eigenvalues from the one-dimensional Schrödinger equation,

$$\left[\frac{-\hbar^2}{2m_r} \frac{\partial^2}{\partial \theta^2} + V(\theta) \right] \psi_j = E_j \psi_j \quad (5.1)$$

where Ψ_j and E_j are the wavefunction and energy of the j^{th} vibrational level. The wavefunctions and the angular variation of the hfc ($A(\theta)$) are used to determine the vibrationally averaged hfc for a vibrational level.

$$\langle A \rangle_j = \frac{\int \Psi_j^* A(\theta) \Psi_j d\theta}{\int \Psi_j^* \Psi_j d\theta} \quad (5.2)$$

The temperature dependence of the hfc's arises from population of vibrational levels that have different averaged hfc values. If one assumes a Boltzmann population of the vibrational levels, the temperature dependence of the hfc's is given by

$$A(T) = \frac{\sum_j \langle A \rangle_j \exp[-(E_j - E_0)/kT]}{\sum_j \exp[-(E_j - E_0)/kT]} \quad (5.3)$$

A drawback to this approach to modeling vibrational averaging effects is that numerous calculations are required to define the potential. As a consequence, all of the radicals studied by Barone and coworkers have been fairly small. The largest ones to have been studied were the radicals formed by hydrogen atom addition to cytosine [167] and thymine [168]. Radicals **5.1-3a** are much larger and more difficult to model due to the numerous substituents and degrees of freedom.

In view of previous experimental and theoretical results that have indicated that the out-of-plane mode dominates the temperature dependence behaviour of the α -proton, I have

attempted to model the effect of this motion on the muon hfc of radicals **5.1a-3a**. Modelling of the vibrational motion of **5.4a** was not attempted as the temperature dependence of A_μ was not determined experimentally. The size of the molecules did not allow for calculations as rigorous as those of Barone *et al.* Instead, I have sought to understand *qualitatively* why radicals with fairly similar structures have very different temperature dependence behaviour.

5.5.1 Inversion potentials of radicals 5.1a-3a

The geometries of the radicals **5.1a-3a** were optimized as a function of the out-of-plane angle at the same level as described in section 5.4.2.1. It was not possible to calculate the hfcs with the EPR-II/III basis sets, or to include solvent models, because of the large number of calculations required. The mesityl rings of **5.2a** were fixed perpendicular to the N1-C2-N3 plane while no constraints were placed upon the orientation of the phenyl rings of **5.3a**.

The potential for the out-of-plane vibration at the radical centre of **5.1a** is coupled to inversion at the adjacent nitrogen atoms. In the minimum energy geometry the isopropyl rings are on the same side of the imidazole ring and on the opposite side to the muon. Inversion occurs at one of the nitrogen atoms when the out-of-plane angle at the radical centre is less than approximately -10° (starting from the minimum energy geometry where $\theta = 40.4^\circ$). This results in the isopropyl groups being on opposite sides of the imidazole ring. Inversion occurs at the second nitrogen atom when θ is less than -15° . This coupling to the inversion at the nitrogen atoms results in a double-well potential that is slightly asymmetric about $\theta = 0^\circ$, with an inversion barrier at approximately $\theta = -5^\circ$ (See Figure 5.13). The nitrogen atoms of **5.2a** are less pyramidal than those of **5.1a** and the double-well potential is less asymmetric. However, it is likely that for both of these radicals vibrational averaging of the other vibrational modes will result in a potential that is symmetric about $\theta = 0^\circ$. The calculated inversion potential for **5.3a** was found to be asymmetric about $\theta = 0^\circ$ due to the dependence of the energy on the orientation of the phenyl rings. At room temperature there should be sufficient torsional motion of the

phenyl rings for the potential to be averaged and produce a symmetric double-well. The inversion barriers for **5.1a-3a** are listed in Table 5.9.

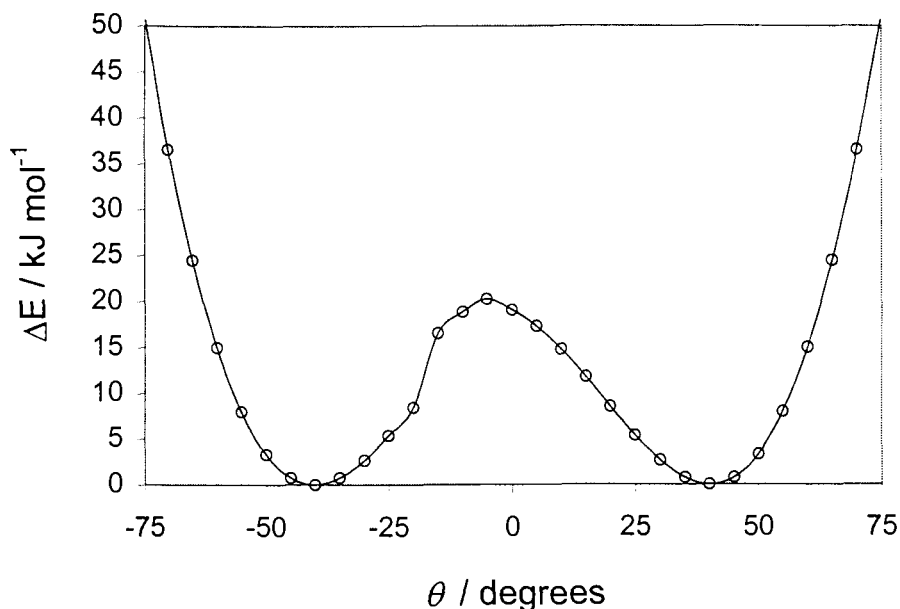


Figure 5.13: Calculated potential (UB3LYP/6-311G**) for the out-of-plane vibrational mode of **5.1a**.

Table 5.9: Inversion barrier heights^a for the out-of-plane vibration at the radical centre for radicals **5.1a-3a**.

Radical	$E^{\text{barrier}} / \text{kJ mol}^{-1}$
5.1a	20.22
5.2a	24.51
5.3a^b	12.33

^a Calculations performed at the UB3LYP/6-311G** level for radical **5.1a** and at the UB3LYP/6-31G level for radicals **5.2a-3a**. ^b Averaged inversion barrier.

5.5.2 Angular variation of hfc's in radicals **5.1a-3a**

The hyperfine coupling constants of the radicals are very sensitive to the geometry at the radical centre. The muon hfc is negative for small out-of-plane angles due to polarization of the C-Mu bond by the unpaired electron [74] and positive for large out-of-plane angles due to hyperconjugation [169]. The ¹³C hfc is positive and increases in magnitude as the

radical centre becomes more pyramidal [170]. The nitrogen hfc decreases by a small amount as the out-of-plane angle increases.

5.5.3 Vibrational wavefunctions

The vibrational wavefunctions for the out-of-plane mode consist of pairs of closely spaced or ‘inversion-doubled’ levels [171]. The splitting between inversion-doubled levels is closely related to the energy of the levels with respect to the inversion barrier. The splitting is small for vibrational levels that are below the barrier and greatly increases for levels that are near to or above the barrier. The shapes of the wavefunctions are also strongly related to the relative energies of the levels and barrier. For levels below the barrier the wavefunctions of the lowest pair of vibrational levels resemble harmonic oscillator wavefunctions centred on each well, and are very similar in shape. This is the situation for most non-muoniated radicals, which usually have several inversion-doubled pairs below the barrier. In contrast, the large out-of-plane vibrational frequency for muoniated radicals (2324 cm^{-1} for **5.1a** at the UB3LYP/6-311G** level) can result in situations where the energy of the vibrational levels is similar to that of the inversion barrier. In cases where the levels have similar or greater energies than the inversion barrier, the vibrational wavefunctions resemble distorted harmonic oscillator functions. The lower level has a significant contribution from small out-of-plane angles, and this results in the averaged hfc for this level being much smaller than that of the upper level. The large frequency of the out-of-plane vibrational mode for muoniated radicals means that there is no significant population of the second inversion-doubled pair of levels.

The magnitude of the muon hfc is expected to increase with increasing barrier height due to the decrease of contributions from small out-of-plane angles to the lower vibrational level. This is in agreement with the relative magnitudes of the A_μ values and the calculated inversion barriers for **5.1a-3a**. The muon and ^{13}C hfc are predicted to have a positive temperature dependence and the ^{14}N hfc is predicted to have a negative temperature dependence, for barriers that are of similar energy, or greater energy, than the ground vibrational level. This is because the lower vibrational level will always have a higher probability of being at small out-of-plane angles, since it can be thought of as the symmetric combination of two harmonic oscillator, while the upper vibrational level is

the asymmetric combination of the same harmonic oscillator functions and this leads to a node at $\theta = 0^\circ$. Larger barrier heights lead to a decrease in the difference between the averaged hfcs of the upper and lower vibrational levels, and this leads to a decrease in the magnitude of the temperature dependence.

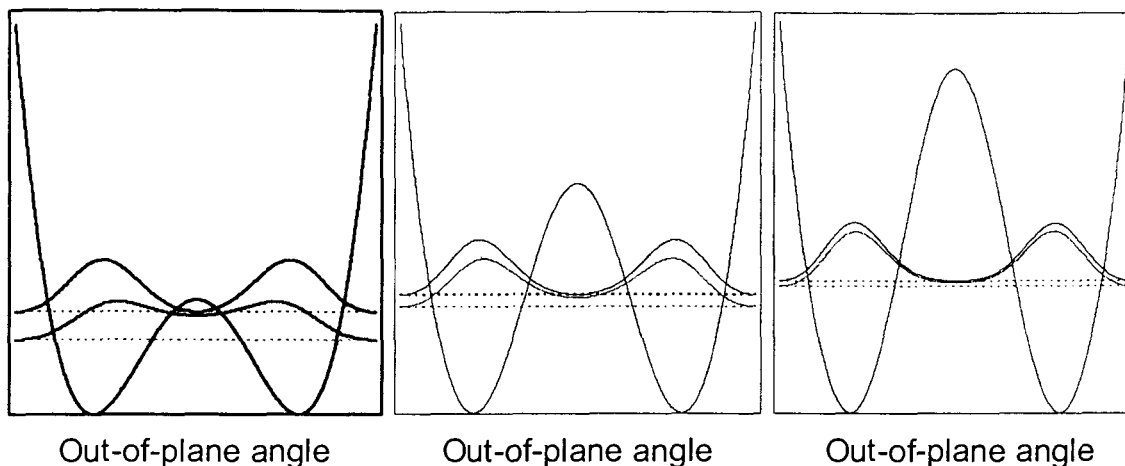


Figure 5.14: Square vibrational wavefunctions for symmetric double-welled potentials with different inversion barriers.

The experimental data for **5.3a** was fitted to equation 5.3 assuming that only one inversion-doubled pair of levels was significantly occupied, and the fitted values are listed in Table 5.10. The large difference between the averaged hfcs of the first and second level and the fairly large energy gap between the pair of levels suggests that the barrier to inversion of this radical is of similar energy to the occupied vibrational levels.

Table 5.10: Fitted parameters for the lowest inversion-doubled pair of levels of radical **5.3a**.

Parameter	Value ^a
A_μ^0	50.39(4) MHz
A_μ^1	365.45(6) MHz
ΔE	1.417(1) kJ mol ⁻¹

^a Statistical uncertainties are shown in parenthesis.

The negative temperature dependence of A_μ for radicals **5.1a** and **5.2a** cannot be explained by only considering the out-of-plane vibration at the radical centre, except for inversion barriers that are much smaller than calculated values. One possibility is that the slight asymmetry of the potential plays a more important role than previously thought, but this is considered unlikely. The levels will still be grouped into inversion-doubled pairs and the lowest wavefunction should have significant contributions from small out-of-plane angles. It is expected that the averaged muon hfc for the ground vibrational level would still be smaller than that of the first excited level. Another possibility is that the heights of the inversion barriers were over-estimated by the quantum calculations. This is unlikely as the barrier would have to be very small and this would cause the vibrationally averaged muon hfc to be much smaller than what was observed experimentally. A more likely explanation is that the negative temperature dependence for A_μ in these radicals is due to the influence of another vibrational mode. The likely candidate is inversion at the nitrogen atoms adjacent to the radical centre, as this motion was found to be coupled with the out-of-plane vibration at the radical centre. This motion is not important for **5.3a** because the nitrogen atoms adjacent to the radical centre are nearly planar.

The geometry of radical **5.1a** was re-optimized with the nitrogen atoms constrained to a planar geometry. The calculated hyperfine parameters in this geometry are $A_\mu = 391.98$ MHz, $A_C = 206.44$ MHz and $A_N = 13.26$ MHz at the UB3LYP/6-311G**//UB3LYP/EPR-III level. All of these values are larger than those obtained from the minimum energy geometry. The inversion potential will be a double-well potential and the vibrational wavefunctions should resemble those shown in Figure 5.13. Since the hfc's are larger for small out-of-plane angles at the nitrogen atoms, the averaged hfc of the lowest vibrational level should be larger than that of the first excited level, leading to a negative temperature dependence for A_μ , A_C and A_N . While this could explain the temperature dependence of the muon hfc it does not explain the increase in A_C with temperature. Vibrational averaging due to inversion at the nitrogen atoms could also be responsible for the experimental A_N values being larger than the calculated values for **5.1a-2a**.

5.6 Future work

There are numerous avenues for future work. An obvious goal would be to measure the temperature dependence of the muon hfc for **5.4a** and the ^{14}N hfc for **5.1a-4a**. The nitrogen hfc are particularly important as they may provide evidence that it is inversion at the nitrogen atoms that is affecting the hfc, or another unconsidered mechanism. Modelling of the vibrational motion in the manner described in this chapter, even at a higher level, is likely to have limited success due to the likelihood of coupling between vibrational modes that influence the hfc. Ab initio / molecular dynamics calculations might be suitable to model the effects of numerous coupled vibrational modes, but at present these studies have been limited to fairly small radicals [172].

A more far reaching goal would be to study the reaction of Mu with carbenes that are not stable under normal conditions. A possible experiment would involve generation of carbenes in an inert matrix that would be irradiated by a muon beam and hopefully generate a wide variety of novel α -muoniated radicals. It would be of great interest to study simpler α -muoniated radicals where more quantifiable information could be obtained. It would also be interesting to study the reaction of muonium with carbene-like systems, such as silylenes and germylenes.

5.7 Conclusions

Muonium adds exclusively to the carbeneic carbon of stable singlet carbenes to produce α -muoniated radicals. The structures of the radicals were assigned by comparing the experimental hyperfine coupling constants with values for the possible structures obtained from density functional theory calculations that empirically included vibrational averaging and solvation effects. The assignment of the radicals was supported by calculations of the energies of the possible products and the barriers to addition of Mu. The temperature dependence of the muon hfc of the 5-muono-1,3,4-triphenyl-1,2,4-triazol-5-yl (**5.3a**) radical could be explained by population of vibrational levels of the out-of-plane mode, while the behaviour of the other radicals suggests that other vibrational modes are important, particularly inversion at the nitrogen atoms adjacent to the radical centre.

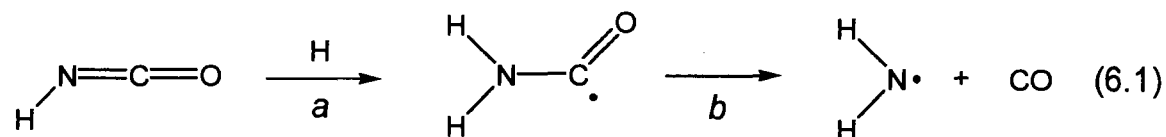
CHAPTER 6.

DETECTION OF MUONIATED ACYL AND THIOACYL RADICALS

6.1 Introduction

The initial goal of this project was to generate muoniated aminyl radicals in order to study the effect of isotopic substitution on the vibrational motion of nitrogen-centred radicals. The only nitrogen-centred muoniated radical to have been previously reported is the *N*-muono-pyridinyl radical, which forms by the reaction of Mu with pyridine [173]. We sought to produce muoniated aminyl radicals via the indirect formation route [174] by targeting molecules that contain the isocyanate functional group. This functional group was chosen because there is evidence that hydrogen atoms react with the isocyanate moiety to produce aminyl radicals [175,176,177,178].

Mertens *et al.* studied the kinetics of the reaction of H with isocyanic acid (HNCO), the simplest isocyanate, in a shock-heated mixture of HNCO in argon between 2340 and 3270 K [175]. The experimental results were consistent with the following reaction sequence.



The hydrogen atom adds to the nitrogen atom of HNCO, producing the amine-substituted acyl (or carbamoyl) radical H₂NCO. The H₂NCO radical rapidly dissociates to the amidogen radical (NH₂) and carbon monoxide. Subsequent theoretical studies by Miller and Melius [176], Nguyen *et al.* [177] and Ma *et al.* [178] confirmed that addition of H to the N of HNCO is the preferred reaction route. Energetically, the H₂NCO radical is the global minimum for reaction 6.1, but this species is short-lived because it is produced in a vibrationally excited state, mainly as a result of the exothermic nature of its formation, and rapidly dissociates.

In contrast, there is experimental evidence that suggests that the H + HNCO reaction does not always lead to the formation of NH₂, particularly when the reaction is performed under different experimental conditions. Petterson *et al.* studied the H + HNCO reaction in a Xe matrix by means of Fourier transform infra-red (FTIR) spectroscopy [179]. Mobile hydrogen atoms were produced by annealing the UV photolysed HNCO/Xe matrix at 50 K. The presence of hydrogen atoms was confirmed by the observation of lines in the FTIR spectrum resulting from the presence of such exotic species as HXeH, HCO, HXeCN, HXeNC and HXeNCO. In addition, new peaks were observed in the FTIR spectrum at 3518.5, ~1800 (quartet), 1555.8 and 1214.4 cm⁻¹. These lines were assigned to the H₂NCO radical and the assignment was corroborated by theoretical calculations. These experimental values correspond well with the fundamental vibrational frequencies of the H₂NCO radical, calculated at the UMP2/6-311++G(3df,3pd) level of theory (3776.4, ~1884.6 (quartet), 1618.3 and 1240.6 cm⁻¹). The amidogen radical, whose fundamental vibrational frequencies are 1499 and 3220 cm⁻¹ [180], was not observed. It is possible that H₂NCO did indeed dissociate to NH₂ and CO, but because these products were kept in close proximity by the matrix, they may have reacted to reform H₂NCO once the excess energy had dissipated. It is also possible that the H₂NCO radical did not decompose because the excess vibrational energy was dissipated by interaction with the matrix.

Given the different results for the H + HNCO reaction under different experimental conditions, it was unclear how Mu would react. A further complication is the choice of the target molecule for the μ SR experiments. Isocyanic acid was not used as a target because it is difficult to work with and is not commercially available. Instead, *tert*-butylisocyanate was used because it is commercially available, relatively stable and a liquid at room temperature. Unfortunately, it was impossible to predict whether an aminyl or an acyl radical would be observed because not only would replacing a hydrogen with a *tert*-butyl group potentially change the thermodynamics of the reaction, but also the reaction would be studied under different experimental conditions from previously published experiments.

The possibility that a muoniated acyl radical could form led us to extend the scope of this study. We chose to study the reaction of Mu with the closely related isothiocyanate functional group. The analogous reaction of hydrogen atoms has not been reported. It was expected that addition of Mu would occur at the nitrogen of the isothiocyanate functional group, and that the resulting thioacyl radical would not dissociate because CS is a poorer leaving group than CO. The target chosen for the μ SR studies was *tert*-butylisothiocyanate because it is similar to the isocyanate compound studied, it is commercially available and it is a liquid at room temperature.

The interest in muoniated acyl radicals is due to the unusual structure of these radicals. Acyl radicals contain a C=O group with the unpaired electron localized on the carbon in a σ orbital. The thioacyl radical is identical except that the oxygen atom has been replaced by sulphur. While acyl radicals have been extensively studied by EPR ([181] and references therein), no acyl or thioacyl radicals have been observed directly by μ SR. Indeed, very few muoniated radicals with the unpaired electron in a σ orbital have been studied by μ SR. The rarity of muoniated acyl radicals makes them an attractive target for study.

The simplest acyl radical is the formyl radical, HCO, which has been studied by EPR [182], even in the gas phase [183]. In contrast, the muoniated isotopomer (MuCO) has not been observed directly, although there is indirect evidence that MuCO is formed by the reaction of Mu with CO. The existence of this species was inferred from the decay of the muon polarization in pure CO gas in longitudinal applied magnetic fields [184]. The decay of the muon polarization was determined to be the result of very fast spin relaxation in the MuCO radical, which would broaden the spectral lines in a TF- μ SR spectrum beyond detection. Cox *et al.* proposed that the fast spin relaxation is due to modulation of the hyperfine coupling at the muon by vibrational motions [185]. Another explanation, which arose from theoretical calculations by Claxton and Cox [186] and Webster [187], is that MuCO is more weakly bound than HCO and the rapid spin relaxation is due to the MuCO radical dissociating. At present, there is no definitive experimental evidence to support either assertion.

Vinyl radicals are closely related to acyl radicals, with both having the unpaired electron in a σ orbital. Only two muoniated radicals with the unpaired electron in a sigma orbital have been observed. The 2-methyl-4-muono-but-2-en-3-yl radical was formed by the addition of Mu to the terminal carbon of 1,1-dimethylallene [188]. The muon is located in a pseudo-methyl group that is attached directly to the radical centre. The position of the muon means that inversion at the radical centre does not result in modulation of the hyperfine coupling at the muon and fast spin relaxation, as in MuCO. The 1,2-bis(trimethylsilyl)-1-muono-2-ethenyl radical was formed by Mu addition to bis(trimethylsilyl)ethyne [189]. Most of the radicals produced by the addition of Mu to a molecule containing a $C\equiv C$ bond [189,190] are not σ radicals. The radical centre is linear due to interactions with the phenyl and trimethylsilyl substituents and the unpaired electron is in a π molecular orbital. The radical centre of the 1,2-bis(trimethylsilyl)-1-muono-2-ethenyl radical is bent due to the steric interactions between the two large trimethylsilyl groups.

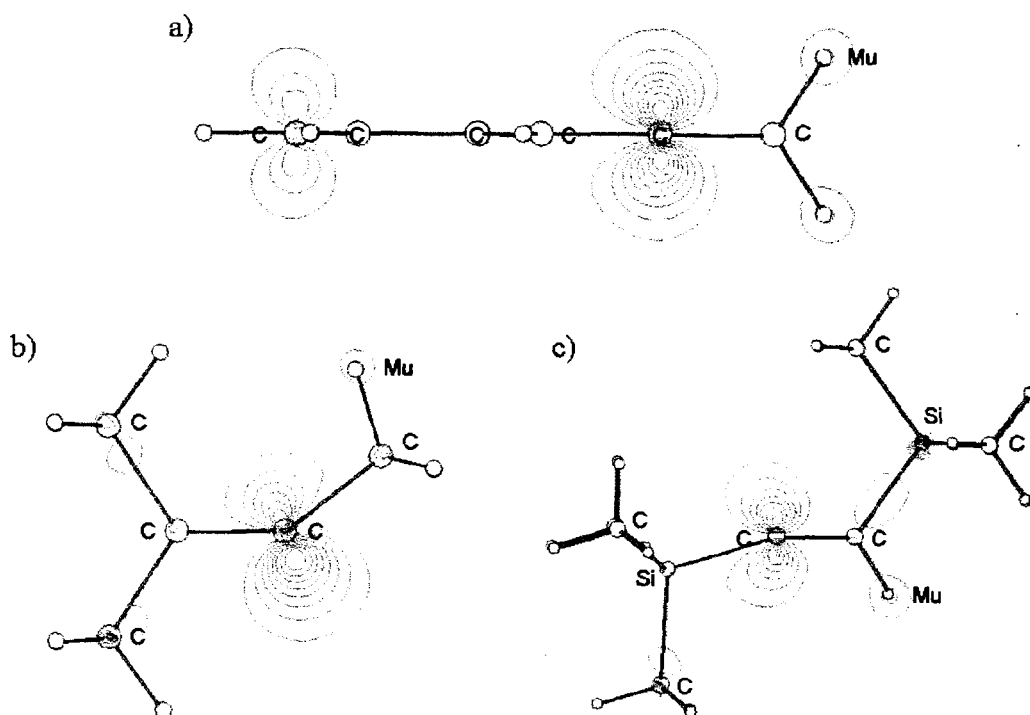


Figure 6.1: Structure and unpaired electron spin density in the a) 2-muono-1-phenyl-1-ethenyl, b) 2-methyl-4-muono-but-2-en-3-yl and c) 1,2-bis(trimethylsilyl)-1-muono-2-ethenyl radicals. (UB3LYP/6-311G)

6.2 Experimental

tert-Butylisocyanate (b.p. 358-359 K) and *tert*-butylisothiocyanate (m.p. 283.6-284.6 K) were purchased from Aldrich Chemicals and used without further purification. The liquids were transferred to stainless steel cells for the μ SR experiments in a glove bag with an argon atmosphere to prevent hydrolysis. The samples were subjected to several cycles of freezing, pumping and thawing to remove dissolved oxygen, and then flame sealed. The samples were stored under an argon atmosphere in order to minimize the danger of oxygen contamination. The TF- μ SR and μ LCR experiments were performed on the M20 beam line at TRIUMF with the HELIOS spectrometer. The details for these experiments are described in Chapter 2.

6.3 Results

Only one type of radical was observed in the TF- μ SR spectrum upon irradiation of *tert*-butylisocyanate with positive muons. The muon hfc (A_μ) was determined from the difference of the radical precession frequencies. The TF- μ SR spectrum was obtained at 274, 298 and 322 K and the corresponding A_μ values are listed in Table 6.1. The TF- μ SR spectrum obtained at 298 K is shown in Figure 6.2.

The μ LCR spectrum was obtained at 298 K. A resonance was observed at 7586.4(16) G with a width of 91.0(38) G. This resonance is consistent with a ^{14}N nucleus with a nitrogen hfc (A_N) of 58.69(31) MHz. The μ LCR spectrum is shown in Figure 6.3.

Table 6.1: Muon hfc (MHz) and relaxation rates (μs^{-1}) of the Mu adduct of *tert*-butylisocyanate between 274 and 322 K.

Temperature / K	A_μ / MHz	λ / μs^{-1}
274	261.33(13)	2.84(43)
298	261.19(31)	4.22(98)
322	260.87(30)	5.28(94)

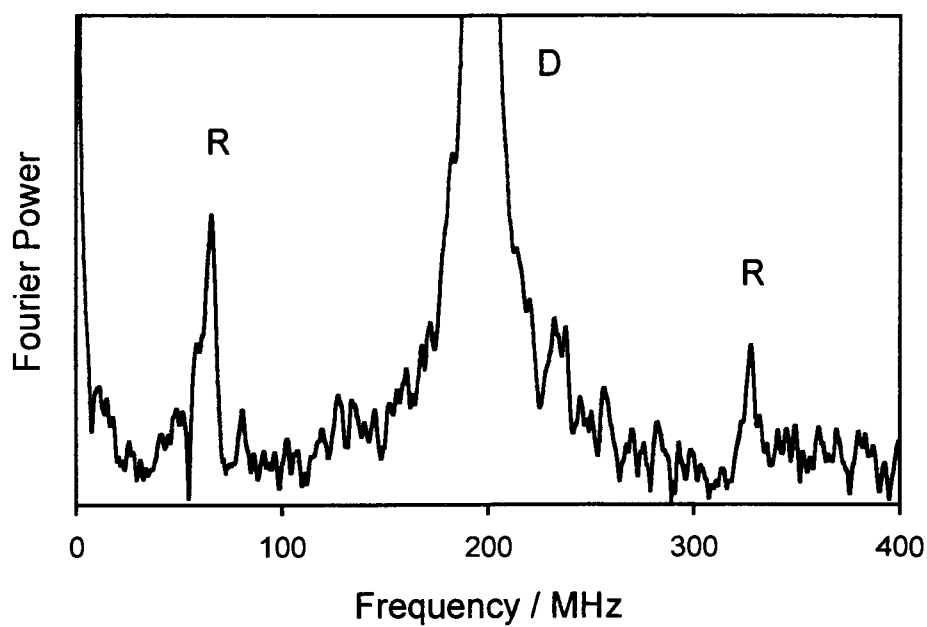


Figure 6.2: TF- μ SR spectrum of *tert*-butylisocyanate at 298 K and an applied magnetic field of 14.5 kG.

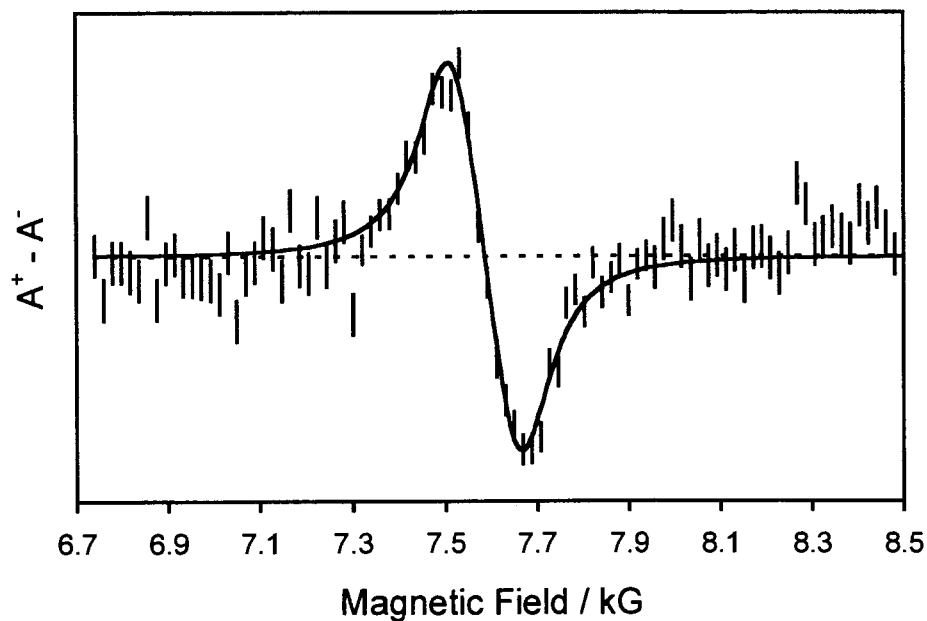


Figure 6.3: μ LCR spectrum of *tert*-butylisocyanate at 298 K.

Two types of radicals were observed in the TF- μ SR spectrum upon the reaction of Mu with *tert*-butylisothiocyanate. Both of these radicals relaxed very rapidly, making observation extremely difficult. The existence of the radicals was confirmed by repeating the TF- μ SR experiment at a different magnetic field and observing that the radical precession frequencies shifted accordingly. TF- μ SR spectra were obtained at four temperatures between 266 and 298 K and the results are listed in Table 6.2 and the spectra at 266 K in applied magnetic fields of 12 and 15 kG are shown in Figure 6.4. No resonance was observed between the fields of approximately 1500 and 15000 G in the μ LCR spectrum at 288 K.

Table 6.2: Muon hfc's (MHz) and relaxation rates (μs^{-1}) for the Mu adducts of *tert*-butylisothiocyanate.

Temperature / K	$A_{\mu}(1)$ / MHz	$\lambda(1)$ / μs^{-1}	$A_{\mu}(2)$ / MHz	$\lambda(2)$ / μs^{-1}
266	100.65(81)	35.79(41)	334.72(27)	9.45(83)
278	115.04(80)	25.36(40)	315.75(59)	7.0(18)
288	118.08(70)	25.98(45)	318.43(29)	2.93(90)
298	121.4(12)	15.28(36)	314.44(26)	2.37(81)

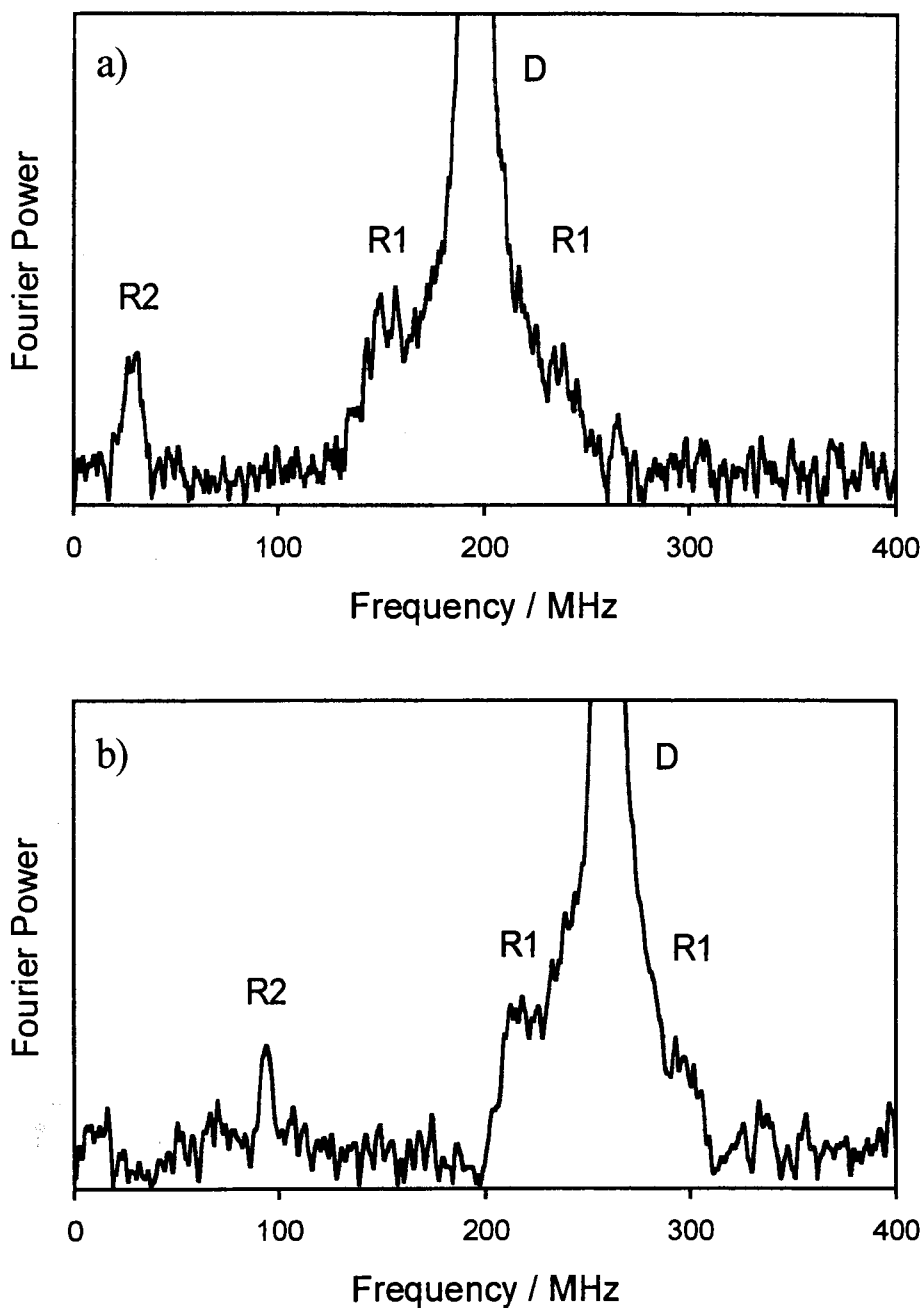


Figure 6.4: TF- μ SR spectra of *tert*-butylisocyanate at 266 K and applied magnetic fields of a) 14.5 kG and b) 19.3 kG.

6.4 Assignment of observed radicals

There are as many as six reactions that could be involved in the addition of Mu to either *tert*-butylisocyanate (6.1) or *tert*-butylisothiocyanate (6.2). These reactions, which are shown in Figure 6.5, could result in the formation of up to four types of radicals for each

target. Several of these radicals have two conformers with different spectroscopic properties, as a result of the partial double bond character of the C-N bond. These conformers have been labelled using the *E* and *Z* nomenclature that is used for double bonds, with reference to the relative positions of the *tert*-butyl group to the acyl (or thioacyl) group. The dihedral angle between the *tert*-butyl group and the acyl group is defined as 180 degrees for the *E* conformer and 0 degrees for the *Z* conformer. The -H and -Mu labels refer to the isotopomer being discussed.

The large number of possible radicals and conformers makes the assignment of the observed radicals non-trivial. The assignment of the observed radical's structure is based upon a comparison of the reduced muon hfc ($A_{\mu}' = A_{\mu} \cdot \gamma_p / \gamma_{\mu}$) and other nuclear hfcs with values for the possible non-muoniated isotopomers determined by both EPR and quantum calculations. Not all of the possible oxygen-containing radicals have been studied by EPR, so, in some cases comparisons could only be made with radicals with similar structures. Very few thioacyl radicals have been studied by EPR, and those that have been have very different structures to the possible sulphur-containing radicals in this experiment. For these radicals, the assignment is based solely on a comparison of the experimental values with calculated values from quantum calculations. The hfcs for related oxygen-containing radicals determined by EPR are given in Table 6.3.

The geometries of all the radicals were optimised at the UB3LYP/6-311++G level of theory. The single point calculations of the hfcs were performed using the unrestricted B3LYP functional and the EPR-III basis set for the carbon, nitrogen and hydrogen atoms and the 6-311++G basis set for sulphur. The C-Mu bond length was increased by 4.9% for the single point calculations to mimic the larger zero-point energy in the C-Mu bond compared with the C-H bond [112]. The calculated hfcs are given in Table 6.4.

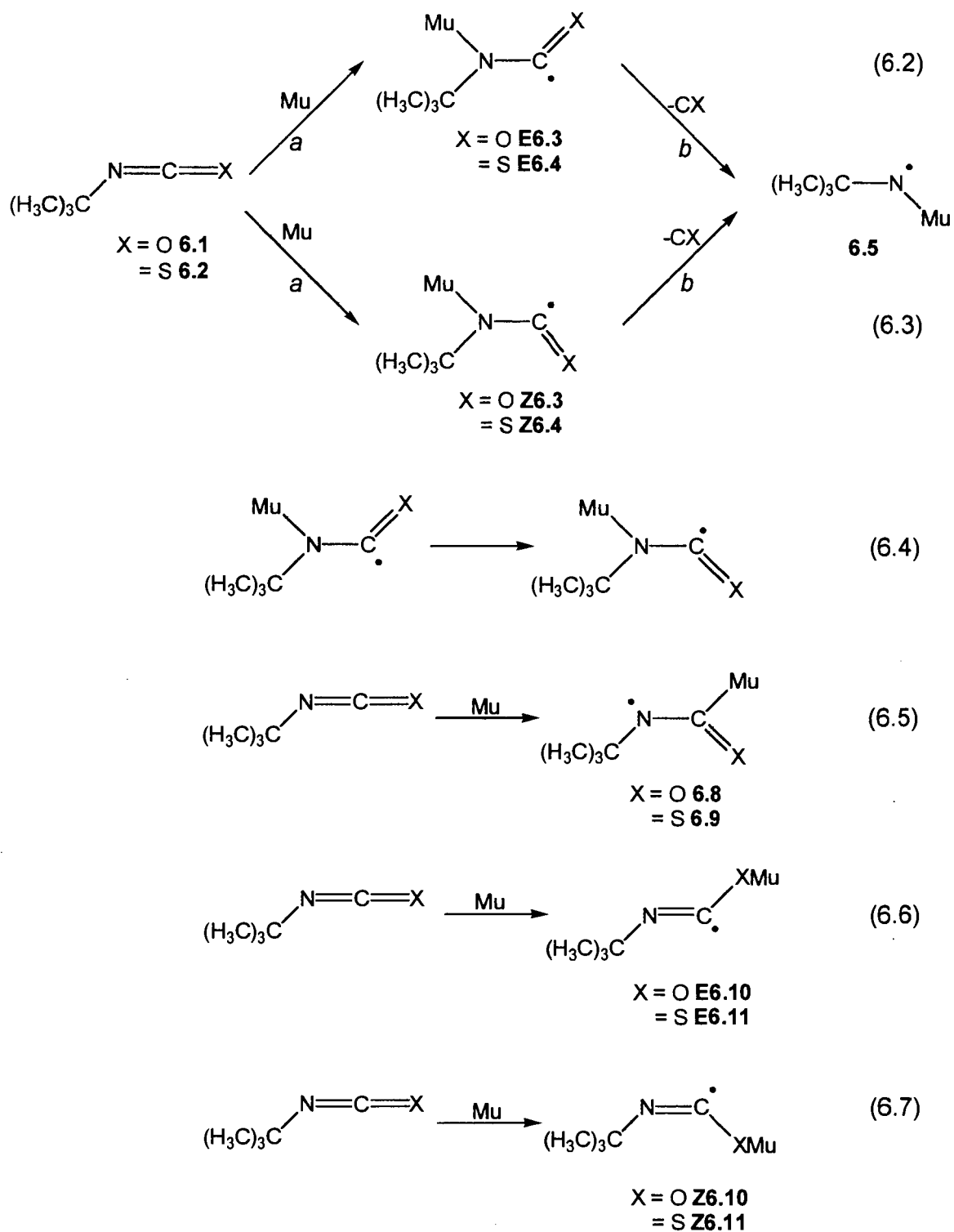
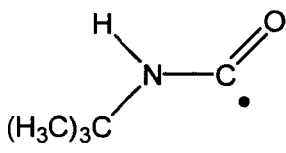
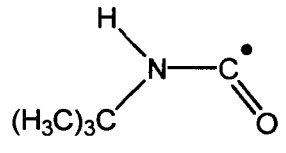
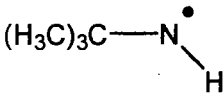
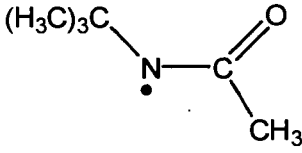
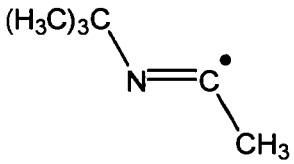


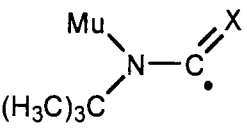
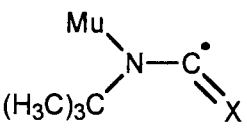
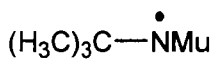
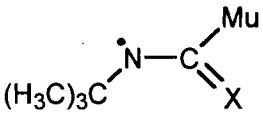
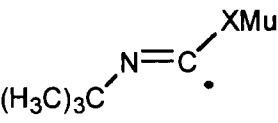
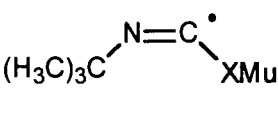
Figure 6.5: Reactions relevant to the addition of Mu to *tert*-butylisocyanate (X = O) and *tert*-butylisothiocyanate (X = S).

Table 6.3: Hfcs (MHz) of related radicals determined by EPR.

Radical	Hfc / MHz	Reference
 <p>E6.3-H</p>	<p>T = 214 K</p> <p>$A_p = 72.0^a$</p> <p>$A_N = 51.8^a$</p>	[191]
 <p>Z6.3-H</p>	<p>T = 214 K</p> <p>$A_p = 2.5^a$</p> <p>$A_N = 57.7^a$</p>	[191]
 <p>6.5-H</p>	<p>T = 77 K</p> <p>$A_p = 70(3)$</p> <p>$A_{\perp}(N) = 0(8)$</p> <p>$A_{//}(N) = 104(6)$</p> <p>$A_N^{iso} = 35(2)$</p>	[192]
 <p>6.12</p>	<p>T = 173 K</p> <p>$A_p^{methyl} = 6.7(0.8)$</p> <p>$A_N = 44.0(1.7)$</p>	[193]
 <p>6.13</p>	<p>T = 275 K</p> <p>$A_p^{methyl} = 6.7(2.2)$</p> <p>$A_N = 44.0(2.0)$</p>	
	<p>T = 172 K</p> <p>$A_p^{methyl} = 240^a$</p> <p>$A_N = 49.0^a$</p>	[194]

a) no errors reported.

Table 6.4: Calculated hfc (MHz) for all the possible radicals that could form by Mu addition to *tert*-butylisocyanate and *tert*-butylisothiocyanate.^a

Radical	Hfc / MHz	
	X = O	X = S
	E6.3-Mu $A_{\mu} = 299.5$ ($A_{\mu}' = 94.1$) $A_{\text{N}} = 68.3$	E6.4-Mu $A_{\mu} = 343.8$ ($A_{\mu}' = 108.0$) $A_{\text{N}} = 28.3$
	Z6.3-Mu $A_{\mu} = 9.1$ ($A_{\mu}' = 2.9$) $A_{\text{N}} = 60.9$	Z6.4-Mu $A_{\mu} = 127.0$ ($A_{\mu}' = 39.9$) $A_{\text{N}} = 19.1$
	6.5 $A_{\mu} = -193.2$ ($A_{\mu}' = -60.7$) $A_{\text{N}} = 31.8$	
	6.8^b $A_{\mu} = 54.0$ ($A_{\mu}' = 17.0$) $A_{\text{N}} = 36.1$	6.9^b $A_{\mu} = 141.1$ ($A_{\mu}' = 44.3$)
	E6.10 $A_{\mu} = -5.7$ ($A_{\mu}' = -1.8$) $A_{\text{N}} = 3.2$	E6.11 $A_{\mu} = -134.0$ ($A_{\mu}' = -42.1$) $A_{\text{N}} = 13.6$
	Z6.10 $A_{\mu} = 33.7$ ($A_{\mu}' = 10.6$) $A_{\text{N}} = 117.9$	Z6.11 $A_{\mu} = 3.2$ ($A_{\mu}' = 1.0$) $A_{\text{N}} = 3.6$

^a Only hfc greater than 5 MHz are reported for nuclei with abundant non-zero spin, except for the muon.

^b Only one minimum energy conformation was found.

The **Z6.3** radical was eliminated because the reduced muon hfc was much larger than the corresponding proton hfc, obtained from EPR experiments by Sutcliffe and Ingold [191]. It was not possible to eliminate any of the other structures based on a comparison with EPR data because the literature hfc are not entirely dissimilar to the hfc obtained in the μ SR experiments. Any differences could be explained by isotope effects due to the light

mass of the muon, by the EPR values being obtained at a different temperature, or by the effect of different substituents. The quantum calculations were used to eliminate the remaining possible structures. Radicals **6.8** and **6.10**, which are formed by the addition of Mu to the carbon or oxygen atoms of *tert*-butylisocyanate, respectively, have calculated hfc values that are substantially different from the experimental values, which allows for these possible structures to be eliminated. We had originally assigned the radical formed by Mu addition to **6.1** to be the muoniated *tert*-butylaminy radical (**6.5-Mu**) based on the agreement between the experimental values, UB3LYP/STO-3G calculations and the EPR values, the energetics of the H+HNCO reaction and that only one type of radical was observed [174]. We now consider this assignment to be in error after considering the signs of the hfc values, which are obtained from the density functional calculations. The position of the μ LCR resonance indicates that A_μ and A_N have the same sign while these hfc values have opposite signs in radical **6.5-Mu**. The observed radical is now assigned to be **E6.3-Mu** due to the good agreement between the experimental hfc values and the hfc values from EPR experiments [191] and quantum calculations.

The two radicals formed by Mu addition to *tert*-butylisothiocyanate correspond to the *E* and *Z* conformers of the *N-tert*-butylthiocarbamoyl radical (**6.4-Mu**) based on the similarities of the computed and experimental muon hfc values. Confidence in the assignment of the radicals would be greater if it was possible to compare another measured hfc value with the calculated values. Unfortunately this is not possible because the fast relaxation rate of the radical signals would broaden any resonance in the μ LCR spectrum beyond detection. Even repeating the experiments with ^{13}C labelled **6.2** would not result in a measurable resonance in the μ LCR spectrum.

6.5 Discussion and calculations

Radicals **6.3-Mu** and **6.4-Mu** are the first muoniated acyl and thioacyl radicals to be observed. The quantum calculations confirm that the majority of the unpaired spin density resides in a σ orbital on the acyl carbon. There is also a small amount of spin density on the neighbouring chalcogen atom. The singly occupied molecular orbitals (SOMO) of **E6.3**, **Z6.3**, **E6.4** and **Z6.4** are shown in Figure 6.6.

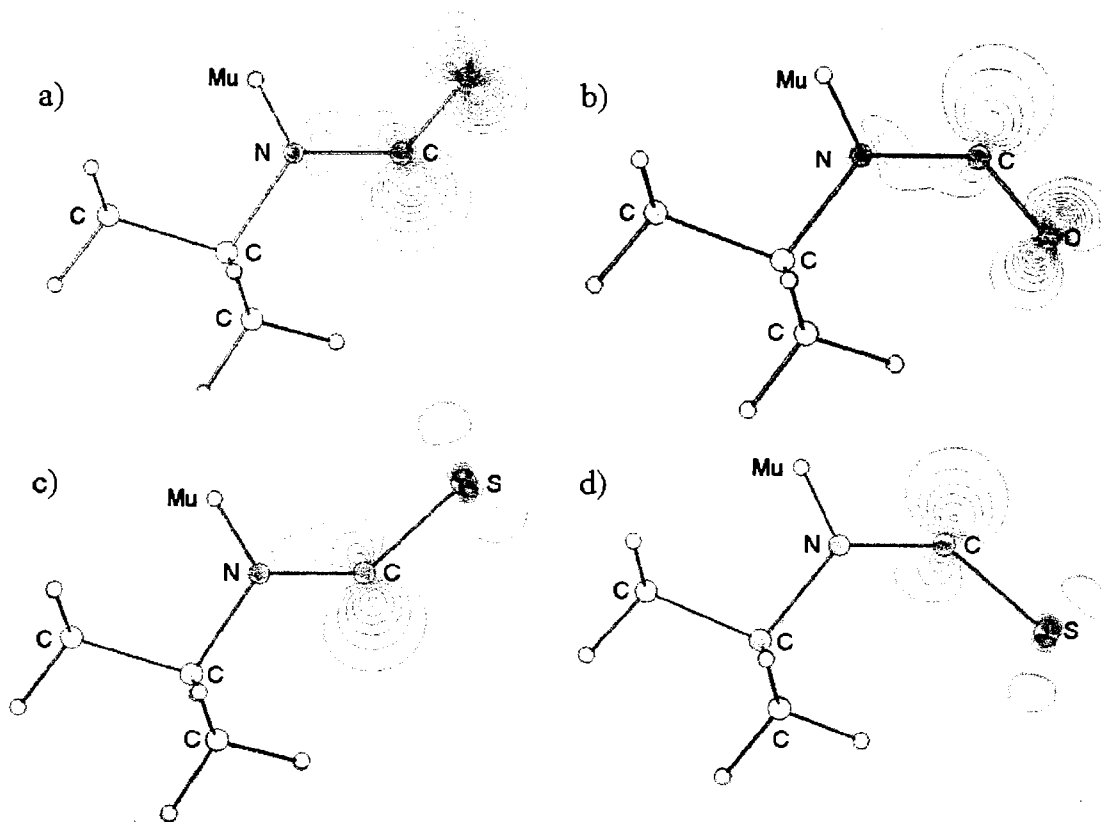


Figure 6.6: Structure and unpaired electron spin density in radicals a) *E6.3*, b) *Z6.3*, c) *E6.4* and d) *Z6.4* obtained from quantum calculations.

The approximation of 4.9% for the increase in the N-Mu bond length was used in the absence of any information on N-Mu bonds. The experimental values of A_μ and A_p (from EPR experiments at 214 K) for *E6.3* can be used to estimate the increase in the N-Mu bond compared with the corresponding N-H bond. The N-Mu bond is slightly longer than the N-H bond because of the higher zero-point energy due to the light mass of the muon and the anharmonic stretching potential. The longer N-Mu bond is more polarizable and this leads to greater spin density at the muon than at the proton. The ratio of the experimental reduced muon hfc and the proton hfc is 1.14. The hfcs are nearly independent of temperature for *E6.3-Mu*. Single point calculations at the UB3LYP/EPR-III level were performed as a function of the N-H bond length and it was found that the coupling at the H (or Mu) increases linearly with the bond length. The calculated hyperfine coupling constants were multiplied by a scaling factor of 0.892 so that the proton hfc for the optimized geometry matches the experimental value. The isotope effect of 14% was reproduced when the N-H bond was increased by 4.2% from

the optimized value. Single point calculations were performed on *E6.4-Mu* and *Z6.4-Mu* that included the scaling factor of 0.892 and the increased bond length of 4.2%. The resulting values (300.5 and 111.0 MHz, respectively) are in better agreement with the experimental values at 298 K than the previous calculated values.

Much like the reaction of H with HNCO, the reaction of Mu with **6.1** has occurred exclusively at the nitrogen atom. Quantum calculations were performed to model reactions 6.2, 6.3 and 6.4 in order to explain why *E6.3-Mu* was observed rather than *6.5-Mu*, why only one conformer of *6.3-Mu* was observed, and why the relaxation rates for the two conformers of *6.4-Mu* differ so greatly. Geometrical parameters of the equilibrium and transition state structures were calculated at the UB3LYP/6-311++G level. The energy was obtained from single point calculations on the UB3LYP-optimised geometry at the UMP2/6-311++G level. The zero point energies were calculated by a Frequency calculation at the UB3LYP/6-311++G level with a scaling factor of 0.89. The zero point energy was calculated for both the muon and proton isotopomers. The thermochemical values are listed in Table 6.5 and the relative energies are shown in Figure 6.7.

Addition of Mu to **6.1** or **6.2** proceeds solely by reaction 6.2a, generating the *E* conformers of radicals *6.3-Mu* and *6.4-Mu*, respectively. This is due to the geometry of the isocyanate and isothiocyanate functional groups, which are not linear, but have the terminal chalcogen atom bent away from the *tert*-butyl group. Mu attacks from the sterically unencumbered side of the molecule, towards which the O (or S) is directed, generating the *E* conformer. The *Z* conformer can form by rotation about the C-N double bond. Other processes that would connect the *E* and *Z* conformers, such as rehybridization at the acyl carbon, were considered but were found to be higher energy processes. The barriers to rotation about the C-N bond (TS4O-Mu and TS4S-Mu, respectively) are below the initial energy of *E6.3-Mu* and *E6.4-Mu*. For a short period after the formation of the radicals, there is rotation about the C-N bond until the excess energy is dissipated, trapping the molecule in either the *E* or *Z* conformation. The *Z6.3-Mu* radical was not observed because the muon hfc (9.1 MHz) is very small and the signal would likely relax rapidly, resulting in the signal being lost in the broad

diamagnetic signal due to muon stops in a magnetic component of the sample cell. The small muon hfc also prevents observation of a resonance in the μ LCR spectrum. The **Z6.4-Mu** radical was observed due to the larger muon hfc.

Table 6.5: The internal, zero point and total energy of the molecules and transition states of reactions 6.2, 6.3 and 6.4 for X = O and S.

Molecule	Energy ^{a,b} / Hartrees	Isotopomer	ZPE ^{a,c} / kJ mol ⁻¹	Total energy/ Hartrees
H	-0.4998098	H/Mu	-	-0.4998098
6.1	-325.0890219	-	353.209	-324.9544917
TS2aO	-325.573	H	358.422	-325.4366748
		Mu	369.303	-325.4325305
E6.3	-325.6268134	H	380.005	-325.4820773
		Mu	439.443	-325.4594382
Z6.3	-325.6295664	H	382.545	-325.4838628
		Mu	445.853	-325.4597501
TS2bO	-325.5810966	H	370.147	-325.4401151
		Mu	430.660	-325.4170670
6.5	-212.5198182	H	349.926	-212.3865384
		Mu	406.045	-212.3651638
CO	-113.0744536	-	13.278	-113.0693000
TS4O	-325.6045139	H	378.173	-325.4604754
		Mu	441.271	-325.4364426
6.2	-647.6645005	-	346.233	-647.5326273
TS2aS	-648.1544313	H	351.547	-648.0205343
		Mu	360.703	-648.0170467
E6.4	-648.2024159	H	374.877	-648.0596327
		Mu	434.966	-648.0367461
Z6.4	-648.2023320	H	376.757	-648.0588328
		Mu	439.966	-648.0347579
CS	-435.439099	-	7.783	-435.5824220
TS4S	-648.1989185	H	374.109	-648.0564280
		Mu	434.146	-648.0335609

^a Geometry optimization: UB3LYP/6-311G**. ^b Single point: UMP2/6-311G**. ^c Zero point energy determined from a Frequency calculation at the UB3LYP/6-311++G level with a scaling factor of 0.89.

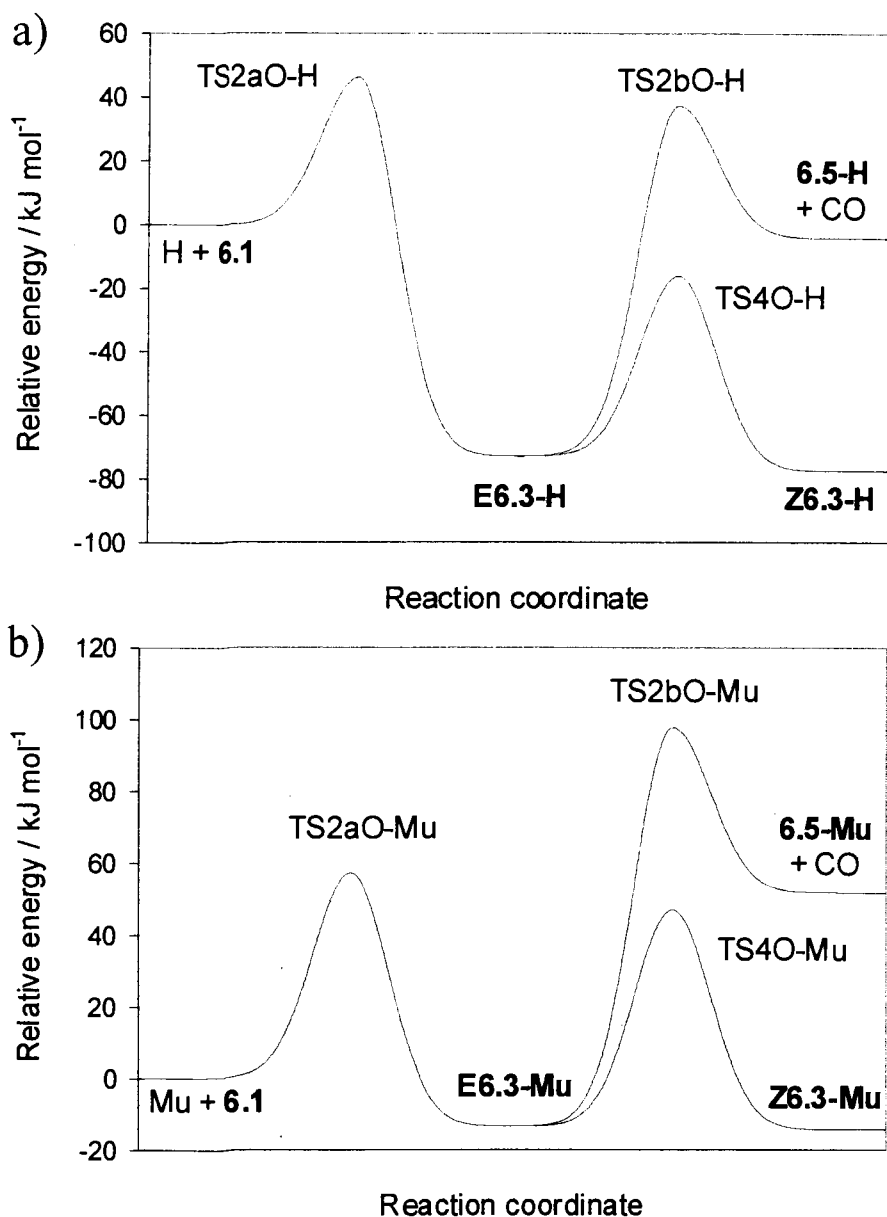


Figure 6.7: Relative internal energies for the reactions of a) H with *tert*-butylisocyanate and b) Mu with *tert*-butylisocyanate.

The relationship between the barriers to formation (TS2a) and dissociation (TS2b) determines which radical is observed. The quantum calculations of Nguyen *et al.* showed that the barrier for hydrogen atom addition to the nitrogen atom of HNCO is 44 kJ mol^{-1} above the barrier to dissociation of H_2NCO [177]. This arrangement means that the H_2NCO radical is produced with enough energy to dissociate, making it a short-lived intermediate, in the absence of any interactions with neighbouring molecules. The barrier

for addition of hydrogen atoms to the nitrogen of *tert*-butylisocyanate (**6.1**) is 9.0 kJ mol^{-1} above the barrier to dissociation, which suggests that the carbamoyl radical (**6.3-H**) should decompose rapidly and that the *tert*-butylaminy radical would be observed. The situation is very different for the addition of muonium to **6.1**. The higher zero-point energy in the N-Mu bond, which is a result of the light mass of the muon, results in the energy of the products being raised in energy with respect to the energy of the reactants. The barrier for addition of muonium to the nitrogen atom of **6.1** is 40.6 kJ mol^{-1} *below* the dissociation barrier. This means that the *N*-muono-*N*-*tert*-butylcarbamoyl radical does not have enough energy to dissociate, so it is this species that is observed and not the muoniated *tert*-butylaminy radical.

The preceding discussion has ignored the effect of entropy, which would favour the dissociation of the acyl and thioacyl radicals. However, it is the relative energies of the barriers to addition of Mu and dissociation that determine whether an aminyl or an acyl radical is observed. The difference in entropy between these two transition states is small. Frequency calculations at the 6-311++G level determined the entropy of TS2aO-Mu and TS2bO-Mu to be 369.2 and $378.1 \text{ J mol}^{-1} \text{ K}^{-1}$, respectively. This difference is negligible compared with the differences in internal energy, so it can be ignored.

The relaxation rates of the radicals can provide information about the radical's internal dynamics and its reactions [195]. The relaxation rate for **E6.3-Mu** increases with temperature, and this could be due to rotation about the C-N bond to form the *Z* conformer, dissociation of the radical to give Mu and **6.1**, or reaction with a neighbouring *tert*-butylisocyanate molecule. The line-widths of the signals for both conformers of **6.4-Mu** decrease with increasing temperature. The likely cause for this behaviour is modulation of the anisotropic hyperfine interactions. This relaxation mechanism results in the relaxation rate being proportional to η/T , where η is the viscosity of the medium. The sample becomes more viscous at lower temperatures, restricting the motion of the radical and causing the relaxation to increase. This is compounded by the decrease in the temperature.

The relaxation rates for **Z6.4-Mu** are several times higher than the relaxation rates for **E6.4-Mu**, which was initially surprising given the similarities in their structures. It is proposed that the difference in the relaxation rates is the result of the different activation energies for the rotation from the *E* to the *Z* conformer compared with the corresponding value for rotation from the *Z* to the *E* conformer. The activation energies are different because of the difference in energy of the *E* and *Z* conformers. The *E* conformer is calculated to be 5.2 kJ mol⁻¹ lower in energy than the *Z* conformer. The ratio of the relaxation rates at 298 K (at which the sample is definitely a liquid) was used to estimate the difference in the energy of the two conformers. The ratio of the relaxation rates is approximately given by the following equation,

$$\frac{\lambda_Z}{\lambda_E} \approx \exp\left[\frac{\delta}{RT}\right] \quad (6.8)$$

where δ is the difference in energy between the two conformers. This expression was derived from the Arrhenius equation, assuming that the pre-exponential factors were the same. The ratio of λ_Z/λ_E at 298 K would be 8.2 using the calculated values. The experimental ratio of λ_Z/λ_E at 298 K is 6.4, which would correspond to a difference of 4.6 kJ mol⁻¹. The relaxation behaviour could be better understood by studying radicals **6.3-Mu** and **6.4-Mu** over a wider temperature range in a solvent that is inert (eliminating the possibility of reaction with the solvent) and has a low melting point (eliminating effects due to the solid state). From such studies it might be possible to determine the barrier to rotation about the C-N bond in these radicals.

6.6 Conclusions

The reactions of muonium with *tert*-butylisocyanate and *tert*-butylisothiocyanate generate novel muoniated acyl and thioacyl radicals, the first of these types of radicals to be directly observed by μ SR. The structures of these radicals were assigned by comparison of the experimental hfcs with values obtained from density functional calculations. The *Z* conformer of the muoniated *N-tert*-butylcarbamoyl radical was not observed because of its low A_μ value but is probably present. The N-Mu bond was estimated to be 4.2% longer than the corresponding N-H bond based on a comparison of the muon and proton hfcs in

the *N-tert*-butylcarbamoyl radical. The results of the theoretical calculations indicate that while the *N-tert*-butylcarbamoyl radical should dissociate to the *tert*-butylaminy radical and CO, the muoniated *N-tert*-butylcarbamoyl radical does not because the larger zero point energy of the muoniated *tert*-butylaminy radical makes the dissociation endothermic. The radicals exhibit unusual relaxation behaviour that warrants further examination.

CHAPTER 7.

SUMMARY

One of the great successes of muonium chemistry has been the study of the effect of the light mass of Mu on the structure and dynamics of muoniated radicals. However, these studies have been mostly limited to alkyl and cyclohexadienyl-type radicals where the muon is attached adjacent to the radical centre. The experiments detailed in this thesis have extended the scope of isotopic studies by producing novel muoniated radicals in which either the muon is attached directly to the radical centre or the unpaired electron is localized in a σ orbital.

The muoniated isotopomers of the methyl radical were produced by the reaction of Mu with ketene and deuterated ketene. The reduced muon hfc is 3% larger than the proton hfc in CH_2Mu due to the difference in the zero-point energy of the C-Mu/H stretching vibration. The temperature dependence of the hfc is unlike that of any other methyl isotopomer in that the magnitude of the hfc increases with increasing temperature. This is due to the out-of-plane bending mode being much higher in energy due to the light mass of the muon, which means that there is negligible population of the first excited state at the low temperatures studied in these experiments. As a result, it is the interaction of the methyl radical with the surrounding solvent molecules that results in the temperature dependence of the hfc. A second radical was observed in ketene and deuterated ketene above 200 K. This radical was the 4-muonomethyl-oxetan-2-on-4-yl radical, which was formed by addition of Mu to the terminal carbon of the C=C bond of diketene. The assignment was confirmed by obtaining TF- μ SR and μ LCR spectra of a pure diketene sample and modelling with density functional theory calculations.

The reaction of Mu with stable singlet carbenes was found to generate α -muoniated radicals. Four carbenes (1,3-bis(isopropyl)-4,5-dimethylimidazol-2-ylidene, 1,3-bis(2,4,6-trimethylphenyl)-imidazol-2-ylidene, 1,3,4-triphenyl-4,5-dihydro-1*H*-1,2,4-triazol-5-ylidene and 1,3-bis(2,4,6-trimethylphenyl)imidazolin-2-ylidene) were studied and in each case Mu added exclusively to the carbeneic carbon. The temperature dependence of the muon hfc was measured for three of the radicals and each radical

behaved very differently. The muon hfc of 1,3-bis(isopropyl)-4,5-dimethyl-2-muono-imidazol-2-yl and 1,3-bis(2,4,6-trimethylphenyl)-2-muono-imidazol-2-yl radicals fell with temperature, while the muon hfc of the 5-muono-1,3,4-triphenyl-1,2,4-triazol-5-yl radical rose with increasing temperature. Theoretical modelling of the out-of-plane mode showed that this vibration could not account for the negative temperature dependence of the 1,3-bis(isopropyl)-4,5-dimethyl-2-muono-imidazol-2-yl and 1,3-bis(2,4,6-trimethylphenyl)-2-muono-imidazol-2-yl radicals. It is likely that the temperature dependence observed for these radicals results from coupling of the out-of-plane vibrational mode with the inversion mode at the pyramidal nitrogen atoms adjacent to the radical centre.

The reaction of Mu with *tert*-butylisocyanate did not produce an α -muoniated radical but instead gave the *N*-muono-*N-tert*-butylcarbamoyl radical. Only the *E* isomer of this radical was observed. The reaction of Mu with *tert*-butylisothiocyanate produced the *N*-muono-*N-tert*-butylthiocarbamoyl radical. In this case it was possible to observe both the *E* and *Z* conformers. The assignment of the radicals was based on a comparison of the experimental hfc with values obtained from DFT calculations. These are the first muoniated acyl radical to be directly observed and their unusual behaviour warrants further examination.

Other studies of α -muoniated radicals are in progress, but were not at sufficient level to be included in this thesis. The muon hfc of the muoniated cyclopentadienyl radical was measured at room temperature [174]. The reduced muon hfc is much larger than the proton hfc of C₅H₅. This was interpreted as resulting from Mu stabilizing one of the Jahn-Teller distorted minimum energy structures. Measurements of the proton hfc of the C₅H₄Mu radical, as well as a temperature dependence study, are necessary to confirm or disprove this model.

This work marks the first big step into the study of the effect of Mu substitution on the vibrational motion at the radical centre. The knowledge of how to make these radicals will surely stimulate research in this area. As described in each of the chapters, there are numerous avenues for future work. In addition to the study of the muoniated

cyclopentadienyl radical mentioned above, future experiments will include a study of the muoniated methyl radical in the gas phase, measuring the hfcs and relaxation rates of *N*-muono-*N*-*tert*-butylcarbamoyl and *N*-muono-*N*-*tert*-butylthiocarbamoyl in different solvents over a wider temperature range, and generating novel α -muoniated radicals by the reaction of Mu with carbenes stabilized in inert matrices at low temperatures.

BIBLIOGRAPHY

- [1] S. H. Neddermeyer and C. D. Anderson, *Phys. Rev.* **54** (1938) 88-9.
- [2] D. C. Walker, Y. C. Jean and D. G. Fleming, *J. Chem. Phys.* **70** (1979) 4534-41.
- [3] D. C. Walker, S. Karolczak, G. B. Porter and H. A. Gillis, *J. Chem. Phys.* **118** (2003) 3233-6.
- [4] D. C. Walker, S. Karolczak, G. B. Porter and H. A. Gillis, *Can. J. Chem.* **81** (2003) 199-203.
- [5] J. R. Kempton, M. Senba, D. J. Arseneau, A. C. Gonzalez, D. M. Garner, J.J. Pan, D. G. Fleming, P. W. Percival, J.-C. Brodovitch and S. K. Leung, *J. Chem. Phys.* **94** (1991) 1046-59.
- [6] P. W. Percival, E. Roduner and H. Fischer, *Chem. Phys.* **32** (1978) 353-67.
- [7] V. Storchak, J. H. Brewer and G. D. Morris, *Phys. Lett. A* **193** (1994) 199-205.
- [8] A. Schenck, *Muon Spin Rotation Spectroscopy: Principles and Applications to Solid State Physics*, Adam Hilger Limited, Bristol and Boston, 1985.
- [9] J. I. Friedman and V. L. Telegdi, *Phys. Rev.* **106** (1957) 1290-3.
- [10] V. W. Hughes, D. W. McColm, K. Ziock and R. Prepost, *Phys. Rev. Lett.* **5** (1960) 63-5.
- [11] E. Roduner, *The Positive Muon as a Probe in Free Radical Chemistry Lecture Notes in Chemistry*, Vol. 49, Springer-Verlag, Heidelberg, 1988.
- [12] A. M. Brodskii, *Zh. Exp. Teor. Fiz.* **44** (1963) 1612-7.
- [13] E. Roduner, P. W. Percival, D. G. Fleming, J. Hochman and H. Fischer, *Chem. Phys. Lett.* **57** (1978) 37-40.
- [14] D. C. Walker, *Muon and Muonium Chemistry*, Cambridge University Press, Cambridge, 1983.
- [15] S. F. J. Cox, *J. Phys. C: Solid State Phys.* **20** (1987) 3187-3319.

-
- [16] J. H. Brewer, in: *Encyclopedia of Applied Physics*, Vol. 11, VCH publishers inc., 1994, pp. 25-53.
- [17] A. Schenck, in: *Nuclear and Particle Physics at Intermediate Energies*, ed. J. B. Warren, Plenum Press, New York, 1975.
- [18] R. L. Garwin, L. M. Lederman and M. Weinrich, *Phys. Rev.* **105** (1957) 1415-7.
- [19] J. H. Brewer, K. M. Crowe, V. S. Evseev, S. S. Gershtein, F. N. Gygax, L. I. Ponomarev and A. Schenck, in: *Muon Physics*, Vol. III, ed. V. W. Hughes and C. S. Wu, Academic Press, New York, 1975 pp 3-139.
- [20] E. Roduner, *Prog. React. Kinet.* **14** (1986) 1-42.
- [21] P. W. Percival, E. Roduner, H. Fischer, M. Camani, F. N. Gygax and A. Schenck, *Chem. Phys. Lett.* **47** (1977) 11-4.
- [22] M. Hemming, E. Roduner, B. D. Patterson, H. Keller and I. M. Savic, *Chem. Phys. Lett.* **128** (1986) 100-6.
- [23] B. Addison-Jones, P.W. Percival, J.-C. Brodovitch, F. Ji, D. Sharma and S. Wlodek, *Hyp. Int.* **87** (1994) 847-51.
- [24] B. Addison-Jones, P.W. Percival, J.-C. Brodovitch and F. Ji, *Hyp. Int.* **106** (1997) 143-9.
- [25] C.J. Rhodes, H. Morris and I. D. Reid, *Magn. Reson. Chem.* **39** (2001) 438-42.
- [26] S. F. J. Cox and I. D. Reid, *Appl. Magn. Reson.* **12** (1997) 227-30.
- [27] B. Webster, K.L. McCormack and R.M. Macrae. *J. Chem. Soc., Faraday Trans.* **93** (1997) 3423-7.
- [28] B. Webster. *Magn. Reson. Chem.* **38** (2000) S16-9.
- [29] I. D. Reid, S. F. J. Cox, U. A. Jayasooriya and G. A. Hopkins, *Magn. Reson. Chem.* **38** (2000) S3-8.
- [30] I. D. Reid, S. F. J. Cox, U. A. Jayasooriya and U. Zimmermann, *Physica B* **326** (2003) 89-93.

-
- [31] P. W. Percival and H. Fischer, *Chem. Phys.* **16** (1976) 89-99.
- [32] G. Le Bras and J. Combourieu, *Int. J. Chem. Kinet.* **5** (1973) 559-76.
- [33] T. Fueno and S. Takane, *Bull. Chem. Soc. Jpn.* **66** (1993) 1944-8.
- [34] E. Roduner, *Hyp. Int.* **19** (1984) 785-91.
- [35] P. W. Percival, H. Fischer, M. Camani, F. N. Gygax, W. Ruegg, A. Schenck, H. Schilling and H. Graf, *Chem. Phys. Lett.* **39** (1976) 333-5.
- [36] M. K. Kubo and K. Nishiyama, *J. Radioanal. Nucl. Chem.* **255** (2003) 175-8.
- [37] R. W. Alder, P. R. Allen and S. J. Williams, *J. Chem. Soc., Chem. Commun.* (1995) 1267-8.
- [38] J. A. C. Clyburne and T. Ramnial, personal communication.
- [39] J. L. Beveridge, J. Doornbos, D. M. Garner, D. J. Arseneau, I. D. Reid and M. Senba, *Nucl. Instr. & Meth. A* **240** (1985) 316-22.
- [40] R. F. Kiefl, *Hyp. Int.* **32** (1986) 707-20.
- [41] <http://www.isis.rl.ac.uk/muons/data%20analysis/wimda/> (March 25, 2004)
- [42] F. L. Pratt, *Physica B* **289-290** (2000) 710-4.
- [43] F. James and M. Roos, MINUIT, CERLIB, CERN computer, 7600 Interim program library (1971).
- [44] P. W. Atkins and R. S. Friedman, *Molecular Quantum Mechanics*, third edition, Oxford University Press, Oxford, 1997.
- [45] I. N. Levine, *Quantum Chemistry*, fifth edition, Prentice Hall, Upper Saddle River, N.J., 2000.
- [46] R. Improta and V. Barone, *Chem. Rev.* **104** (2003) 1-26.
- [47] D. M. Chipman, *Theor. Chim. Acta.* **82** (1993) 93-115.
- [48] T. Ziegler, *Chem. Rev.* **91** (1991) 651-67.

-
- [49] W. Koch and M. C. Holthausen, *A Chemist's Guide to Density Functional Theory*, Wiley, Weinheim, 2001.
- [50] V. Barone, in: *Recent Advances in Density Functional Methods*, ed. D. P. Chong, World Scientific, Singapore, 1995, pp. 287-334.
- [51] L. A. Eriksson, in: *Density Functional Methods in Chemistry and Materials Science*, ed. M. Springborg, John Wiley & Sons, Chichester, 1997, pp. 125-148.
- [52] S. F. Boys, *Proc. Roy. Soc. (London)* **A200** (1950) 542-54.
- [53] P. Hohenberg and W. Kohn, *Phys. Rev. A* **136** (1964) 864-71.
- [54] W. Kohn and L. J. Sham, *Phys. Rev. A* **140** (1965) 1133-9.
- [55] Æ. Frisch and M. J. Frisch, *Gaussian 98 User's Reference*, Gaussian Inc., Pittsburgh, 1998.
- [56] L. A. Eriksson, V. G. Malkin, O. L. Malkina and D. R. Salahub, *Int. J. Quantum Chem.* **52** (1994) 879-901.
- [57] L. A. Eriksson, V. G. Malkin, O. L. Malkina and D. R. Salahub, *J. Chem. Phys.* **100** (1994) 5066-75.
- [58] <http://www.gaussian.com/> (March 25,2004)
- [59] *Gaussian 98, Revision A.11.3*, M. J. Frisch, G. W. Trucks, H. B. Schlegel, G. E. Scuseria, M. A. Robb, J. R. Cheeseman, V. G. Zakrzewski, J. A. Montgomery, Jr., R. E. Stratmann, J. C. Burant, S. Dapprich, J. M. Millam, A. D. Daniels, K. N. Kudin, M. C. Strain, O. Farkas, J. Tomasi, V. Barone, M. Cossi, R. Cammi, B. Mennucci, C. Pomelli, C. Adamo, S. Clifford, J. Ochterski, G. A. Petersson, P. Y. Ayala, Q. Cui, K. Morokuma, N. Rega, P. Salvador, J. J. Dannenberg, D. K. Malick, A. D. Rabuck, K. Raghavachari, J. B. Foresman, J. Cioslowski, J. V. Ortiz, A. G. Baboul, B. B. Stefanov, G. Liu, A. Liashenko, P. Piskorz, I. Komaromi, R. Gomperts, R. L. Martin, D. J. Fox, T. Keith, M. A. Al-Laham, C. Y. Peng, A. Nanayakkara, M. Challacombe, P. M. W. Gill, B. Johnson, W. Chen, M. W. Wong, J. L. Andres, C. Gonzalez, M. Head-Gordon, E. S. Replogle, and J. A. Pople, Gaussian, Inc., Pittsburgh PA, 2002.

-
- [60] <http://www.scm.com/> (March 25, 2004)
- [61] <http://www.msg.ameslab.gov/GAMESS/GAMESS.html> (March 25,2004)
- [62] G. Herzberg, *The Spectra and Structures of Simple Free Radicals; an Introduction to Molecular Spectroscopy*, Cornell University Press, Ithica, 1971.
- [63] G. Herzberg and J. Shoosmith, *Can. J. Phys.* **34** (1956) 523-5.
- [64] D. E. Milligan and M. E. Jacox, *J. Chem. Phys.* **47** (1967) 5146-56.
- [65] A. Snelson, *J. Phys. Chem.* **74** (1970) 537-44.
- [66] J. Pacansky and J. Bargon, *J. Am. Chem. Soc.* **97** (1975) 6896-7.
- [67] L. Y. Tan, A. M. Winer and G. C. Pimentel, *J. Chem. Phys.* **57** (1972) 4028-37.
- [68] C. Yamada, E. Hirota and K. Kawaguchi, *J. Chem. Phys.* **75** (1981) 5256-64.
- [69] S. Davis, D. T. Anderson, G. Duxbury and D. J. Nesbitt, *J. Chem, Phys.* **107** (1997) 5661-75.
- [70] J. K. Kochi, in: *Advances in Free Radical Chemistry, Volume 5*, ed. G. H. Williams, Academic Press, New York, 1975, pp. 189-316.
- [71] J. A. Weil, J. R. Bolton and J. E. Wertz, *Electron Paramagnetic Resonance*, John Wiley & Sons, New York, 1994.
- [72] N. M. Atherton, *Principles of Electron Paramagnetic Resonance*, Ellis Horwood, Prentice-Hall, New York, 1993.
- [73] Landolt-Börnstein: "Numerical data and functional relationships in science and technology" *Magnetic Properties of Free Radicals, New Series*, edited by H. Fischer.
- [74] H. M. McConnell and D. B. Chesnut, *J. Chem. Phys.* **28** (1958) 107-17.
- [75] I. A. Zlochower, W. R. Miller, Jr. and G. K. Fraenkel, *J. Chem. Phys.* **42** (1965) 3339-40.
- [76] G. B. Barbutt, H. D. Gesser and M. Fujimoto, *J. Chem. Phys.* **48** (1968) 4605-14.
- [77] H. Fischer and H. Hefter, *Z. Naturforsch. Teil A* **23** (1968) 1763-5.

-
- [78] J. M. Riveros and S. Shih, *J. Chem. Phys.* **50** (1969) 3132-3.
- [79] R. W. Fessenden, *J. Phys. Chem.* **71** (1967) 74-83.
- [80] T. Yamada, K. Komaguchi, M. Shiotani, N. P. Benetis and A. R. Sørnes, *J. Phys. Chem. A* **103** (1999) 4823-9.
- [81] T. Shiga and A. Lund, *J. Phys. Chem.* **77** (1973) 453-5.
- [82] D. M. Chipman, *J. Chem. Phys.* **78** (1983) 3112-32.
- [83] P. Botschwina, J. Flesch and W. Meyer, *Chem. Phys.* **74** (1983) 321-8.
- [84] V. Barone, A. Grand, C. Minichino and R. Subra, *J. Chem. Phys.* **99** (1993) 6787-98.
- [85] F. M. Bickelhaupt, T. Ziegler and P. von R. Schleyer, *Organometallics* **15** (1996) 1477-87.
- [86] R. W. Carr, Jr., I. D. Gay, G. P. Glass and H. Niki, *J. Chem. Phys.* **49** (1968) 846-52.
- [87] F. Slemr and P. Warneck, *Ber. Bunsenges. Phys. Chem.* **79** (1975) 152-6.
- [88] J. V. Michael, D. F. Nava, W. A. Payne and L. J. Stief, *J. Chem. Phys.* **70** (1979) 5222-7.
- [89] H. Umemoto, S. Tsunashima, S. Sato, N. Washida and S. Hatakeyama, *Bull. Chem. Soc. Jpn.* **57** (1984) 2578-80.
- [90] P. Frank, K. A. Bhaskaran and T. Just, *J. Phys. Chem.* **90** (1986) 2226-31.
- [91] J. E. Bennett and B. Mile, *J. Chem. Soc. Faraday Trans. 1*, **69** (1973) 1398-1414.
- [92] K. Sung and T. T. Tidwell, *J. Org. Chem.* **63** (1998) 9690-7.
- [93] J. Lee and J. W. Bozzelli, *Int. J. Chem. Kinetics* **35** (2003) 20-44.
- [94] A. I. Vogel, *Vögel's Textbook of Practical Organic Chemistry*, 5th edition, revised by B. H. Furniss, Longman, London, 1989, pp. 100-102.
- [95] S. Andreades and H. D. Carlson, *Organic Syntheses, Coll. Vol. V* (1973) 679-84.
- [96] G. J. Fisher, A. F. MacLean and A. W. Schnizer, *J. Org. Chem.* **18** (1953) 1055-7.

-
- [97] H. Paul and H. Fischer, *Helv. Chim. Acta* **56** (1973) 1575-94.
- [98] R. Livingston and H. Zeldes, *J. Am. Chem. Soc.* **88** (1966) 4333-6.
- [99] E. Hirota and C. Yamada, *J. Mol. Spectrosc.* **96** (1982) 175-82.
- [100] E. G. Janzen and G. A. Coulter, *Tetrahedron. Lett.* **22** (1981) 615-8.
- [101] I. Al-Bala'a and R. D. Bates Jr., *J. Mag. Reson.* **73** (1987) 78-89.
- [102] P. J. Chmielewski, A. Jezierski, Z. Siatecki and J. Sienkiewicz, *Radiat. Phys. Chem.* **45** (1995) 891-7.
- [103] B. Fernandez, O. Christiansen, O. Bludsky, P. Jørgensen and K. V. Mikkelsen, *J. Chem. Phys.* **104** (1996) 629-35.
- [104] R. M. Stratt and S. G. Desjardins, *J. Am. Chem. Soc.* **106** (1984) 256-7.
- [105] H. Tachikawa, *J. Phys. Chem. A* **102** (1998) 7065-9.
- [106] M. Igarashi, T. Ishibashi and H. Tachikawa, *THEOCHEM*, **594** (2002) 61-9.
- [107] C. P. Poole, Jr. and H. A. Farach, *Relaxation in Magnetic Resonance*, Academic Press, New York, 1971.
- [108] H. Paul, *Chem. Phys. Lett.* **32** (1975) 472-5.
- [109] P. W. Atkins and D. Kivelson, *J. Chem. Phys.* **44** (1966) 169-74.
- [110] R. E. D. McClung, *J. Chem. Phys.* **57** (1972) 5478-91.
- [111] J. Hwang, D. Kivelson and W. Plachy, *J. Chem. Phys.* **58** (1973) 1753-68.
- [112] E. Roduner and I. D. Reid, *Israel J. Chem.* **29** (1989) 3-11.
- [113] P. G. Blake and H. G. Davies, *J. Applied Chem. Biochem.* **22** (1972) 491-3.
- [114] K. Sung and T. T. Tidwell, *J. Org. Chem.* **63** (1998) 9690-9697.
- [115] F. O. Rice and J. Greenberg, *J. Am. Chem. Soc.* **56** (1932) 2132-2134.
- [116] N. G. Polyanskii, Yu I. Temchin, V. N. Shtyrkov and V. V. Nikulina, *Zhurnal Prikladnoi Khimii* **44** (1971) 2586-8.

-
- [117] E. Roduner, W. Strub, P. Burkhard, J. Hochmann, P. W. Percival, H. Fischer, M. Ramos and B. C. Webster, *Chem. Phys.* **67** (1982) 275-85.
- [118] D. Buttar, R. M. Macrae, B. C. Webster and E. Roduner, *Hyp. Int.* **65** (1990) 927-36.
- [119] C. Heller and H. M. McConnell, *J. Chem. Phys.* **32** (1960) 1535-9.
- [120] P. W. Percival, J.-C. Brodovitch, S.-K. Leung, D. Yu, R. F. Kiefl, G. M. Luke, K. Venkateswaran and S. F. J. Cox, *Chem. Phys.* **127** (1988) 137-147.
- [121] D. Yu, Ph. D. thesis, Simon Fraser University.
- [122] M. Shiotani, N. Isamoto, M. Hayashi, T. Fängström and S. Lunell, *J. Am. Chem. Soc.* **122** (2000) 12281-12288.
- [123] M. Cossi, V. Barone, R. Cammi and J. Tomasi, *Chem. Phys. Lett.* **255** (1996) 327-335.
- [124] D. Griller, K. U. Ingold, P. J. Krusic and H. Fischer, *J. Am. Chem. Soc.* **100** (1978) 6750-2.
- [125] I. Carmichael, *J. Phys. Chem.* **89** (1985) 4727-32.
- [126] J. Pacansky and M. Yoshimine, *J. Phys. Chem.* **90** (1986) 1980-3.
- [127] W. Kirmse, *Carbene Chemistry*, Academic Press, New York: 1971.
- [128] M. Jones, Jr. and R. Moss, *Carbenes*, Wiley, New York: 1973.
- [129] A. Igau, H. Grutzmacher, A. Baceiredo and G. Bertrand, *J. Am. Chem. Soc.* **110** (1988) 6463-6.
- [130] A. J. Arduengo, R. L. Harlow and M. Kline, *J. Am. Chem. Soc.* **113** (1991) 361-3.
- [131] D. Enders, K. Breuer, G. Raabe, J. Runsink, J. H. Teles, J.-P. Melder, K. Ebel and S. Brode, *Angew. Chem. Int. Ed. Engl.* **34** (1995) 1021-3.
- [132] A. J. Arduengo, III, J. R. Goerlich and W. J. Marshall, *J. Am. Chem. Soc.* **117** (1995) 11027-8.

-
- [133] L. Pauling, *J. Chem. Soc. Chem. Commun.* (1980) 688-9.
- [134] K. K. Irikura, W. A. Goaddard, III and J. L. Beauchamp, *J. Am. Chem. Soc.* **114** (1992) 48-51.
- [135] A. J. Arduengo, III, *Acc. Chem. Res.* **32** (1999) 913-21.
- [136] D. Bourissou, O. Guerret, F. P. Gabbaï, and G. Bertrand, *Chem. Rev.* **100** (2000) 39-91.
- [137] W. A. Hermann and C. Köcher, *Angew. Chem. Int. Ed. Engl.* **36** (1997) 2162-9.
- [138] W. A. Hermann, *Angew. Chem. Int. Ed. Engl.* **41** (2002) 1276-91.
- [139] A. H. Cowley, *J. Organomet. Chem.* **617-618** (2001) 105-9.
- [140] D. Enders, K. Breuer, G. Raabe, J. Simonet, A. Ghanimi, H. B. Stegmann and J. H. Teles, *Tetrahedron Lett.* **38** (1997) 2833-6.
- [141] L. Pause, M. Robert, J. Heinicke and O. Köhl, *J. Chem. Soc. Perkin Trans. 2* (2001) 1383-8.
- [142] R. Weiss and N. Kraut, *Angew. Chem. Int. Ed. Engl.* **41** (2002) 311-4.
- [143] C. Heinemann, T. Müller, Y. Apeloig and H. Schwarz, *J. Am. Chem. Soc.* **118** (1996) 2023-38.
- [144] C. Boehme and G. Frenking, *J. Am. Chem. Soc.* **118** (1996) 2039-46.
- [145] T. Boehland, F. Temps and H. G. Wagner, *J. Phys. Chem.* **91** (1987) 1205-9.
- [146] N. Kuhn and T. Kratz, *Synthesis* (1993) 561-2.
- [147] E. Roduner, G. A. Brinkman and P. W. F. Louwrier, *Chem. Phys.* **73** (1982) 117-30.
- [148] V. G. Malkin, O. L. Malkina, L. A. Eriksson and D. R. Salahub, in: *Modern Density Functional Theory, A Tool for Chemistry*; J. M. Seminario and P. Politzer, Eds.; Elsevier: New York, 1995.
- [149] A. D. Becke, *J. Chem. Phys.* **98** (1993) 1372-7.

-
- [150] N. Rega, M. Cossi and V. Barone, *J. Chem. Phys.* **105** (1996) 11060-7.
- [151] V. Barone in *Recent Advances in Density Functional Methods Part 1*; D. P. Chong, Ed.; World Scientific Publishing Co.: Singapore, 1996 p.287-334.
- [152] D. Yu, P. W. Percival, J.-C. Brodovitch, S.-K. Leung, R. F. Kiefl, K. Venkateswaran and S. F. J. Cox, *Chem. Phys.* **142** (1990) 229-36.
- [153] J. R. Morton, F. Negri and K. F. Preston, *Phys. Rev. B* **49** (1994) 12446-50.
- [154] M. A. Boxwell, T. A. Claxton and S. F. J. Cox, *J. Chem. Soc. Faraday Trans.* **89** (1993) 2957-60.
- [155] V. Barone, C. Minichino, H. Faucher, R. Subra and A. Grand, *Chem. Phys. Lett.* **205** (1993) 324-30.
- [156] V. Barone and R. Subra, *J. Chem. Phys.* **104** (1996) 2630-7.
- [157] V. Barone, C. Adamo, Y. Brunel and R. Subra, *J. Chem. Phys.* **105** (1996) 3168-74.
- [158] A. J. Arduengo, III; H. V. R. Dias, R. L. Harlow and M. Kline, *J. Am. Chem. Soc.* **114** (1992) 5530-4.
- [159] J.-C. Brodovitch, B. Addison-Jones, K. Ghandi, S. Kecman, I. McKenzie and P. W. Percival, Manuscript in preparation.
- [160] P. W. Percival, B. Addison-Jones, J.-C., Brodovitch, K. Ghandi and J. Schüth, *Can. J. Chem.*, **77** (1999) 326-331.
- [161] J.-C. Brodovitch, B. Addison-Jones, K. Ghandi, I. McKenzie, P. W. Percival, and J. Schüth, *Can. J. Chem.*, **81** (2003) 1-6.
- [162] J. Villa, J. C. Corchado, A. González-Lafont, J. M. Lluch, and D. G. Truhlar, *J. Phys. Chem. A* **103** (1999) 5061-74.
- [163] B. S. Jursic, *J. Chem. Soc. Perkin Trans. 2* (1997) 637-641.
- [164] J. K. Kochi, P. Bakuzis and P. J. Krusic, *J. Am. Chem. Soc.* **95** (1973) 1516-26.
- [165] V. Barone, A. Grand, C. Minichino and R. Subra, *J. Phys. Chem.* **97** (1993) 6355-61.

-
- [166] V. Barone and C. Minichino, *Theochem.* **330** (1995) 365-76.
- [167] C. Adamo, M. Heitzmann, F. Meilleur, N. Rega, G. Scalmani, A. Grand, J. Cadet and V. Barone, *J. Am. Chem. Soc.* **123** (2001) 7113-7.
- [168] F. Jolibois, J. Cadet, A. Grand, R. Subra, N. Rega and V. Barone, *J. Am. Chem. Soc.* **120** (1998) 1864-71.
- [169] R. Behrson, *J. Chem. Phys.* **24** (1958) 1066-72.
- [170] M. Karplus and G. K. Fraenkel, *J. Chem. Phys.* **35** (1961) 1312-23.
- [171] B. L. Burrows, M. Cohen and T. Feldmann, *Can. J. Phys.* **76** (1998) 129-41.
- [172] H. Tachikawa, M. Igarashi and T. Ishibashi, *Chem. Phys. Lett.* **352** (2002) 113-9.
- [173] C. J. Rhodes, H. Morris and I. D. Reid, *Magn. Reson. Chem.* **39** (2001) 438-442.
- [174] I. McKenzie, J.-C. Brodovitch, K. Ghandi, S. Kecman, and P. W. Percival, *Physica B* **326** (2003) 76-80.
- [175] J. D. Mertens, K. Kohsehoinghaus, R. K. Hanson and C. T. Bowman, *Int. J. Chem. Kinetics* **23** (1991) 655-668.
- [176] J. A. Miller and C. F. Melius, *Int. J. Chem. Kinetics* **24** (1992) 421-432.
- [177] M. T. Nguyen, D. Sengupta, L. Vereecken, J. Peeters and L. G. Vanquickenborne, *J. Phys. Chem.* **100** (1996) 1615-1621.
- [178] S.Y. Ma, Y. Q. Ji and R. Z. Liu, *Acta Chimica Sinica* **55** (1997) 110-116.
- [179] M. Pettersson, L. Khriachtchev, S. Jolkkonen and M. Rasanen, *J. Phys. Chem. A* **103** (1999) 9154-9162.
- [180] D. E. Milligan and M. E. Jacox, *J. Chem. Phys.* **43** (1965) 4487-93.
- [181] C. Chatgilaloglu, D. Crich, M. Komatsu and I. Ryu, *Chem. Rev.* **99** (1999) 1992-2069.
- [182] F. J. Adrian, E. L. Cochran and V. A. Bowers, *J. Chem. Phys.* **36** (1962) 1661-72.
- [183] J. A. Brivati, N. Keen and M. C. R. Symons, *J. Chem. Soc.* (1962) 237.

-
- [184] J. J. Pan, D. G. Fleming, M. Senba, D. J. Arseneau, R. Snooks, S. Baer, M. Shelley, P. W. Percival, J.-C. Brodovitch, B. Addison-Jones, S. Wlodek and S. F. J. Cox, *Hyp. Int.* **87** (1994) 865-70.
- [185] S. F. J. Cox, R. M. Macrae, W. G. Williams and D. G. Fleming, *Hyp. Int.* **87** (1994) 871-6.
- [186] T. A. Claxton and S. F. J. Cox, *Phil. Mag. B* **72** (1995) 267-273.
- [187] B. Webster, *Chem. Soc. Faraday Trans.* **93** (1997) 205-210.
- [188] C. J. Rhodes, M. C. R. Symons, E. Roduner and C. A. Scott, *Chem. Phys. Lett.* **139** (1987) 496-8.
- [189] C. J. Rhodes, M. C. R. Symons, C. A. Scott, E. Roduner and M. J. Heming, *Chem. Soc. Chem. Commun.* (1987) 447-8.
- [190] D. A. Geeson, M. C. R. Symons, E. Roduner, H. Fischer and S. F. J. Cox, *Chem. Phys. Lett.* **116** (1985) 186-91.
- [191] R. Sutcliffe and K. U. Ingold, *J. Am. Chem. Soc.* **103** (1981) 7686-7687.
- [192] M. C. R. Symons, *J. Chem. Soc. Perkin Trans II* (1973) 797-803.
- [193] R. Sutcliffe, D. Griller, J. Lessard and K. U. Ingold, *J. Am. Chem. Soc.* **103** (1981) 624-628.
- [194] A. G. Davies, J.-Y. Nedelec and R. J. Sutcliffe, *Chem. Soc. Perkin Trans. II* (1983) 209-211.
- [195] E. Roduner, *Hyp. Int.* **8** (1981) 561-9.